Dewatering Through Mud Mounds on the Continental Fore-arc of Costa Rica

Dissertation

zur Erlangung des Doktorgrades

der Mathematisch-Naturwissenschaftlichen Fakultät

der Christian-Albrechts-Universität zu Kiel

vorgelegt von

Noémi Fekete

Kiel

2006

Referent/in:	Prof. Dr. Timothy J. Reston
Korreferent/in:	PD. Dr. Ingo Grevemeyer
Tag der mündlichen Prüfung:	12. 06. 2006
Zum Druck genehmigt:	Kiel, 14. 06. 2006

Der Dekan

Table of contents

Summary

The scientific aim of SFB 574 has been to investigate the role of fluid and volatile recycling in subduction zones. Within this context, the present work sets out to study the contribution of mounds, found abundantly on the Pacific margin of Central America, to the dewatering of continental fore-arc. Our targets are twofold: to determine the structure and mechanism of mud domes on one hand, and to identify and locate alternative fluid pathways through the subsurface on the other.

The geophysical method applied through the analyses is primarily seismo-acoustic. An extensive set of multibeam bathymetric, parametric echosounder, and high-resolution multichannel seismic data provides means for a multi-frequency approach. *In situ* heat flow measurements are utilized to calibrate the thermal parameters of sediments and to supplement conclusions regarding the temperature regime within the upper few hundred meters below the seafloor.

Structural investigations near a single large mound reveal it to be of diapiric origin. Based on the observed deformation and sediment deposition patterns in its vicinity, a local tectonic model of the Mound Culebra area is constructed, along with several hypotheses so as to assess the model's spatial extent of validity. Potential dewatering-related features are discussed.

Thermal modelling, allowed by the widespread presence of gas hydrates in the subsurface, helps identify probable locations of heat and fluid advection as well as evaluate their relative importance. Conclusions are also drawn about the local thermal state of downgoing lithosphere beneath the Mound Culebra area, from the perspective of its documented coldness and proposed explanations.

In order to extend our results beyond the locality of investigations, observations near an additional group of mounds are presented. Differences in the local tectonics point to the influence of a subducting ridge, which overprints deformation patterns and causes a probable decrease of venting through the Hongo domes. With a comparison between the study areas, a possible fate of mud mounds on the Central American margin is outlined.

Zusammenfassung

Das wissenschaftliche Ziel des SFB 574 ist es, die Rolle des Recycling von Fluiden und Volatilen in Subduktionszonen zu untersuchen. In diesem Zusammenhang betrachtet diese Arbeit den Beitrag der Schlammhügel (Mounds) zur Entwässerung des kontinentalen Fore-arc. Zahlreiche Mounds wurden auf dem mittelamerikanischen Kontinentalrand gefunden. Die Ziele dieser Arbeit sind zweifach: die Struktur und den Mechanismus von Schlammhügeln zu bestimmen, und alternative Fluid-Aufstiegswege durch den Untergrund zu identifizieren.

Bei der Analyse wird überwiegend die seismo-akustische Methode angewendet. Ein umfassender Datensatz aus Multibeam Bathymetrie, Sediment Echolot, und hoch-auflösender Mehrkanal-Seismik ermöglicht die Untersuchung in verschiedenen Frequenzbereichen. *In situ* Wärmeflussmessungen werden verwendet, um die thermischen Parameter der Sedimente zu kalibrieren, und ergänzende Schlussfolgerungen über den Temperaturzustand in den obersten Hunderten von Metern unter dem Meeresboden zu treffen.

Strukturelle Untersuchungen in der Nähe eines einzelnen großen Mounds weisen auf seine diapirische Herkunft hin. Gestützt auf den in der Umgebung beobachteten Deformations- und Sedimentablagerungsmustern wird ein lokales tektonisches Modell des Mound Culebra Gebietes vorgestellt. Das räumliche Ausmaß seiner Gültigkeit wird auf der Basis von mehreren Hypothesen eingeschätzt. Potenzielle Entwässerungsstrukturen werden kurz diskutiert.

Weit verbreitete Gashydratvorkommen ermöglichen die thermische Modellierung und helfen somit bei der Identifizierung wahrscheinlicher Wärme- und Fluid-Aufstiegsstellen, sowie bei der Evaluierung von deren relativer Bedeutung. Schlussfolgerungen werden gezogen über den lokalen thermischen Zustand der abtauchenden Platte unter dem Gebiet des Mound Culebra hinsichtlich ihrer in der Literatur dokumentierten anomalen Kälte und den dazu vorgeschlagenen Erklärungen.

Um die Ergebnisse räumlich erweitern zu können, werden Beobachtungen über eine zusätzliche Gruppe von Mounds vorgestellt. Unterschiede in der lokalen tektonischen

Lage weisen auf den Einfluss eines subduzierenden Rückens hin, der die Deformationsmuster überschreibt und eine wahrscheinliche Abnahme des Fluidausflusses durch die Hongo Mounds verursacht. Mit einem Vergleich zwischen den beiden Untersuchungsgebieten wird das mögliche Schicksal der Schlammdiapire des Mittelamerikanischen Kontinentalrandes dargestellt.

Összefoglalás

Az SFB 574 kutatásának tárgya a szubdukciós zónákban található folyadékok és illók sorsának vizsgálata. Jelen dolgozat ebben a kontextusban született, s a sárkupolák (mounds) szerepének megismerését tűzte ki céljául, melyeket nagy számban találni Közép-Amerika csendes-óceáni partjainál. Célkitűzésünk kettős: egyrészről a sárkupolák szerkezetének, működési mehanizmusának tanulmányozása, másrészről pedig további lehetséges folyadékútvonalak felismerése és lokalizálása.

A felhasznált geofizikai módszerek jobbára a szeizmo-akusztika köréből kerülnek ki. Kiterjedt adatbázis teszi lehetővé a többfrekvenciás megközelítést, melyben éppúgy megtalálhatók a tengerfenék-térképek, mint a szediment-echográfiai és nagy-felbontású sokcsatornás szeizmikus szelvények. Az üledékek hőtani paramétereinek kalibrálásához, és a tengerfenék alatti felső néhányszáz méter hőtani állapotára vonatkozó felismeréseink kiegészítéséhez *in situ* hőáram-méréseket használtunk föl.

Egy magányosan álló sárkupola közelében végzett vizsgálatok annak diapirikus eredetét fedik föl. A környéken megfigyelhető deformációs és üledéklerakódási kép alapján felállítható egy, a szűk környezet tektoniáját leíró modell, több, ennek érvényességi körét elemző elmélettel együtt. Bemutattunk több geológiai szerkezetet, melyek valószínűsíthető szerepet játszanak a kontinensszegély víztelenedésében.

A felszín alatt nagy mennyiségben előforduló gázhidrátok jelenlétének köszönhetően alkalom nyílt hőtani modellszámításra, mely segítséget nyújt fölfelé irányuló hő- és folyadékáramok felismeréséhez, valamint fontosságuk becsléséhez. A Mound Culebra terület alatt lemerülő lemez helyi termikus állapotát illető felismeréseinket a lemez különlegesen alacsony hőtartalmának, és ehhez tartozó ismert magyarázatoknak a fényében vitattuk.

Egy másik munkaterületről való megfigyelések is helyet kaptak a dolgozatban, hogy eredményeinket térben kiterjeszthessük. A tektonikus környezetek közti eltérés oka egy, a lemerülő lemezen található hegyhát, mely megváltoztatta a deformációs képet, és valószínűsíthetőleg jelentősen csökkentette az Hongo-dombokon át történő

folyadékáramlást. A két terület összehasonlítása alkalmat adott a közép-amerikai szegély sárdiapírjai egy lehetséges életmenetének felvázolására is.

Foreword

Convergent margins present a fascinating variety of geoscientific questions. Many of these are of social relevance, because they exert utmost influence on everyday life. Earthquakes, volcanic eruptions, and tsunamis are well-know dangers associated primarily with subduction systems - far less public awareness is given to such processes as, for instance, devolatilization, which has the potential to cause medium to long-term changes in the Earth's climate.

The fluid content of subsurface is definitive of its physical behaviour. Whether within the pore space or bound in minerals, water controls fundamental characteristics such as the rheology or thermal properties of rocks, and is also responsible for a large amount of material migration below the surface. It can dissolve chemical species and carry them over huge distances laterally, where they interact with other materials; or transport them several kilometers vertically, to release them to the ocean and atmosphere.

The following work represents a small part in a series of investigations carried out to study the behaviour and budget of fluids and volatiles in subduction zones. Its main goal is to assess the role of mud diapirism / mud volcanism in the dewatering of continental fore-arc, and to locate and quantify upward fluid transport with the help of thermal considerations. To achieve this goal, the following topics are presented in individual chapters:

Chapter 1 leads you through the regional geological settings of the Central American Subduction System. It describes the scientific goals of our investigations in detail. Finally, it introduces the two target areas: Mound Culebra, and the Hongo mounds.

Chapter 2 describes each part of the data set, illuminating data acquisition and processing procedures as well as data quality and challenges.

Chapter 3 - 5 constitute the bulk of this dissertation: a characterization of subsurface structure as well as the thermal properties of the Mound Culebra area are given, followed by a comparison of observations to those near the Hongo mounds.

Results are summarized in Chapter 6. A short outlook is also given here.

1
Introduction

1.1 Geological settings

Convergence and erosion

The Pacific convergent margin of Central America is formed by the subduction of the Cocos Plate beneath the Caribbean Plate (Fig. 1.1). Due to their relative rotation, convergence rates decrease from the southeast, averaging at 85 mm/a in northern Costa Rica. Analysis of GPS measurements and seismic slip directions of shallow-thrust subduction earthquakes indicates a partitioning of the Cocos-Caribbean convergence into displacement normal and parallel to the Middle America trench (MAT), the latter occurring possibly in the form of dextral strike-strip earthquakes along the Central American volcanic arc (DeMets, 2001).

The most prevailing type of convergent margins around the world is that dominated by subduction erosion. As demonstrated by results of the Ocean Drilling Program Leg 170 (Kimura et al, 1997), it is also erosional processes rather than accretion that form the features of the continental plate in Central America. Subduction erosion is indicated primarily by a rapid subsidence of the margin. Near-shore breccia formed some 16 - 17 Ma ago has been found near the trench at 4000 m depth, in an upright position and covered by a full sequence of foraminifera, indicating gradually increasing water depths (Meschede et al., 1999, Vannucchi et al. 2001). This observation would be hard to explain satisfactorily in the context of a dominantly accretionary setting.

Structure of the continental crust

The margin wedge offshore Nicoya peninsula is built up of a high-velocity (> 4 - 4.5 km/s) material, separated by a regionally extensive seismic discontinuity from the low-velocity (~ 2 - 2.5 km/s) sequence of slope sediments (Fig. 1.2). This prominent horizon, called "rough surface" or "base-of-slope sediment (BOSS)" can be traced from near the trench to the Nicoya coastal area and for hundreds of kilometers parallel to it, and correlated to the unconformity, which separates post-Paleogene beds from the underlying Nicoya complex on land. Thus, the high-velocity wedge material is interpreted to be of ophiolitic origin and possibly is the continuation of lithological
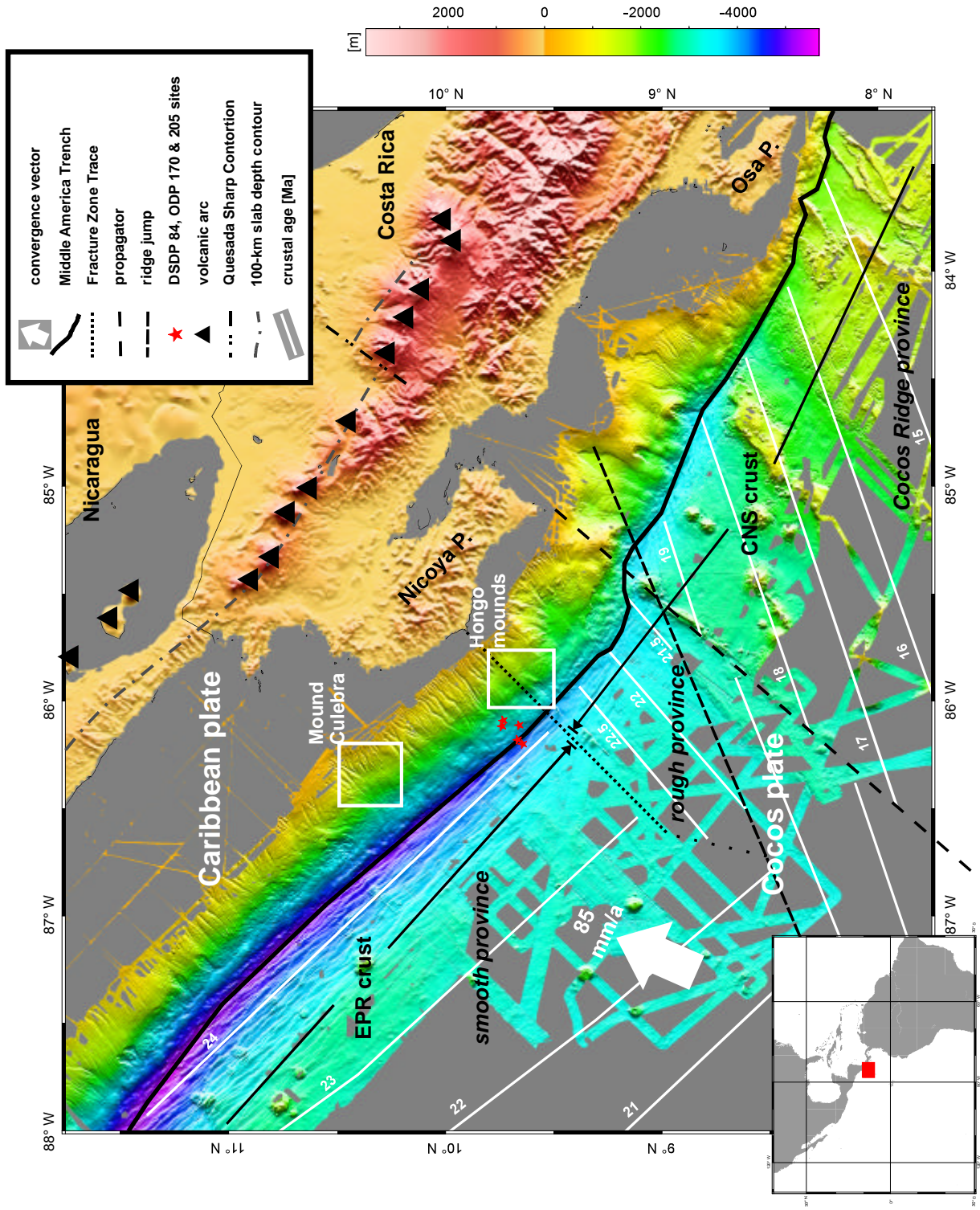
Figure 1.1 Bathymetric map of the Pacific Central America, showing major tectonic elements after Barckhausen et al., 2001 and Protti et al., 1994 as well as the two study areas (Mound Culebra and Hongo, white rectangles). The Cocos plate subducts beneath the Caribbean plate at a speed of approximately 85 mm / a (DeMets, 2001). The two oceanic domains, produced the Cocos-Nazca Spreading Center ("Cocos Ridge" and "rough" provinces southward) and the East Pacific Rise ("smooth province" in the north), respectively, are characterized by significant differences in lithospheric structure. See text for details. The color scale will remain the same throughout all bathymetric figures.
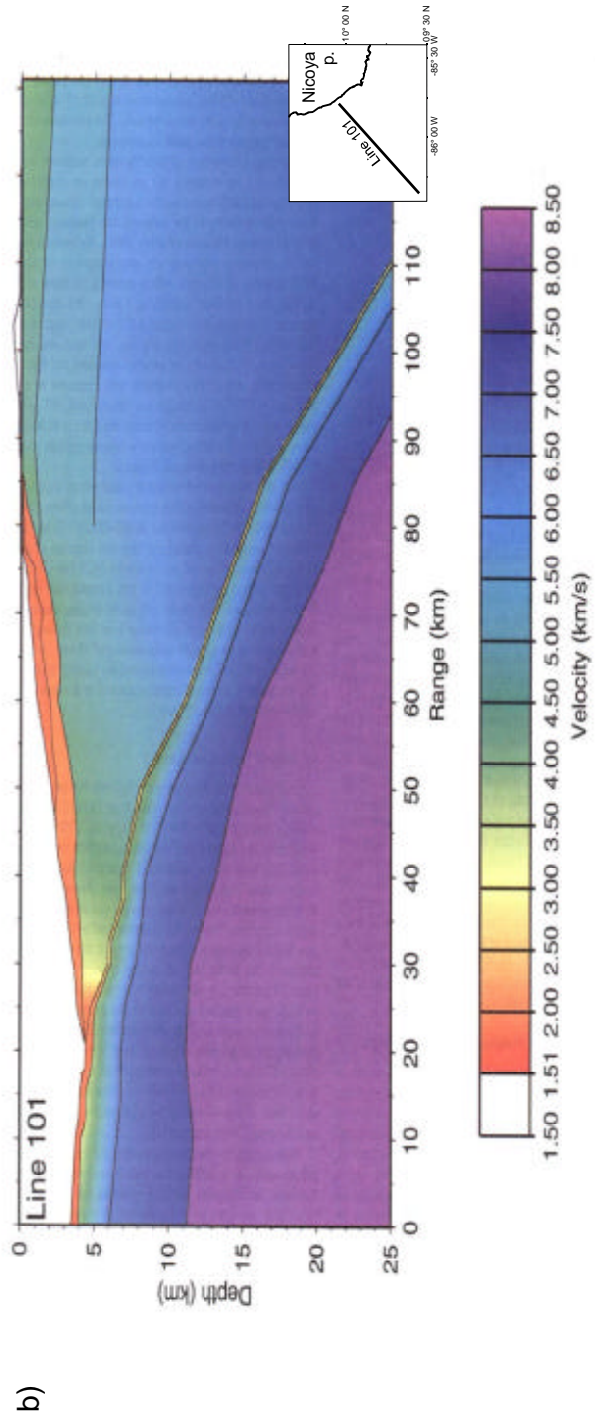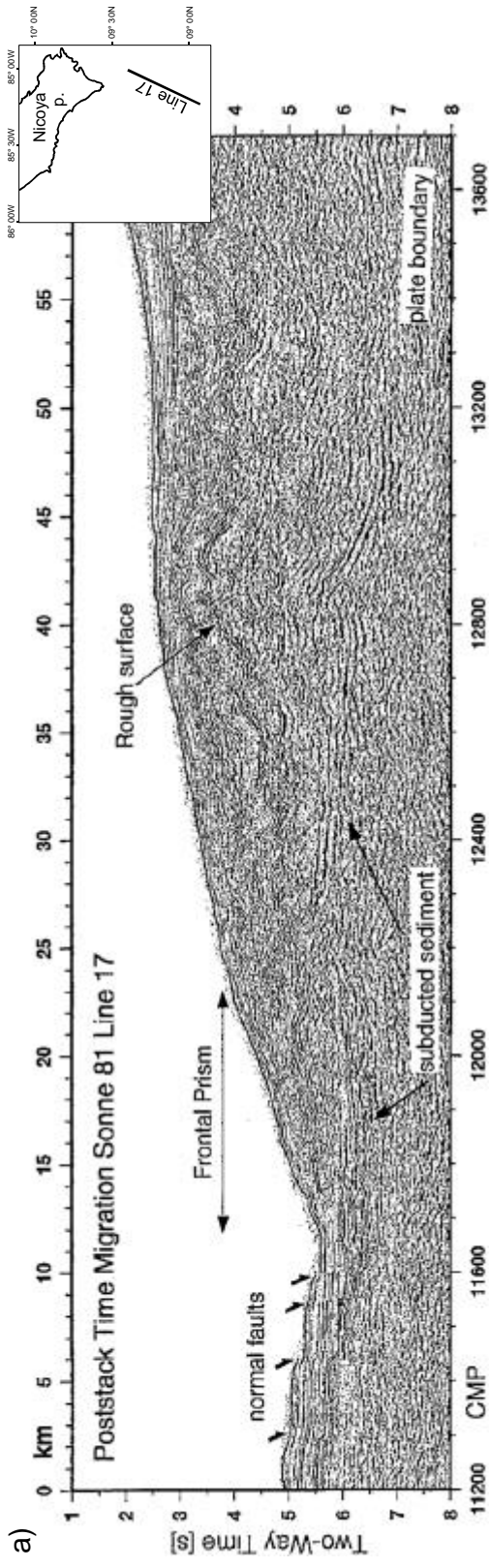
Figure 1.2 a) Seismic cross-section of the margin south of Nicoya peninsula, after von Huene et al., 2000, showing normal faulting on the incoming plate, a narrow frontal prism, and the "rough surface". b) Velocity model derived from wide-angle data offshore central Nicoya peninsula, after Christeson et al. (1999). The "rough surface" corresponds to a regional discontinuity separating low-velocity (~ 2-2.5 km/s) sediments from high-velocity (> 4-4.5 km/s) material of probable ophiolitic origin.

units found on shore (Meschede et al., 1999, Vannucchi et al. 2001). Analysis of wide-angle seismic data reveals a similar situation offshore Nicaragua (Walther et al. 2000).

The width of the frontal prism does not exceed 10 km along the entire studied segment and is quite stable despite the variable nature of crust subducting beneath it. This only changes at locations of recent seamount subduction (von Huene et al., 2000). The prism is interpreted to be made up of either old accreted oceanic material or, more probably, slumped slope sediments from the continent, as accretion is thought to have stopped 7 Ma ago (Morris et al., 2002).

Sediment deposition rates arcward of the MAT are not well constrained. DSDP Leg 84 determined 165 m/Ma during the late Pleistocene, 125 m/Ma in early to late Pliocene strata, but only 13 m/Ma in the early Pliocene. This very low value possibly implies the presence of an unconformity (Kimura et al., 1997). Ash stratigraphy on the continental side (Kutterolf, pers. comm.) indicates recent deposition rates of 150 - 200 m/Ma.

Subduction characteristics show systematic spatial variation along the MAT. A stepback of the volcanic arc from the coastline southeastward of the Nicaragua - Costa Rica border coincides with a gradual shallowing of earthquake depths (Protti et al., 1994), possibly in connection with slab tear at depth. Sediment signature of the incoming plate in the chemistry of output volcanic material (e.g. [10]Be isotopic ratio) decreases toward central Costa Rica, as does the angle of subduction.

Variable incoming plate properties

The above changes can in part be attributed to the segmentation of incoming oceanic crust. In the southeast, subducting material was created at the Cocos-Nazca Spreading Center (CNS) and underwent the influence of the Galapagos hotspot 14 - 12 Ma ago (Walther 2003, Sallares et al., 2000, Barckhausen et al., 2001). The resulting thickened, buoyant crust at the Cocos Ridge is responsible for a lower subduction angle and an uplift of southern Costa Rica (Fisher et al., 1998, Meschede et al., 1999). Its arrival at the MAT 6.5 - 6 Ma ago is thought to be seen as a sudden increase of

subsidence of the continental margin. Calculated mass removal rate changes remarkably from 45 km^3/Ma/m inferred over 16.5 Ma, to a post-6.5 Ma rate of 107 - 123 km^3/Ma/m (Vannucchi et al., 2003). This enhanced erosion may provide an explanation for low [10]Be values in the volcanic output of southern Costa Rica: estimated continental contribution from then on may have accounted for as much as ten times the subducted oceanic sediments, thus suppressing its isotopic signature (Vannucchi et al., 2003). Alternatively, oceanic sediments may also be underplated, as perhaps seen from seismic velocity duplexes at the bottom of the overriding plate (Christeson et al. 1999). Due to this process, they are no longer part of the source material for the volcanic arc and cause a lack of incoming sediment signature.

Northwest of the Cocos Ridge flank, the oceanic crust is covered up to 40% by seamounts. When these enter the MAT, they change local deformation patterns considerably. During the early phase of their subduction, seamounts cause a local retreat of the margin by eroding prism material. Compression and uplift occurs at their front, coupled with extensive deformation. Once these features pass, slope behind them is destabilized, displaying local subsidence and large-scale slumping in their wake (Ranero and von Huene, 2000). Crustal ages of this "rough province" at the trench increase towards central Nicoya up to a maximum of 22.7 Ma.

Opposite the peninsula, a small subducting ridge (Fracture Zone Trace, FZT) was identified from magnetic anomalies to mark the boundary between CNS crust and material produced at the East Pacific Rise (EPS) (Barckhausen et al, 2001). The transition is accompanied by a downward step of the basement of 100 - 200 m northwestward and significant changes of the physical properties of the downgoing plate. It is associated with variations in upper plate tectonics and subducting slab characteristics. Oceanic seafloor of this northwestern domain is relatively smooth, but upon approaching the trench becomes segmented by large-scale normal faulting running roughly parallel to the deformation front. Fault offsets reach 50 - 100 m off northern Costa Rica and rise to as much as 500 m at the trench further north (Ranero et al., 2003). The crustal age of incoming plate at the MAT is 24 Ma. On the Nicaraguan side of the FZT, crustal thickness from wide-angle data was found to be about 5 km and slightly increasing towards Nicoya (Walther et al., 2000, Ranero and von Huene 2000). Average sediment thickness is between 400 - 500 m, the entire

column of which is thought to subduct at least below the margin wedge. This is supported by the narrowness of the frontal prism and by stratigraphical correlations between ODP Leg 170 sites (Kimura et al., 1997).

Oceanic heat flow

Heat flow of the northwestern segment of the incoming plate is anomalously low compared to both global mean values (60 - 80 mW/m^2) and those predicted by conductive thermal models of crust of this age (95 - 120 mW/m^2). Average values of 20 - 40 mW/m^2 indicate an intensive cooling of the oceanic crust (Fisher et al., 2003). A complex hydrothermal circulation has been suggested (Silver et al., 2000) to explain the 70% lack of heat, with seawater entering the oceanic basement through pathways probably opened by bend faulting (Ranero et al., 2003) or through basement outcrops, combined with unusually high lateral permeability of oceanic basement (Fisher et al., 2003). Modelling shows that a circulation system of several 100 to 1000 m depth and relative pressures of $?_B > 0.8$ are required to account for the heat flow deficit (Langseth and Silver, 1996, Fisher et al., 2003).

Heat flow measured above the CNS crust differs significantly. Values of 105 - 115 mW/m^2, although above global average, are consistent with conductive models. The discrepancy between the two domains is perhaps explained by the noticeable absence of basement outcrops near the MAT on CNS-generated seafloor. Alternatively, it may be caused by "hydrogeologic compartmentalization" through off-axis magmatic and tectonic activity, associated with the formation of the Cocos Ridge. This is expected to limit large-scale heat extraction from CNS crust even if permeability is locally comparable to hypothesized values in the EPR domain.

Fore-arc dewatering

The tectonics of the continental side displays mostly extensional characteristics. Out-of-sequence thrust faults are only found near the deformation front, where underthrusting of oceanic sediments causes an oversteepening of the upper plate (Meschede et al., 1999). Further landward, normal faulting prevails, possibly cutting through the entire wedge (Shipley et al., 1992, McIntosh et al., 1993). Basal erosion is

thought to be responsible for a simultaneous subsidence, progradation, and coastal retreat (Meschede et al., 1999). The morphology of the entire continental slope suggests a widespread occurrence of mass wasting processes (Ranero and von Huene, 2000) (Fig. 1.3).
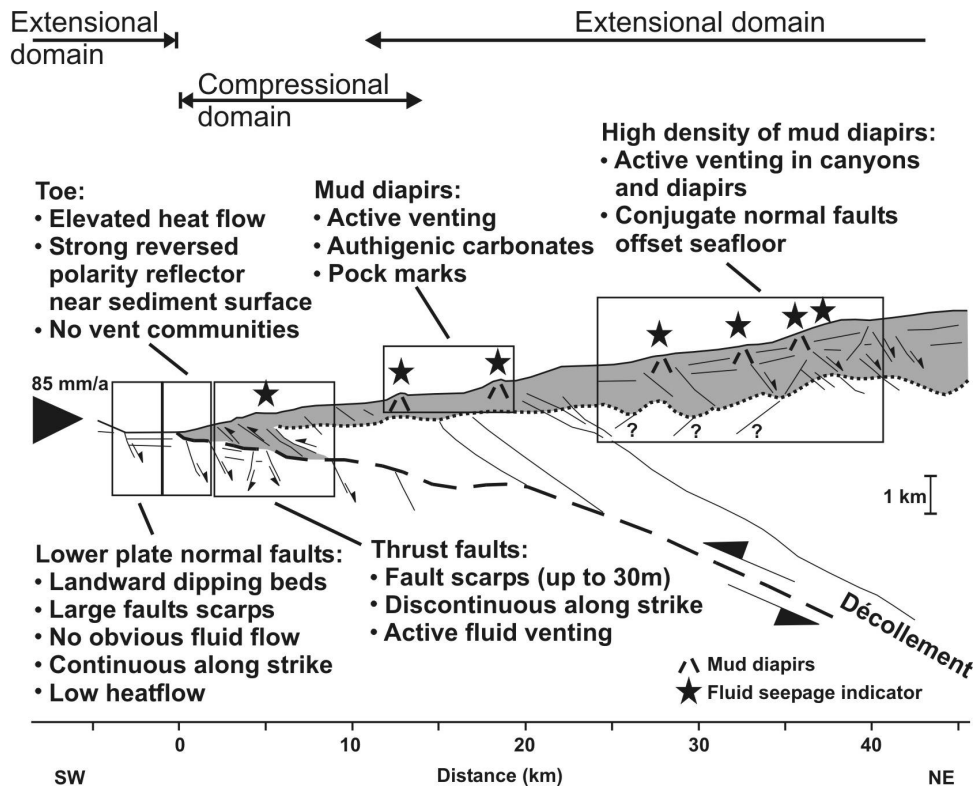

Figure 1.3 Schematic cross-section of the margin offshore northern Costa Rica after Moerz et al., 2005. Summary of dewatering-related features and tectonic properties after McAdoo et al., 1996, Ranero and von Huene, 2000, and Meschede et al., 1999.

Shipley et al. (1990) show dewatering of underthrust sediments to occur rapidly behind the trench. Seismic data image downgoing sequences to decrease in thickness to 30% of their original value within the first few kilometers after subduction, which is attributed to pore water loss and compaction. However, non-uniform dewatering keeps lower sediment layers undercompacted and pore pressures elevated. Dewatering upwards can only occur along vertical conduits or faults, while lateral flow requires high local permeability (Saffer et al., 2000). The hydrology of sediments appears decoupled from that of the basement (Silver et al., 2000). Deep-seated fluids migrate

along the decollement and fault system, with the former possibly acting as a barrier separating upper and lower plate flow (Chan and Kastner, 2000, Kopf et al., 2000, Hensen and Wallmann, 2005).

Several independent fluid flow systems have been identified at the location of ODP 170 sites. One is a sediment and upper plate system, which itself is composed of three subunits. These are a) the underthrust sediments, probably dewatering rapidly along narrow, high-permeability channels to the decollement, b) the zone of decollement, characterized by fluids of decreased chlorinity, and c) the deformed wedge and slope apron, chemically influenced by the decollement. Underneath, active flow of modified seawater within the upper oceanic crust happens at rates of 1 - 5 m/a, and beside being responsible for anomalously low crustal heat flow, it probably causes the alteration of the basaltic crust (Silver, 2000).

Although dewatering was expected to be most vigorous at the deformation front (Shipley et al., 1990), geological signs of fluid expulsion are almost entirely missing and are more abundant towards the middle slope. No vent communities were found near the trench. Large, localized heat flow anomalies are also absent - a phenomenon that may be explained by fluids not carrying significant heat and/or diffusive or episodic outflow. However, mud diapirs, mud volcanoes, and probable conduits have been observed in large numbers further landward. Their direct relation to fluid expulsion is evidenced by abundant presence of venting-associated communities on the surface, and locally elevated methane content in the water column (Kahn et al., 1996, McAdoo et al., 1996, McIntosh and Silver, 1996, Bohrmann et al, 2002, Mau et al., 2006).

Heat flow of the fore-arc

Heat flow measurements on the continental margin yield unusually low and constant values. This on one hand has been explained by reheating of the anomalously cool downgoing plate through subduction (burial) and frictional heating (Langseth and Silver, 1996), as well as by dewatering in the prism, although no flow rates were determined. Heat advection here maybe non-conclusive of the amount of dewatering because shallow fluids are not necessarily warm. Diffusive expulsion at 1 mm/a was

inferred at the prism toe and faster, though still slow, disperse flow further landward (Kahn et al., 1996).

The thermal state and dewatering pattern are intimately interrelated with gas hydrate presence at the Central American continental margin. Clathrate-containing sediment samples were recovered at DSDP Leg 84 and ODP Leg 170 sites. Further landward, the widespread occurrence of a negative-polarity bottom simulating reflector (BSR) in seismic images points to hydrates forming in the sediment (e.g. Pecher et al., 2001). Their chemical stability being primarily a function of temperature and pressure, the location and extent of gas hydrate stability field is strongly affected by heat advection, fluid migration, and slope stability. On the other hand, clathrates display a range of mechanical influence in the sediments, varying from cementation effects to reduction of porosity, and this way they influence both fluid pathways and slope stability directly.

1.2 Objectives

The special research initiative "Volatiles and Fluids in Subduction Zones" started its work at the Middle America Trench in 2001. During the last 5 years, its goal has been to investigate material transport into, at, and out of convergent plate margin settings, with special focus on climatic relevance as well as the potential to trigger natural disasters.
It is within this framework that the following investigations have been carried out. Our main objectives are "to study fluid flow and transient storage in the fore-arc region using geophysical techniques".

The scientific targets are twofold. On one hand, the role of mud mounds in fore-arc dewatering is to be studied. These features may develop through mud diapirism or mud volcanism, depending on the timing and speed of the upward movement of material. The other object of investigation is gas hydrates, which store significant amounts of methane and higher hydrocarbons in crystalline form within the hydrate stability zone, and occur widespread in the fore-arc subsurface.
The relevance of mud mounds lies in their support of upward transport of mud, fluid, and gas, promoting the dewatering and devolatilization of the continental margin

wedge and possibly of the subducting complex underneath. Thereby they have great implications for the volatile budgets of such systems, and also influence the thermal settings. The nature and importance of the contribution of mud mounds is controlled by their structure, mechanisms, local tectonic setting, life span, source region, and strength of activity.

Gas hydrates have recently been recognized for their importance in questions concerning climate, and natural hazards. Their relevance lies, on one hand, in the large amount of methane stored in compact hydrate form, and on the other, in the sensitivity of gas hydrates to changes in ambient temperature and pressure. Since hydrates exist in the pore space of sediments, their presence may increase the stability of shallow strata. Upon dissociation, this cementing effect is replaced by an overpressure due to volume expansion, creating potential slide planes. Free methane may subsequently find its way into the water column and the atmosphere, adding to the amount of greenhouse gases.

Possible causes of hydrate dissociation include uplift associated with seamount subduction, or warming caused by the upward migration of fluids. But fore-arc dewatering is tightly coupled to the occurrence of gas hydrates in additional ways. Their abundance is controlled by migrating fluids, which supply hydrate constituents. On the other hand, hydrate presence also influences available migration pathways. Furthermore, the vertical extent of hydrate stability zone is an excellent indicator of temperature and pressure variations within the sediments.

We set out to study the above-described processes with the help of a multi-frequency seismo-acoustic data set. Our primary goals are to identify fluid escape pathways within the fore-arc, such as conduits feeding mud domes, or permeable fault surfaces. To determine the nature of mounds, and find indications as to their source region, history of activity, and probable future fate. To evaluate their importance in terms of both individual and cumulative contribution to fore-arc dewatering. To assess the thermal state of subsurface through the extent of gas hydrate stability zone, the base of which can often be imaged seismically. To investigate its spatial variability, in order to locate heat transfer associated with the upward migration of fluids. And finally, to combine our observations into a general model which broadens our understanding of fore-arc dewatering through mud mounds at convergent margins.

1.3 Mound Culebra

For a detailed structural study of mud mounds on the Costa Rican fore-arc, a single large mound called Culebra has been chosen. It is located northwest of Nicoya peninsula (10° 18' N / 86° 18' W), approximately 35 km landwards of the MAT and in 1630 m water depth, opposite the subducting "smooth domain" of EPR crust. Discovered in freshly acquired bathymetric data in early 2002, Mound Culebra attracted interest being the largest mound that had been found off the shores of Costa Rica[1], and was preliminarily interpreted a mud volcano. It became a recurring target of R/V SONNE and METEOR cruises SO-163, M54, and SO-173, with data collected in its vicinity including detailed multibeam bathymetry, backscatter, ocean floor video observations, magnetics, CTD measurements, multicorer samples, dredging (Weinrebe and Flueh, 2002); sediment cores, heat flow profiles, and direct fluid flux measurements (Soeding et al., 2003, and Flueh et al., 2004), along with a large set of surface and deep-towed multi-frequency active seismic data.

A short overview of data and results relevant for our investigations is provided for background information.

Morphology and fluid venting

Mound Culebra lies on the middle slope of the continental margin. In map view, it is an elliptical feature of some 120 m of elevation and has a lateral extent of approximately 1.5 x 1 km, its major axis oriented to 244° of N. The upper plate off northern Nicoya peninsula is carved by canyons, most of which end landwards of the mound. Towards greater water depths, approximately slope-parallel bathymetric steps form the seafloor morphology. Around and northwest of Culebra, the continental slope is locally less steep, possibly indicating recent sediment deposition, and that canyons are active in terms of downslope material transport (Weinrebe and Flueh, 2002). High backscatter patches of the 30 kHz sidescan sonar TOBI (towed ocean bottom instrument) show rugged topography and/or a hard crust on Mound Culebra's top, modifying preliminary interpretations to a possible chemocherm mound. This is supported by observations from several ocean floor video (OFOS) and TV-guided

---

[1] Subsequent cruises discovered a large number of mounds off Nicaragua and noted increasing mound size northward (Flueh et al, 2004).

grab runs, which found no evidence of mud flows but ground-truthed high backscatter areas for massive outcropping carbonates. Indirect indication of a possible fault zone ("Culebra Fault"), roughly slope-parallel and appearing to divide the mound crest in two, was also found both in OFOS and TOBI observations. An abundant but scattered presence of chemosynthetic organisms, such as vesycomid clams or pogonophoran tubeworms, indicate ongoing outflow of methane- and sulphur-rich fluids at low rates (Han et al, 2004), as do elevated CH_4 concentrations in the water column samples from the summit and the northwestern flank. However, attempts to verify fluid outflow by sediment and pore water sampling have often remained unsuccessful, implying its either strongly localized, episodic, or diffusive nature.

Core and pore water information

Analysis of shallow cores from Mound Culebra have revealed it to contain numerous mud clasts which are often tectonically deformed, brecciated, overconsolidated, or cemented by carbonate. It also contains carbonate chimneys, indications of secondary hydrofracturing, and other evidence of fluid migration. These observations suggest that at least part of Culebra's material originated at greater depths, undergoing rotation and deformation during ascent, and imply the significant role of simultaneous fluid venting (Moerz et al., 2005b). Its thin sedimentary cover suggests that mud eruptions, if ever present, ceased at least a few thousand years ago and since then the mound's activity is limited to pure fluid and gas venting (Soeding et al., 2003). Heat flow measurements as well as pore water chemistry lead to the assumption that, except for one location, the mound top is characterized mostly by seawater inflow, while warmer, salt-depleted fluids escape at its base. Chemically, pore fluids appear to be characteristic of seawater recharge, H_2S discharge, or low chlorinity regimes (Hensen et al., 2004).

Water column investigations

Water column sampling has found implications of a methane source on the mound's eastern summit and possibly on its northwestern flank, correlating well with the extent of clam-inhabited areas. An additional methane anomaly above the southwestern slope was found without any sign of a local bottom source. Initial observations of the

methane content of seawater to evenly decrease from northeast to southwest above the mound have not been confirmed. Beyond spatial heterogeneity, repeated water column investigations also indicate high temporal variation of Mound Culebra's venting activity over a time span of months to years, perhaps related to an influence of regional seismic cyclicity. The data set points to generally low fluid advection rates throughout the entire Culebra area, with methane being dissolved in advecting fluids rather than degassing in form of bubbles. A conservative estimate of the mound's methane output is thought to fall between 3 x 10^4 - 6 x 10^5 mol/year (Mau et al., 2006).

Culebra Fault

Investigations at Mound Culebra have included studies of the extension of the hypothetical Culebra Fault. About 4.5 km to the southeast, bathymetric data show a fresh-looking headwall scarp - a possible result of slumping caused by movement along the fault- crossed by a gully. High backscatter values in the sidescan sonar data, which are a result of abrupt topographic variation, are accompanied by a methane plume in the water column, elevated methane and low chlorinity content of pore fluids, and the presence of venting-associated organisms. Figure 1.4 shows the locations of the above listed investigations at Mound Culebra during R/V SONNE and METEOR cruises SO-163, M54 and SO-173. A detailed location map of the data used in this work is presented in Chapter 2.

1.4 The Hongo mounds

The Hongo mounds were first studied during R/V SONNE cruise SO-144, an expedition focussing mainly on the effects of changing properties of the subducting plate on the tectonics of overriding system. Previous research in the vicinity (cruises SO-81: multichannel seismics and SO-107: magnetic profiling) addressed problems concerning, among others, gas hydrate detection (e.g. Pecher, 1996), as well as questions of dewatering of the continental slope (e.g. Kahn et al., 1996). Next to additional magnetic lines, swath bathymetric and narrow-beam echosounder profiling, SO-144 investigations included an OFOS and a CTD mission above a circular sea
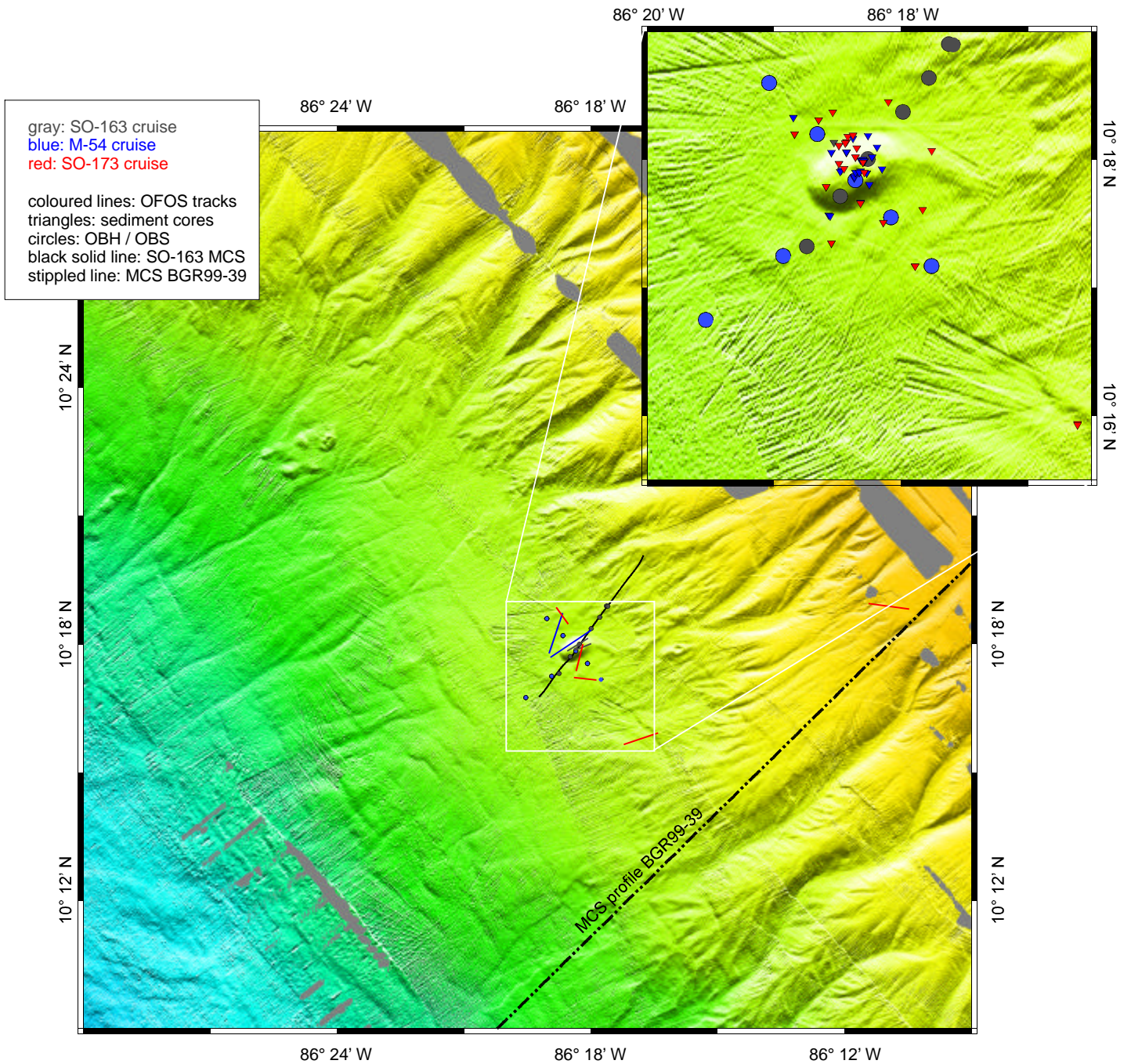
Figure 1.4 Bathymetry of Mound Culebra, with locations of various investigations carried out in the mound vicinity. Insert shows close-up of area marked in white. Map does not show data set used in this study (compare with Figure 2.2). OFOS: ocean floor observation system, OBH / OBS: ocean bottom hydrophone / seismometer, MCS: multichannel seismic profile.

floor hill at 9° 39.5' N / 85° 52.9' W, preliminarily interpreted as mud volcano (Bialas et al., 1999).

Based on the observed carbonate precipitates, patches of chemosynthetic organisms (Calyptogena, Pogonophora, bacterial mats), and elevated methane values in the bottom waters, the mound was identified as a site of active, though not vigorous, venting. Bohrmann et al. (2002) describe the mud dome as being 1000 m in diameter, approx. 100 m tall, with a central depression of 30 m and characterized by an abundance of chemosynthetic organisms.

The Hongo area became a target of scientific interest anew in spring 2002 during the R/V SONNE cruise SO-163, which aimed at investigating volatile and fluid budgets in subduction systems and especially at studying their climatic and disaster-triggering relevance. Several smaller mounds were identified and investigated in the vicinity of the "SO-144 OFOS 10 mud volcano", now named Mound Jaguar, by a number of geophysical/geological methods, including bathymetric and echosounder mapping, multi-frequency deep-towed sidescan sonar imaging, sea floor video observations (OFOS), active and passive seismic experiments. The structures were found to be generally near-circular, of a few hundred meters in diameter, and several tens of meters high. The results obtained confirmed the connection between all seven studied mounds and fluid/methane venting by recognizing circular/elongated patches of high backscatter as locations of carbonate precipitates and by finding several examples of typical vent biota, while no sign of recent mud flows was found. Some of the mounds are completely covered by sediments, but some display massive carbonate outcrops - the possibility is thus not to exclude, that they are largely or entirely made up of these. Generally, venting activity was interpreted to mostly have taken place in the past rather than at present. Normal faulting was also inferred in the area from bathymetric observations, with a possible controlling connection to the existence and location of mounds. Active seismic experiment yielded a 1D velocity model of the upper sediment cover (~4 km thick), with values ranging between 1.5 - 2 km/s. A six-week seismological experiment with ten ocean bottom hydrophones (OBH) was carried out above the central area in hope to identify venting-related microseismic activity. Indeed series of dual-frequency events ("Hongos") were recorded, preliminarily interpreted as signs of a two-phase activity, which after relocation and temporal
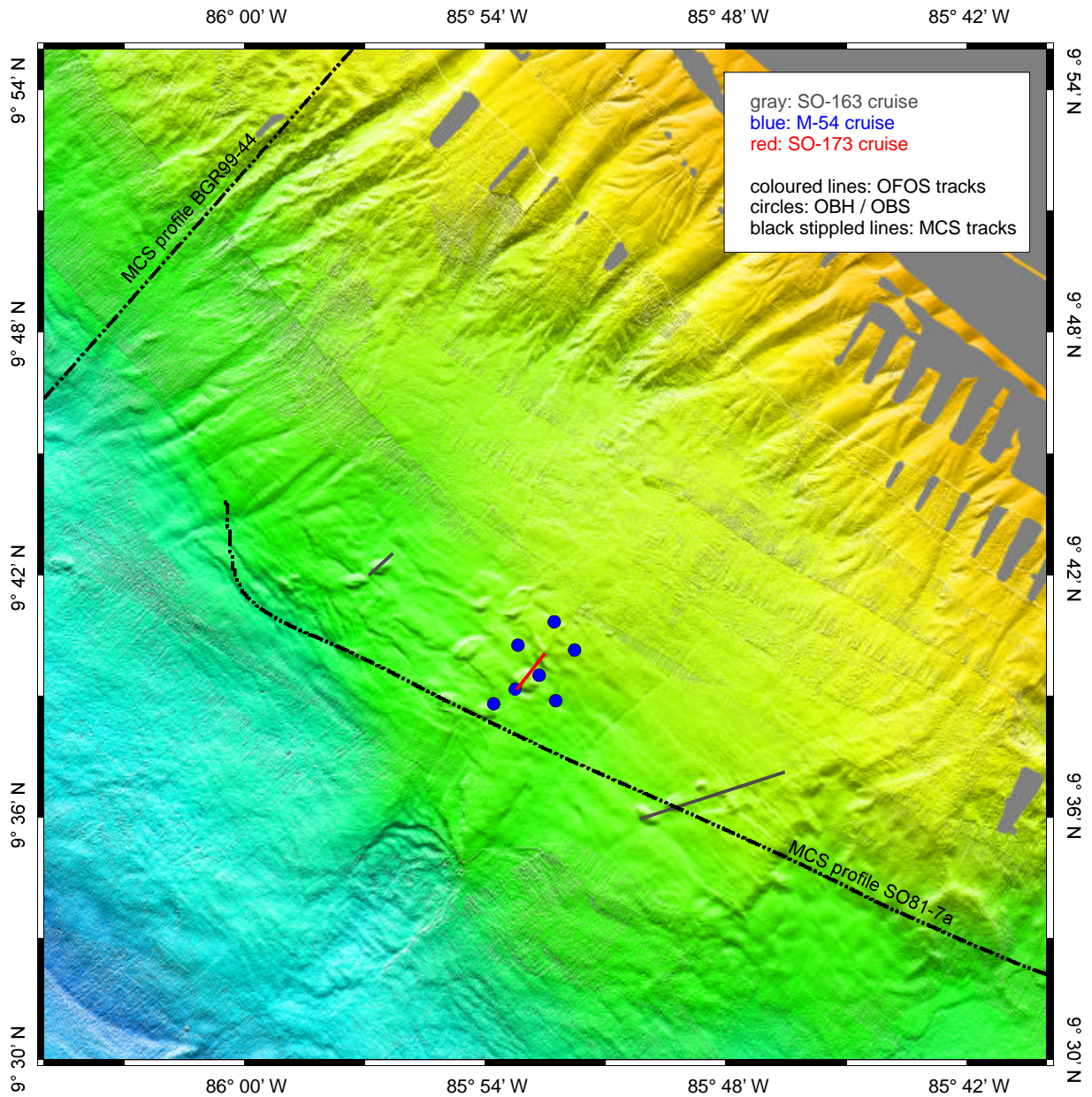
Figure 1.5 Bathymetry of the Hongo area, with locations of various investigations carried out in the vicinity of the mounds. Map does not show data set used in this study (compare with Figure 2.3). Abbreviations as in Figure 1.4.

tracing were shown to have probably been of anthropogenic origin. No other events implying local fluid migration were registered (Weinrebe and Flueh, 2002).

In summer 2002, another extensive geophysical/geological expedition took place offshore Costa Rica. Within its scope, first a tight grid of sediment echosounder and high-resolution multichannel seismic profiles were acquired in the Hongo area, supplemented by seven OBH recording the shots on the sea floor. After preliminary processing, data showed clear indications of gas hydrate presence and of an elevated free gas content in the shallow subsurface. (Spiess, Weekly Reports M54-1). Apart from seismic investigations, two heat flow transects were measured in the vicinity, starting seaward of the trench and advancing upslope. The one running southwest of the central mound area shows normal or slightly decreased values, while the other profile, only 35km further northeast, displayed significantly decreased heat flow. An overview of various investigations carried out in the area is shown in Fig. 1.5.

2
Description of data

Our investigations utilize seismo-acoustic data of four types. A detailed description is given in this chapter of their characteristics, location, quality, and the processing steps necessary for their interpretation.

2.1 Two sets of multibeam bathymetric data

Bathymetric data are used to provide details on surface information as well as a link of results from related work above the seafloor (e.g. water column investigations) to subsurface features. Maps are produced with the help of General Mapping Tool by Wessel and Smith (Wessel and Smith, 1998).

For general surface information of the region, Simrad EM 120 recordings are used. An example is shown in Figure 2.1a. The acquisition system is a multibeam echosounder, which operates by sending out acoustic signals at around 12 kHz and recording energy returned from the seafloor. The data set is a collection from several cruises to the area and covers both target areas fully within at least 5 nm measured from the center. With the latest part - data from R/V SONNE cruise SO173-1 - integrated in 2005, a grid cell size of 25 m has been achieved at both localities.

At Mound Culebra, another data source has been used in parallel (Fig. 2.1b), collected with the Hydrosweep (Hydrographic multibeam sweeping survey echosounder, operating at 15.5 kHz) system during R/V METEOR cruise M54-1. This set of data, available since 2002, was hand-edited and gridded by the author using MB-System (copyright Caress and Chayes, 1993-2005) and reached an average horizontal resolution of 50 m. The central part is of excellent data quality, while it deteriorates visibly around the edges. Hydrosweep profiles at the Hongo area (126 lines above a slightly larger area than that of Culebra) have not been processed yet.

The two bathymetric data sets are used simultaneously, because both have certain important advantages with respect to the other. The primary drawback of the Hydrosweep map is the fact that the area of good coverage is strongly limited. Several features in the vicinity are not covered, which may be of relevance for a final interpretation, such as a group of small mounds northwest of Mound Culebra, or the change of slope steepness landwards (see Fig. 1.4). A minor disadvantage is the
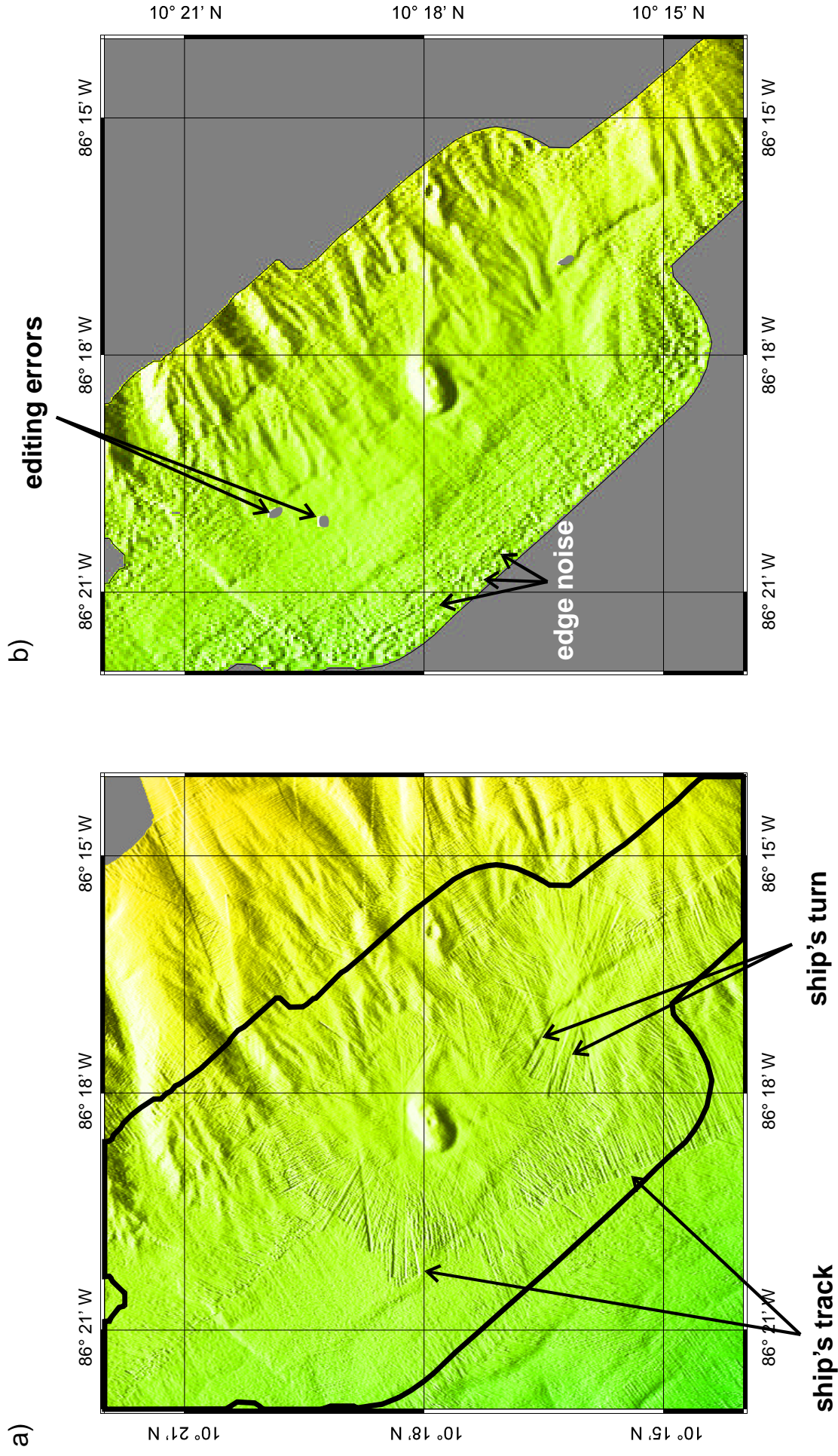
Figure 2.1 Two types of bathymetric data set above Mound Culebra. a) Data compiled from several cruises and acquisition systems (eg. Simrad EM 120). Erronous pings (thin lines about 1 nm long, where water depths differ systematically from that of the vicinity) are related for instance to changes in ship's course. Black line marks data extent of 2.1b. Color scale is the same as in Figure 1.1. b) Hydrosweep bathymetric data collected during cruise M54-1. Illumination and color scale as in 2.1a. Data quality visibly deteriorates towards the edges, especially in the SW. While the compilation (left) covers several additional relevant trench-parallel linear bathymetric features, topography in the image center is richer in details in the Hydrosweep map due to excellent data coverage.

existence of editing errors, which are due to the lack of experience of the author with the processing of such data. However, these are easy to identify and few in number, therefore they do not influence morphological observations. Neither of these problems is present in the Simrad data. On the other hand, the strength of Hydrosweep data is that 39 profiles were recorded above an area of about 7.5 x 13 km and within just two days. This yielded an unusually high data point density and provided an extensive crosschecking possibility, which improved accuracy significantly. Grid cell size was chosen such that even the edges show a satisfactory quality - the central area, where coverage was higher, could easily be gridded with a 15 m cell size. The short acquisition time of these data minimized variations arising from sea state, water velocity distribution, and weather changes, from instrument variation due to aging and to resetting of system parameters.

In contrast, the Simrad data set is a collection of several cruises, which had to be merged. None of these provided the focussed data quantity above the target areas as did Hydrosweep, but they covered a larger area with useful sampling density. Ship course changes, always an enhanced source of error, could not be simply deleted from the data, and are thus often visible as single cross-track lines with the width of a full beam (Fig. 2.1a). The same is true for entire track segments, possibly where the coverage of two cruises join with little overlap. Topography on the whole appears less pronounced in the compiled map, probably a result of smoothing and spatial filtering of the data.

In light of the above, it would be useful for further investigations near the Hongo mounds to process the Hydrosweep bathymetric profiles, as the unusually large amount of concentrated information is likely to give a bathymetric map of unprecedented detail in the area.

2.2 "Parasound" parametric sediment echosounder profiles

Echosounder data are widely used in marine sedimentological investigations (e.g. Damuth, 1980, Melles and Kuhn, 1993, Spiess, 1993). Parametric systems make use of wave interference to create a more focussed beam of energy and thus achieve higher lateral resolution (Spiess, 1993). In this case, a hull-mounted transducer sends

out acoustic signals vertically downwards at two frequencies, 18 kHz and 22 kHz, simultaneously. Non-linearity in wave interference produces useful pings of strongly focussed energy around the difference frequency of 4 kHz, with an aperture of the pilot wave (4°). Ping rate is controlled by the water depth (~ 2.1s for depths between 1000 - 2000 m). Reflections from the sea floor and shallow subsurface are picked up by the same transducer and signals between 2 - 6 kHz are transferred to a digital recording unit. A time window of 267 ms (~ 200 m), its delay after pings set manually by an operator, is saved on hard disk. Although the ship's movements (roll, pitch and yaw) are compensated for, the small aperture angle makes Parasound data sensitive to rugged sea floor topography as reflections from steep slopes will reach the receiver with greatly decreased energy or not at all. However, a footprint of approximately 7% of the water depth makes the equipment a powerful tool to study small-scale sediment characteristics.

Parasound profiles were acquired simultaneously to Hydrosweep bathymetric and seismic data at both target areas, and to a deep-towed seismic survey above Mound Culebra during the R/V SONNE cruise SO-173 (Fig. 2.2). Before interpretation, raw data were bandpass-filtered between 1.5 - 6.5 kHz to eliminate electronic noise picked up during recording. The envelope of the seismogram was then resampled from 40 kHz to 8 kHz, converted to standard SEG-Y format with SEGYDECO (courtesy of MTU, University of Bremen) and read into Kingdom Suite (copyright Seismic Micro-Technology, 1993-2003). An example profile is shown in Fig. 2.3. Several profiles were paper printed with SEDRUCK (courtesy of MTU, University of Bremen) after additional graphical and numerical S/N enhancement, which consisted of individual noise level calculation from the top of traces and subtracting the value from each trace, suppression of negative polarities, and a constant amplitude scaling. Thus, an image of the envelope function (with increased signal energy) was obtained, and supplemented interpretations.

Parasound data represent a number of challenges related to data acquisition (see Fig. 2.3). Steep slopes are hard to trace because of the low portion of vertically reflected energy that reaches the receiver. Instead, beyond 2° inclination, only backscatter energy is recorded. In consequence, care must be taken when interpreting reflection amplitude variations, especially where this correlates to seafloor morphology. It is our

Figure 2.2 Location of seismo-acoustic data set near Mound Culebra. Red lines: processed MCS profiles from M54-1. For easier orientation, the profile names are given. These include dip lines (from northwest to southeast) GeoB02-417, GeoB02-421, GeoB02-425, GeoB02-427, GeoB02-424, GeoB02-428, GeoB02-426, and GeoB02-417, as well as strike lines (from trench towards the coast) GeoB02-418, GeoB02-422, GeoB02-452, GeoB02-416, GeoB02-442, GeoB02-438, GeoB02-432, GeoB02-423, GeoB02-430, GeoB02-433, GeoB02-437, GeoB02-420, GeoB02-449, GeoB02-447, GeoB02-445 and GeoB02-429. Black lines: all other profiles along which echosounder and bathymetric data presented here were collected. Stippled line shows deep seismic profile BGR99-39.
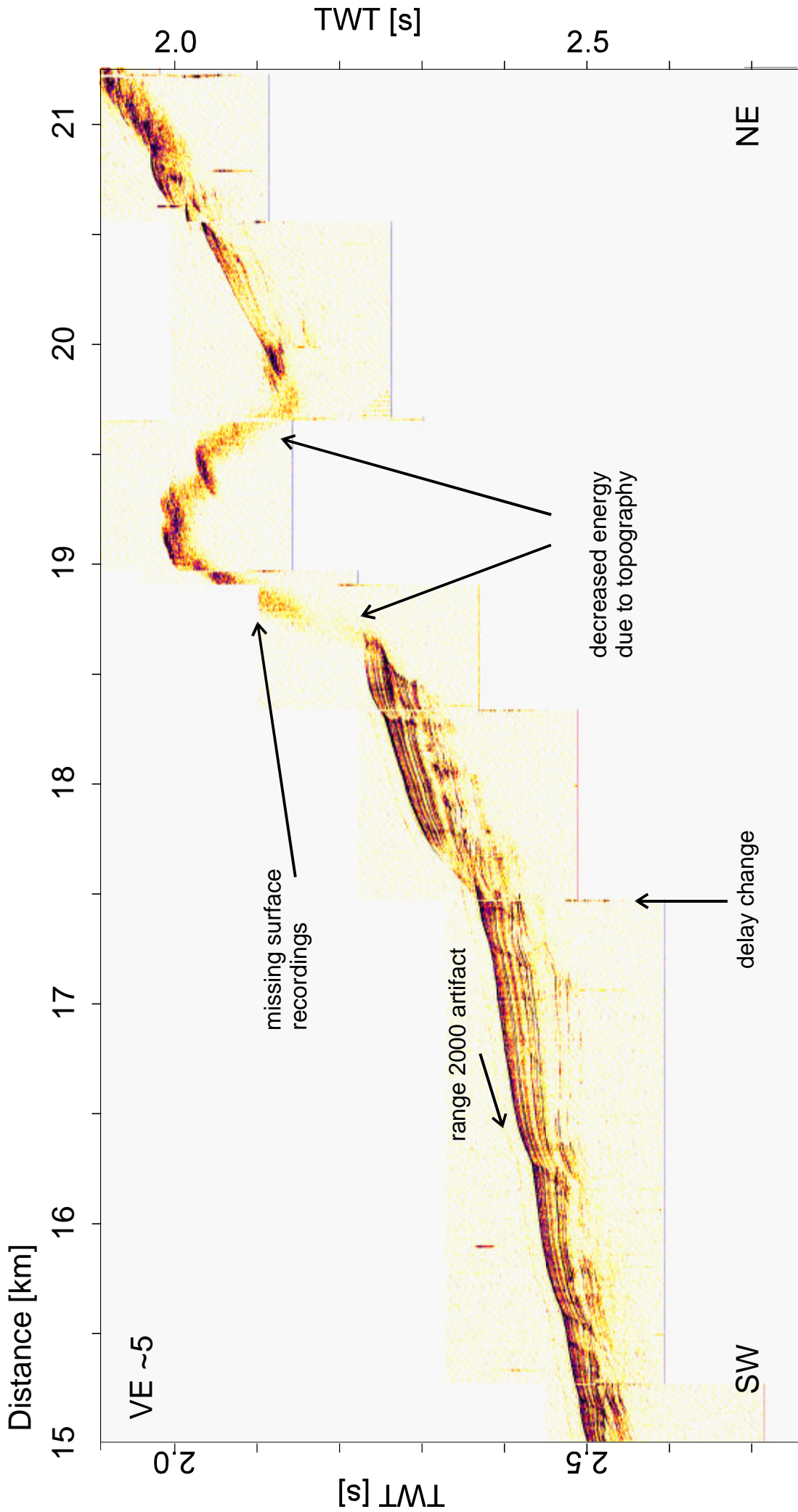
Figure 2.3 Example echosounder profile, showing typical challenges in the data. Steep topography such as mound flanks causes weak returns. Erroneous recording window results in parts of the vertical section missing. Delay change is written in the header last, causing the first echo with new delay to appear at the old depth. Finally, when measuring range is set to 2000 m, a weak echo precedes all arrivals 18 ms earlier.

experience however, that satisfactory signal return is observed somewhat beyond the theoretical limit of 2° slope.

Since the recording window is set manually at all time during data acquisition, the operator's lack of experience may result in the fact that the relevant time interval - i.e. that including seafloor and subsurface reflections - is not or only in part included in the recording, This becomes a major problem especially above mound features, where bathymetry may vary by a 100 m within a few minutes. Owing to hardware setup - the transducer being directed slightly forward, - the problem is asymmetrical and more pronounced downslope.

When the time delay is modified, actual data recording time is changed first, which then is registered in the trace header. This results in some cases in erroneous header values, that traces are plotted at the wrong depth and create vertical stripes in the image. However, for the usual number of delay changes, this does not significantly influence overall visual profile quality and was therefore not manually corrected.

At water depths slightly below 2000 m, an additional artifact is present, inherent in the acquisition system itself. Before every group of five emitted towards the seafloor, a longer 18 kHz signal is sent out 18 ms before the others to determine the water depth. Insufficient blanking creates a weak precursor of reflections and the seismogram is shifted in time. This is mostly visible only before the seafloor arrival and does not influence observations, however, at crossing profiles recorded with different range setting, seafloor at the intersection point has to be shifted manually. Such a mistie analysis often proves useful also between lines recorded by the same parameter settings.

Another noteworthy challenge is that of diffraction hyperbolae. Although the footprint is small, hyperbolae are present especially at bathymetric steps. Migration of the data is theoretically possible (Keil, 1995) but would require tedious static corrections on the order of centimeters. While this maybe feasible, invested computation time would outweigh the benefits for present investigations.

Parasound data are used in this study to bridge the gap between surface and subsurface information. An average line separation of 650 m in the margin-parallel direction provides reasonably high lateral resolution. With a wavelength of 37.5 cm, an actual vertical resolution on the decimeter scale is achieved. Penetration seldom exceeds 70 ms (50 m) throughout the target areas, mostly due to their morphology and

sedimentary properties. Side echoes are eliminated by the directivity of useful energy and receiver setup. Last, but not least, Parasound is an optimally quick tool to look at sedimentary processes in detail because of the low processing effort needed.

2.3 Multichannel seismic profiles

The main bulk of this study is based on high-resolution MCS (multichannel seismic) data. Its characteristics, preprocessing and processing sequence, and related challenges are therefore described here at some length. Of the large number of profiles collected, a smaller set of overview profiles were selected for processing. These consist of 24 lines at Mound Culebra and 16 profiles in the Hongo area, and are shown in Figures 2.2 and 2.4, respectively.

Data acquisition

One larger and two smaller GI guns were used as seismic sources, with volumes of 4.1 L and 1.7 L, respectively, operating with an air pressure of 150 bar. With the former in the middle, these sources were towed some 20 m behind the vessel and shot alternatingly at a shot rate of 10 s, equivalent of an approximate shot distance of 25 m at our average speeds of 5 kn. Lateral gun separation was maintained at approximately 20 m with the help of shear boards, metal boards mounted above the side guns in order to provide a constant outward pull away from the ship's track. A gun identifier signal - positive and negative spikes for starboard- and portside guns and none for the big one, Figure 2.5 - was recorded on channel 23 to enable a subsequent separation of individual sources, adding the possibility to triple the number of acquired profiles and allow for 3D processing. Around Mound Culebra however, only the largest GI gun was used, to maximize energy and penetration depth. Working deck settings are shown in Figure 2.6.

The seismic signal was received by a 96-channel surface streamer of 600 m active length, with two sets of 48 hydrophone groups at group separations of 12.5 m. The small "groups" consist of 2 or 3 hydrophones and are designed to fit very-high-resolution investigations in shallow water or high-frequency recordings from a watergun source, while the large groups, used in this study, contain 13 hydrophones
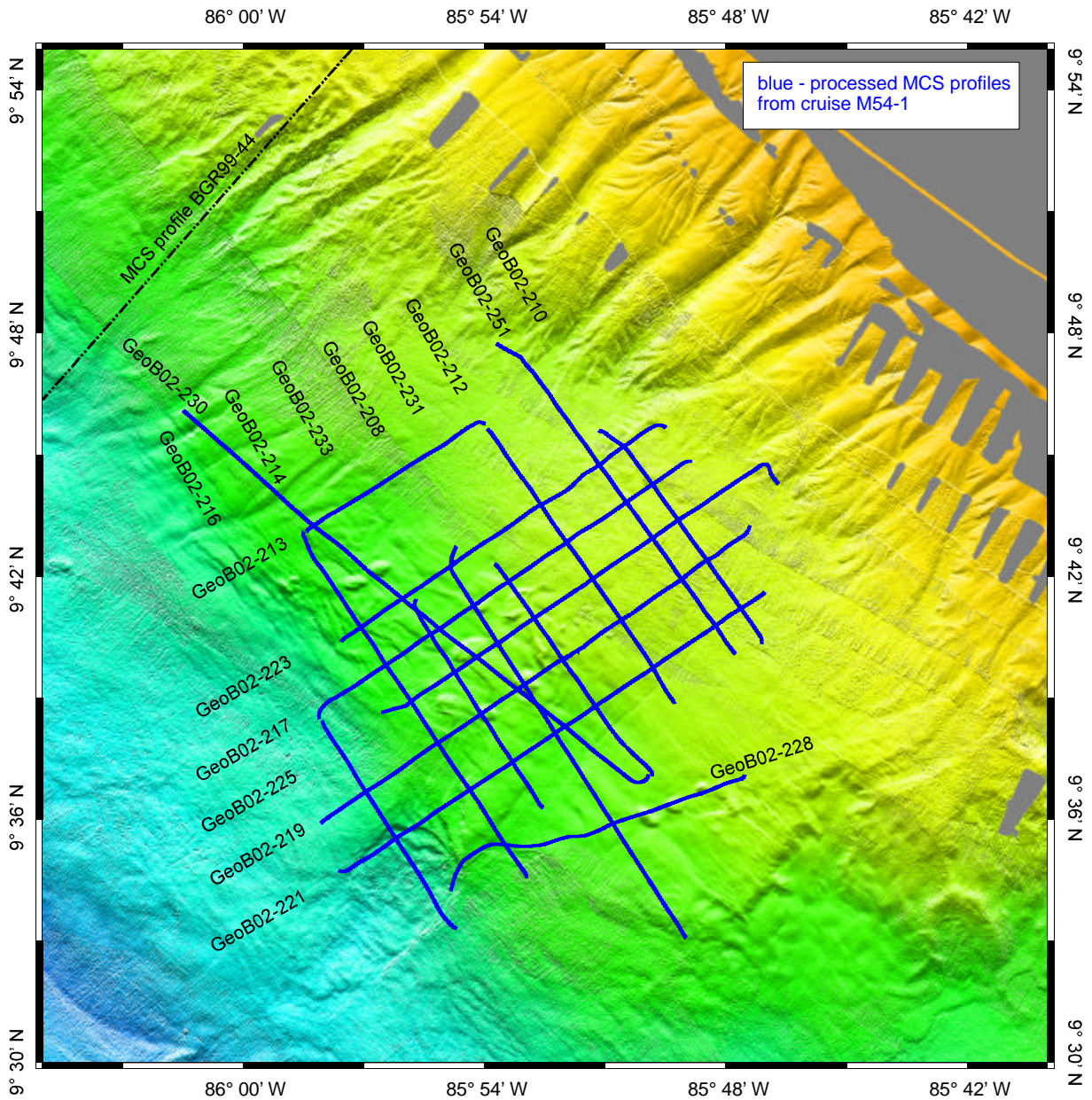
Figure 2.4 Location of seismo-acoustic data set in the Hongo area. Blue lines: processed MCS profiles from M54-1. For easier orientation, the profile names are given. These include dip lines (from northwest to southeast) GeoB02-213, GeoB02-223, GeoB02-217, GeoB02-225, GeoB02-219, GeoB02-221, and GeoB02-228, as well as strike lines (from trench towards the coast) GeoB02-216, GeoB02-214, GeoB02-233, GeoB02-208, GeoB02-231, GeoB02-212, GeoB02-251, and GeoB02-210, and the oblique GeoB02-230. Stippled line shows deep seismic profile BGR99-44.

shots with   shots with
portside gun   middle gun

0.35 sec

delay change at ffid 806
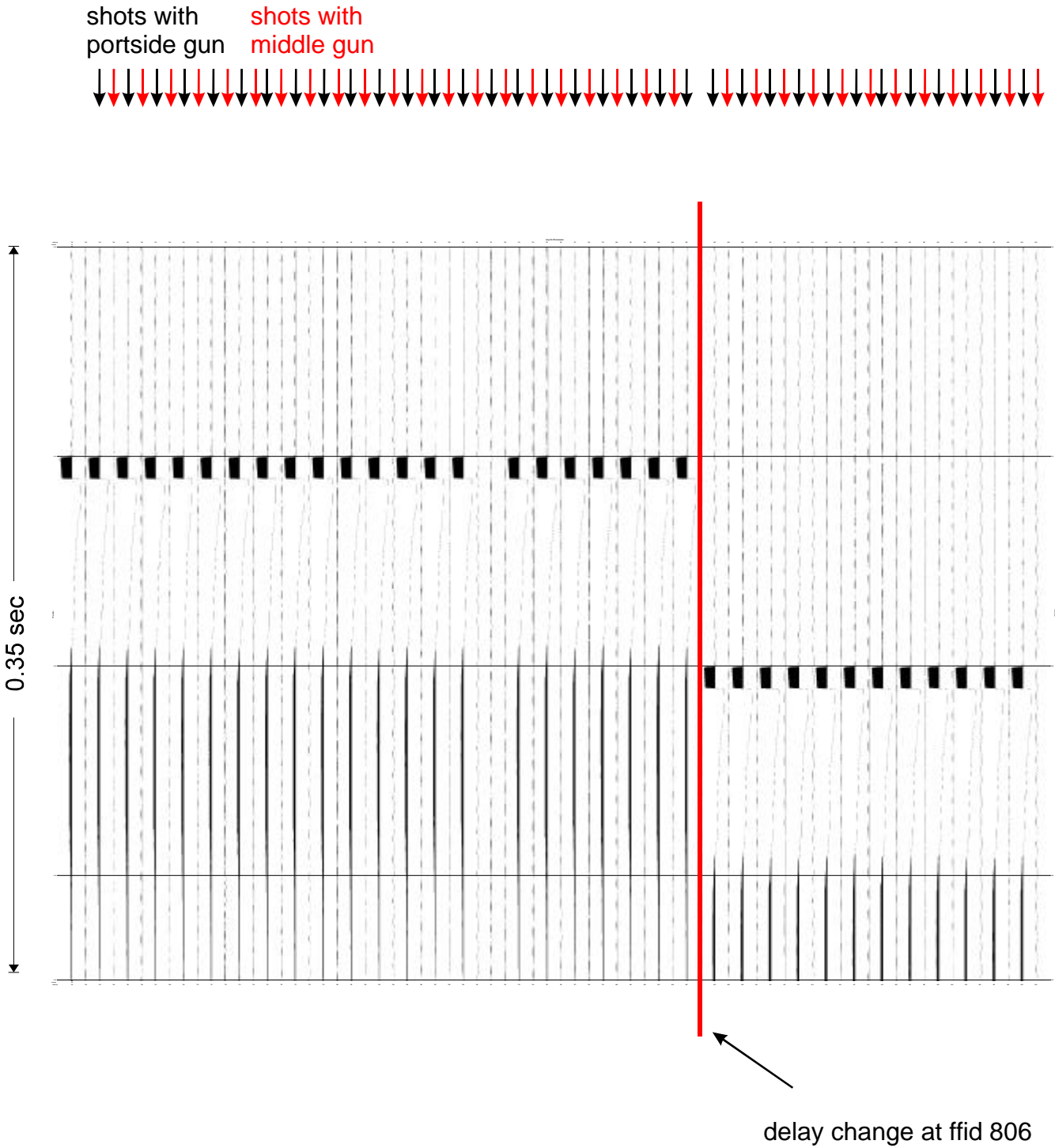
Figure 2.5 The alternating use of several sources requires the recording of a gun identifier, to enable subsequent splitting of data according to individual sources. Negative spike marks a shot with the portside gun (red arrows), empty trace marks a shot with the middle gun. Source identifiers are also useful in the exact location of recording delay changes within the profile.
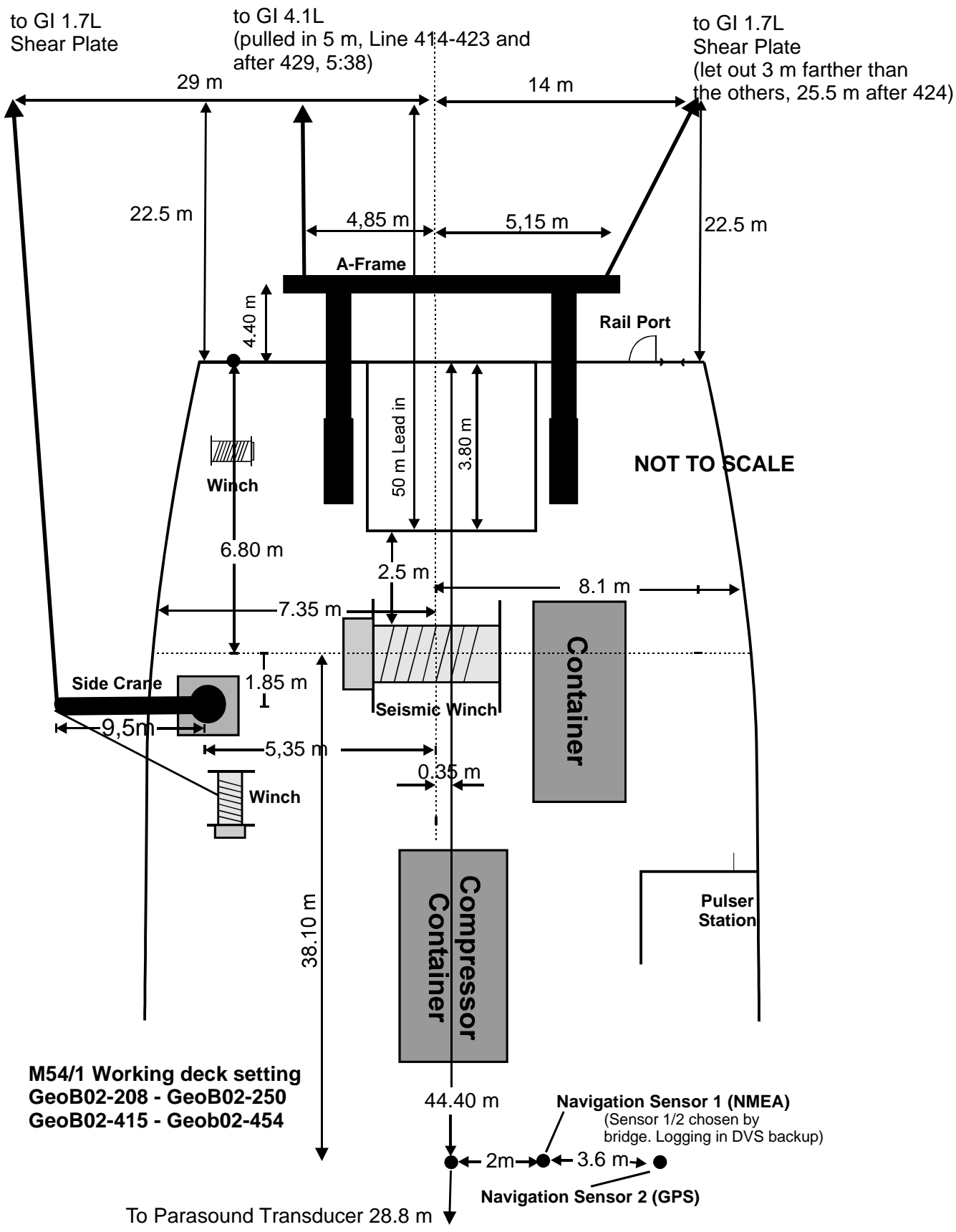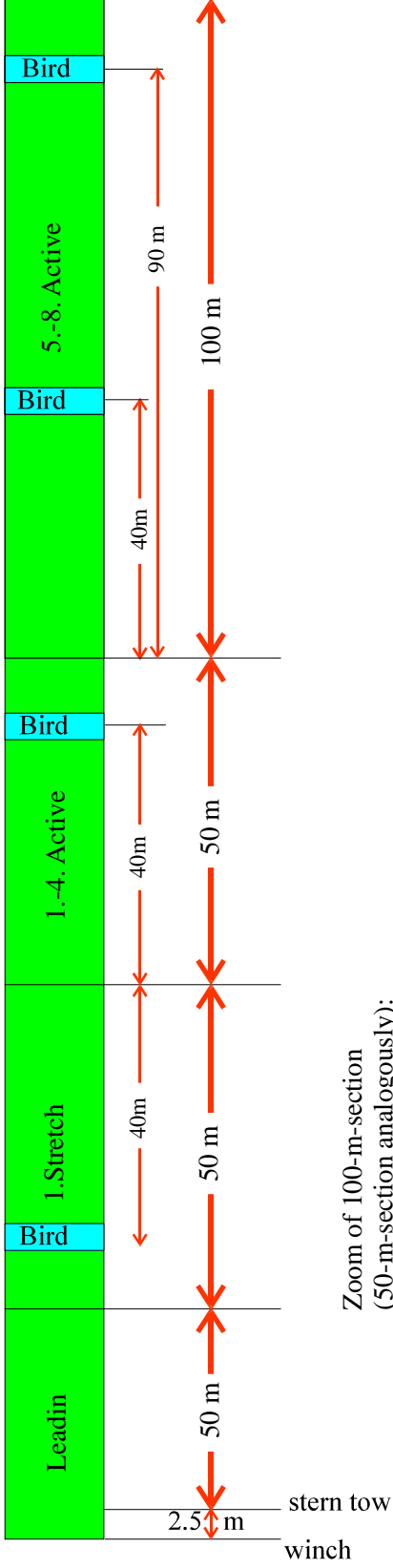
to GI 1.7L
Shear Plate

to GI 4.1L
(pulled in 5 m, Line 414-423 and
after 429, 5:38)

to GI 1.7L
Shear Plate
(let out 3 m farther than
the others, 25.5 m after 424)

29 m

14 m

22.5 m

4,85 m

5,15 m

22.5 m

A-Frame

4.40 m

Rail Port

50 m Lead in

3.80 m

NOT TO SCALE

6.80 m

2.5 m

8.1 m

7.35 m

Container

Side Crane

1.85 m

Seismic Winch

Winch

9,5m

5,35 m

0.35 m

Winch

38.10 m

**Compressor
Container**

**Pulser
Station**

**M54/1 Working deck setting
GeoB02-208 - GeoB02-250
GeoB02-415 - Geob02-454**

44.40 m

Navigation Sensor 1 (NMEA)
(Sensor 1/2 chosen by
bridge. Logging in DVS backup)

2m

3.6 m

Navigation Sensor 2 (GPS)

To Parasound Transducer 28.8 m

Figure 2.6 Working deck setting. Top view of ship (moving downwards), with location of sources, receiver, and reference point of navigation, by Zuehlsdorff (pers. comm.).

M54/1 - streamer configuration

Profil GeoB02-208 bis GeoB02-250
Profil GeoB02-415 to GeoB02-423

Information:
1 stretch of 50 m with swapped plugs, 4 sections of 50 m, 4 sections of 100 m
1 adaptor between short and long sections
3 GI guns, 2 shear plates, see protocol / deck plan
short groups onto Bison 1, long groups onto Bison 2

Leadin — 1.Stretch — 1.-4. Active — 5.-8. Active — Bird

50 m — 40m — 50 m — 50 m — 40m — 50 m — 40m — 100 m — 90 m

2.5 m — stern tow — winch

Zoom of 100-m-section
(50-m-section analogously):

98,3 — 90,6 — 86,3 — 78,1 — 73,3 — 65,6 — 61,3 — 53,1 — 48,3 — 40,6 — 36,3 — 28,1 — 23,3 — 15,6 — 11,3 — 3,1
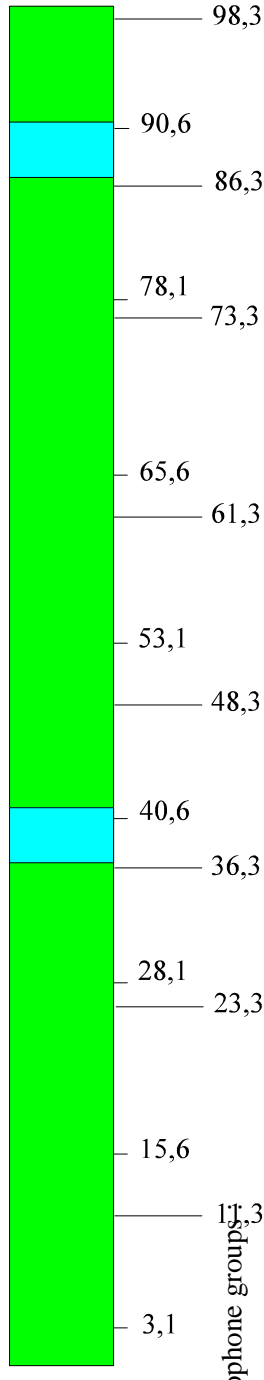
position of large hydrophone groups :

position of small hydrophone groups :

Bird	Position	Offset
MTC 3	Stretch	62.5
Digi 11	Active 1	142.5
-	Active 2	-
Digi 13	Active 3	242.5
MTC 4	Active 4	292.5
Digi 12	End of Active 5	393
MTC 6	End of Active 6	493
Digi 14	End of Active 7	593
Digi 15	End of Active 8	693

preferred streamer depth	3 m
depth of GI 4.1L	2 m
depth of both GI 0.4L	1.5 m

Figure 2.7 Schematic image of seismic streamer configuration, with location of hydrophone groups as well as "birds", by Zuehlsdorff (pers. comm.). Together with the working deck setting (Figure 2.6), they provide acquisition geometry necessary for processing.

each, and are devised to provide information of deeper targets (see streamer setup in Figure 2.7). Bird locations as well as source and receiver depths are also listed.

Streamer position was controlled and logged by eight "birds" of two types ("Digi" and "MTC"). These house a pressure sensor and a magnetic compass and measure heading and depth values of a given streamer segment every 10 s. Via the bird control units, it is also possible to change their preferred vertical position in the water by adjusting their wing angles, thus optimizing streamer attitude.

Data from the two sets of channels were recorded independently on two separate recording units (Bison 1 and 2), sampled at 4kHz, and written on DLT tapes. In order to economize with storage space, a water depth dependent delay was inserted between shots and the start time of recording, which varied between 0.5s and 4 s in steps of 500 ms. Positioning was achieved by DGPS technique.

Preprocessing

Preprocessing was done with the help of a handful of scripts and Fortran codes (called GeoApp), written / provided by the MTU UHB. Its purpose was to prepare data for standard seismic processing, primarily by calculating data geometry. Geometrical information relies greatly on an elaborate processing of bird data, so that hydrophone group locations are known accurately at the time of every shot. Birds used came from two manufacturers and the two types were handled separately. After an estimation of general profile direction, heading and depth data were cleaned of outliers, smoothed, and interpolated. Bird data were merged after visual quality control to serve as input for further calculations. A conversion from magnetic to geographic headings was carried out for the particular time of year and geographic location, with the necessary coefficients taken from the web site of National Geophysical Data Center. Headings and depths were then combined with shot times, relative gun and streamer positions, navigation data, and desired binning parameters, to calculate a full set of header values including absolute source and receiver positions, offset, source and receiver statics, cdp (common depth point) numbers and co-ordinates. Bin size was chosen 30 m with an along-track bin separation of 10 m. Traces were assigned to individual cdps. Beside the updated header file containing data geometry, several quality control

files were produced in the form of statistics to find any errors in this crucial part of data handling (see Appendix for examples).

Seismic data processing

Because of numerous challenges inherent in the data, processing sequence could only be automated to a low degree. This meant that the effort to bring individual lines to a satisfactory level did not decrease significantly throughout the processing phase. Therefore, a subset of the data was selected for investigations at each target area, such that a satisfactory overview of structures was attained. For Mound Culebra, 24 profiles between lengths of 10 - 25 km have been processed to a constant velocity time migration. Average line separation upslope remains below 1000 m and is around 500 m in the strike direction. The two longest sections (a dip and a strike line, both 35 km long) underwent subsequent velocity analysis (for their locations, see Fig. 2.2). Above the Hongo mounds, the same procedure up to a constant velocity migration was carried out on 16 profiles of similar lengths (Figure 2.4). A grid of lines about 2-3 km apart was obtained. No velocity analysis has been performed on these profiles.

Processing was carried out with Seismos[2]. After reading the data files from tape, the first step was to integrate calculated geometry in the trace headers. With the help of field protocols, traces then were expanded to their actual length with zero samples at the beginning - to compensate recording delay, - and at the end - to match trace lengths within the line (Fig. 2.8). At the same time, source and receiver static corrections were applied, with trigger error corrections where necessary.

Trigger jumps of 5, 10 and 15 ms in both directions were a common feature in the Culebra data (Fig. 2.9) and required a checking of each shot in receiver gathers (single channel data). Accurate locations of delay changes within the profiles were also identified this way. Two good-quality channels were then used to verify corrections before they were applied to the entire line. In parallel, shot gathers were examined to

---

[2] Processing of several lines was first performed at the University of Bremen, with the help of Vista Windows (tm Seismic Image Software Ltd., Calgary, CAN). These lines were also reprocessed with Seismos.
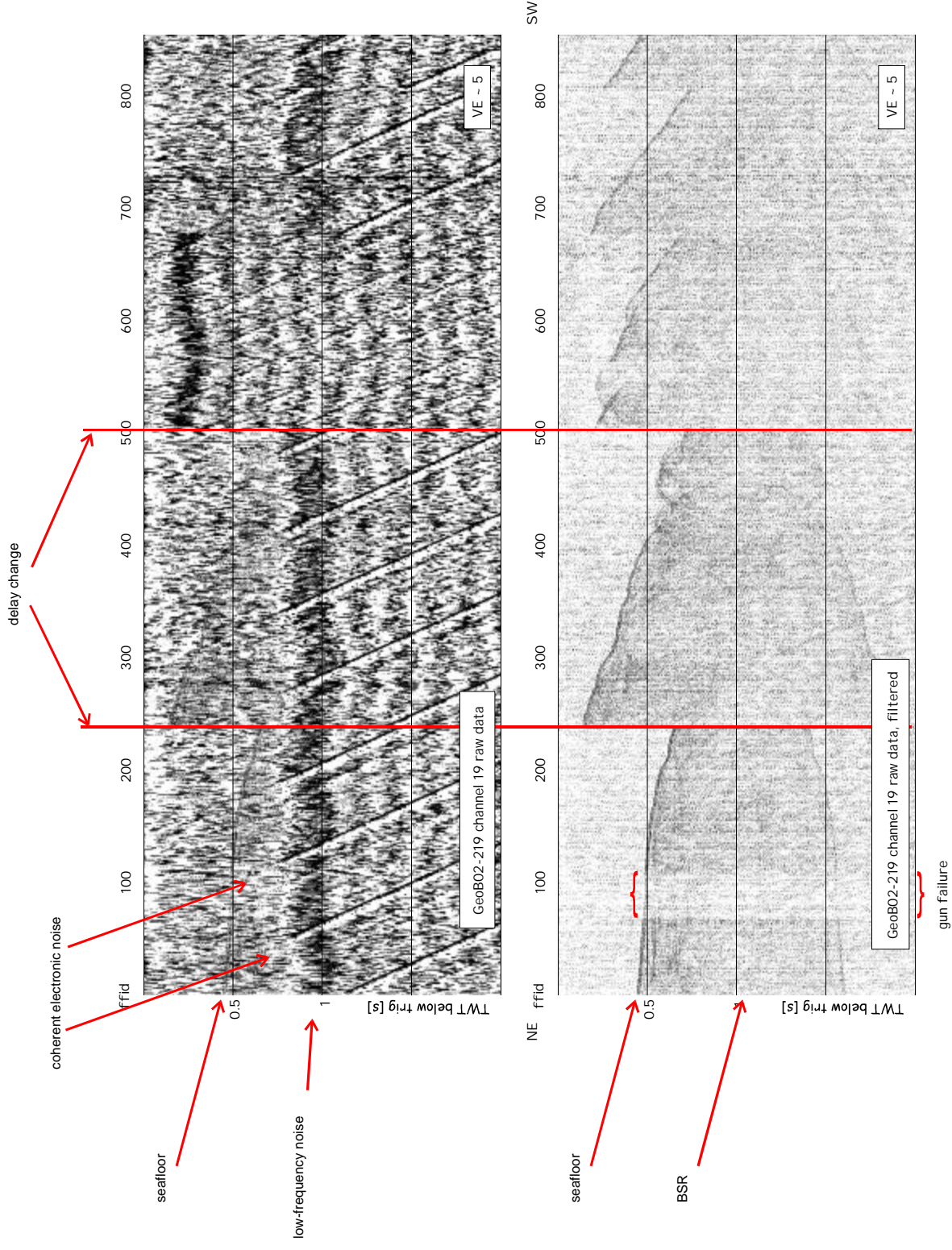
Figure 2.8 Example of seismic raw data from the Hongo mounds, single channel section with two guns shooting alternatingly. Top: unfiltered, bottom: filtered. ffid: shot number. Vertical red lines show locations where recording delay was changed. "Gun failure" marks interval where only the small source was functioning. Low-frequency and coherent dipping noise mask most subsurface reflections.
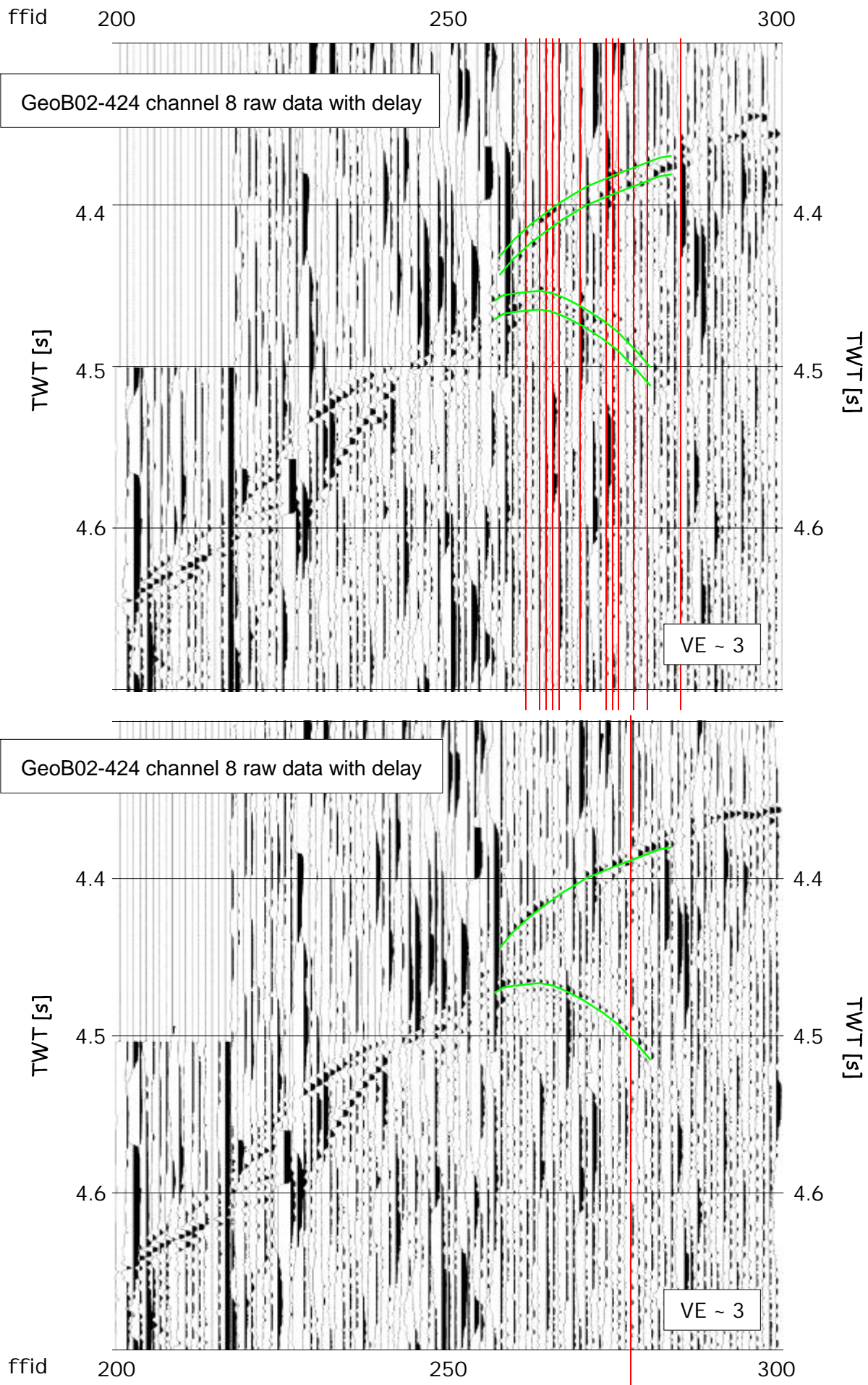
Figure 2.9 Trigger jumps in the raw data make it difficult to follow reflections (top, eg. green horizons). With appropriate time correction applied to individual shots (eg. for traces marked with red: +10 ms), arrivals line up (bottom image), revealing remaining erronous traces.
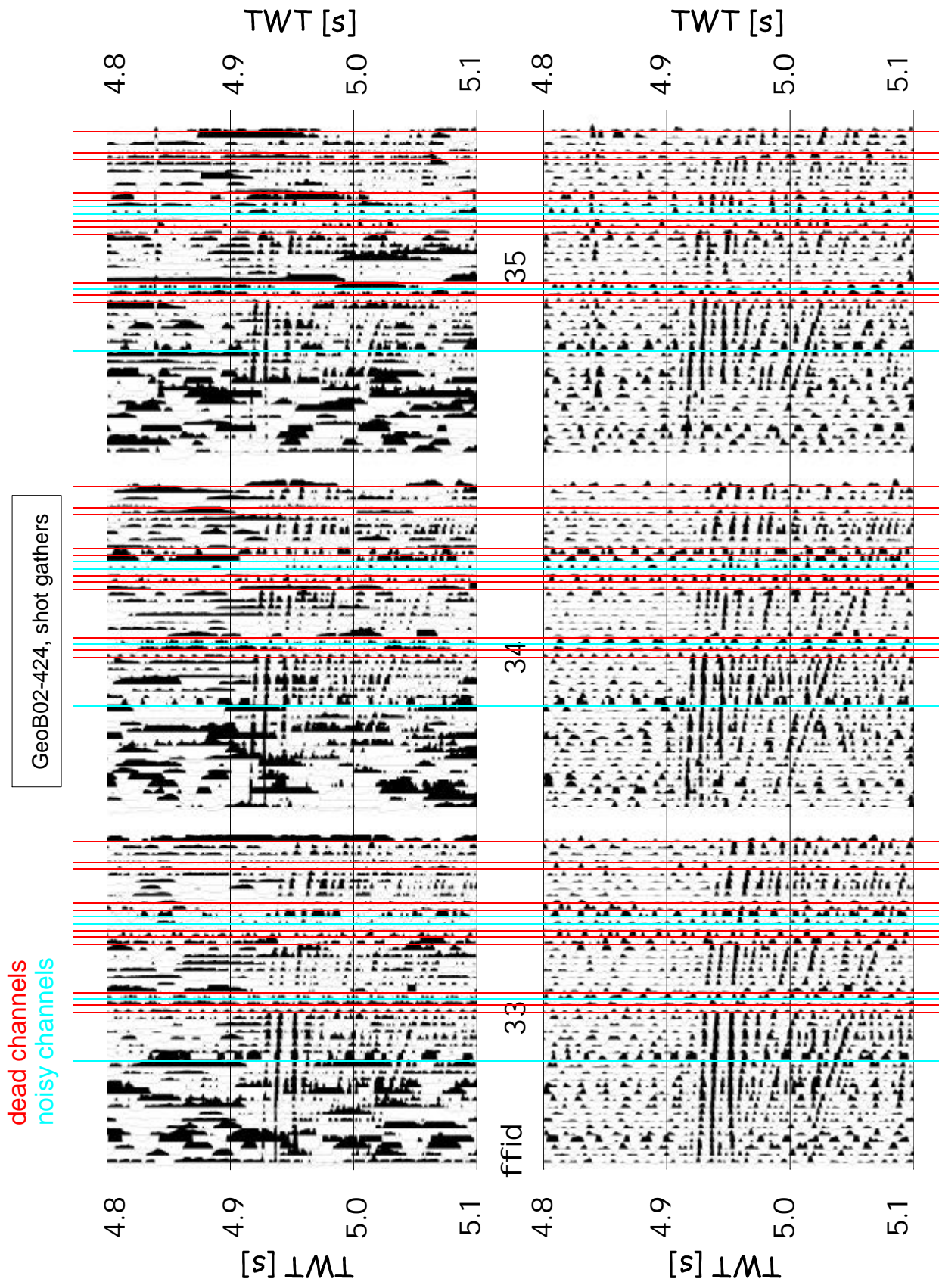
Figure 2.10 Channels which remain dead (red) or very noisy (blue) throughout the shots are eliminated before further processing in order to improve S/N ratio. Top: unfiltered data, bottom: filtered data.

select dead or very noisy channels (Fig 2.10). These appeared to remain fairly consistent in the Culebra profiles and were eliminated from further processing.

A different approach was adopted for the Hongo profiles. Most of these were acquired with two alternating sources of different size and position, which had to be separated first. Based on the information in the auxiliary channel and using reflection amplitudes as control, data were split into "small gun sections" and "big gun sections" with shot rates of 20 s each (Figure 2.11). Channel 23 was also helpful in locating delay changes accurately, a necessary supplement where this piece of information was masked by noise in receiver gathers. However, profiles with the smaller source proved to be of insufficient energy to image deeper than 100 - 200 ms and were of no use for this study by themselves. On the other hand, decreased coverage of cdps from only the larger gun also presented a serious challenge for imaging quality. Therefore, a compromise solution had to be found. A simple calculation can show that at a bin radius of 30 m, the two sources can be considered collocated with respect to arrival times (Figure 2.12). This allows the merging of data from the two sources before stacking, although signal forms from the first few channels may be affected.

Channel quality varied greatly throughout the Hongo sections, possibly as a result of slightly worse weather conditions and the resulting need of hardware maintenance of the sources. This made it necessary to split every profile into 48 single-channel lines and check the quality of each. As a side effect, this also served to easily detect trigger jumps occurring in the data. These were however scarce and of a uniform +5 ms.

Once time integrity of the profiles was restored, data needed to be cleaned of noise. Apart from dead channels and bad shots, noise occurred in the following forms: 1) randomly distributed high-amplitude spikes of possibly electronic origin. These were reduced by setting samples with amplitudes beyond a threshold to an interpolated value. 2) Bands of coherent noise crossing the sections at certain angles. To remove these, NMO-corrected shot gathers were examined for horizontal bands of anomalous amplitudes. Samples were then interpolated to the median value within the design window. 3) Low-frequency disturbances were suppressed by the application of a zero-phase Kaiser bandpass filter with corner frequencies of 30 - 35 - 250 - 300 Hz. Data at this point were resampled to 1 ms.
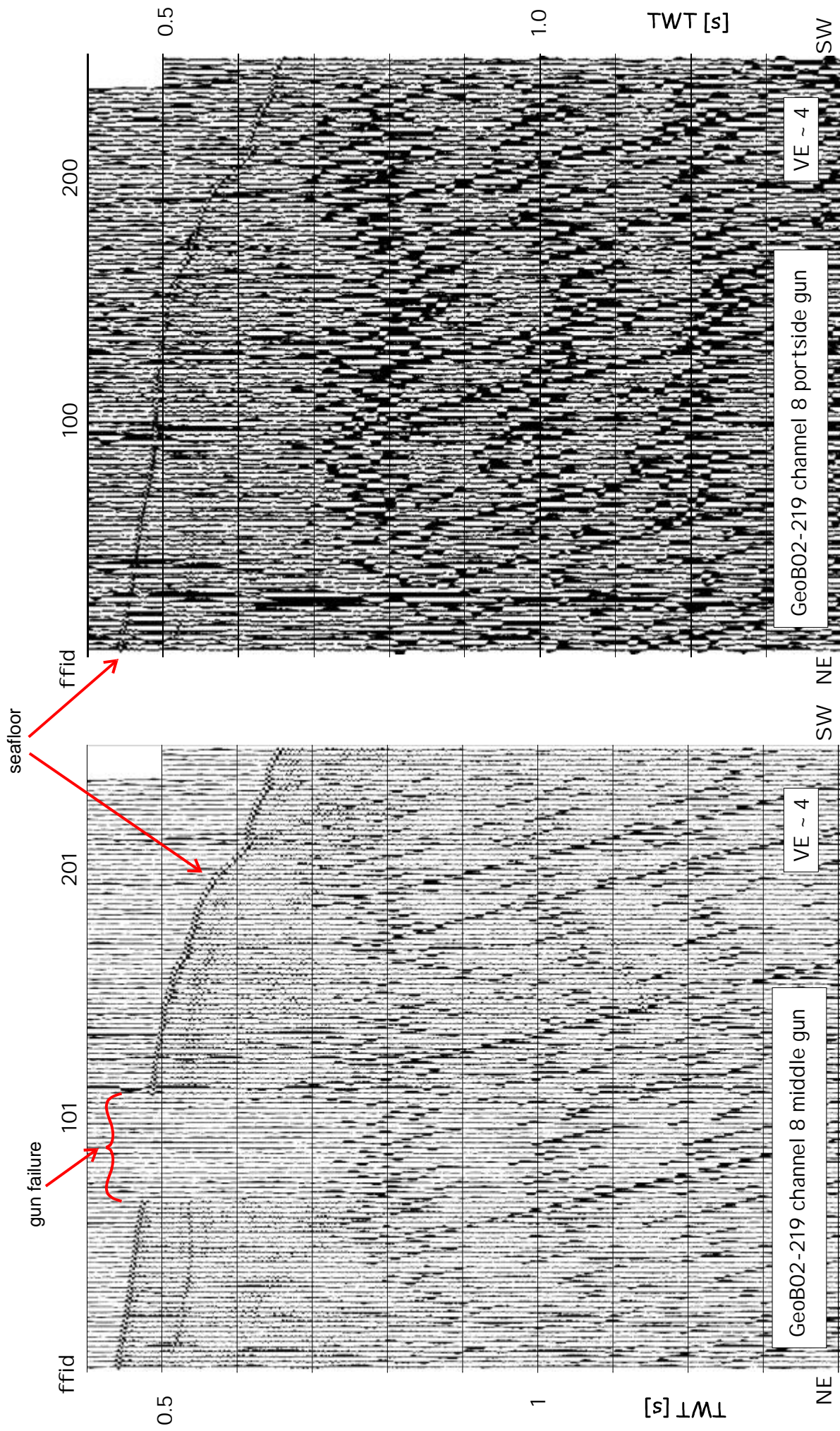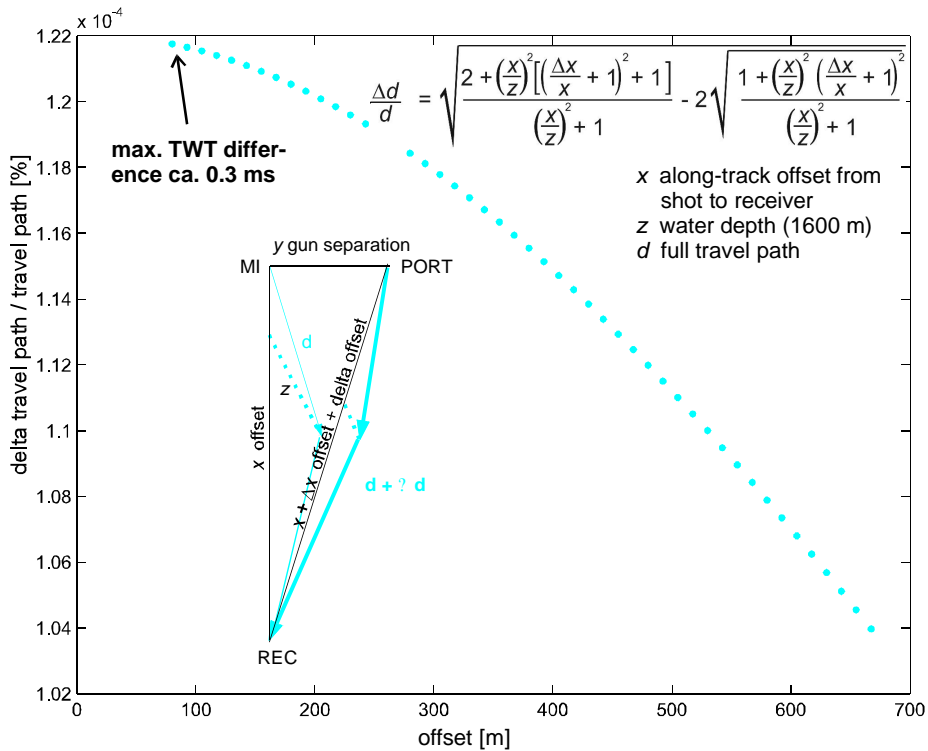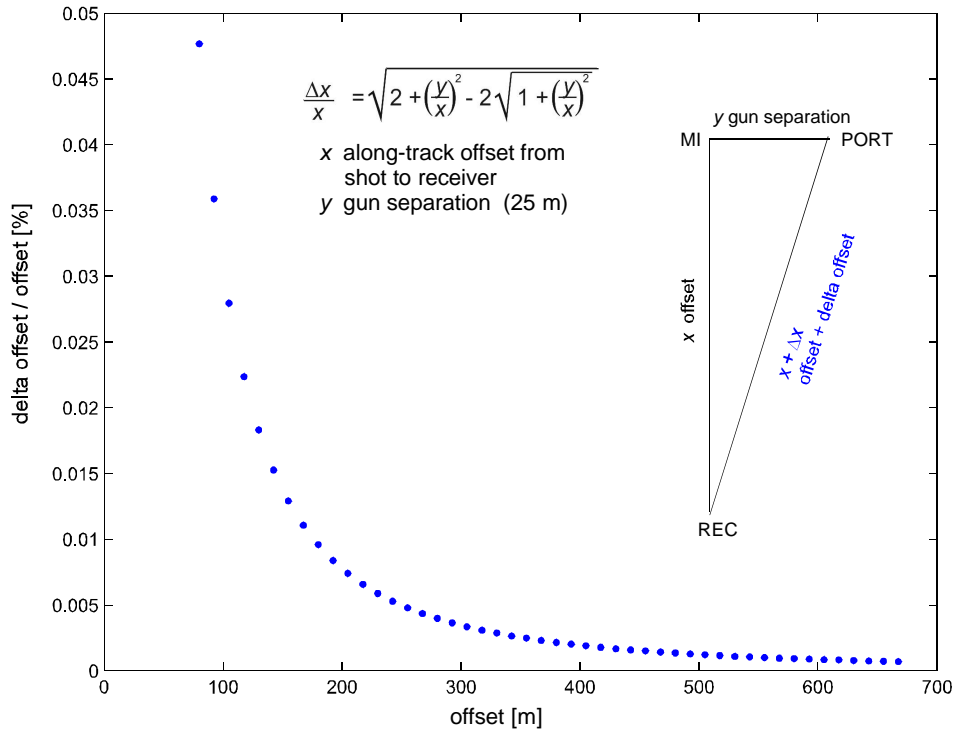
Figure 2.11 Data split according to source. Left: 4.1 L GI gun. Right: 0.4 L GI gun. Scaling is such that seafloor reflection looks similar. This reveals the much higher relative noise level in the port side section, that makes them suboptimal for separate processing. Note different amplitude scaling to make small signal visible.

Top figure equation:

$$\frac{\Delta x}{x} = \sqrt{2 + \left(\frac{y}{x}\right)^2 - 2\sqrt{1 + \left(\frac{y}{x}\right)^2}}$$

x along-track offset from shot to receiver
y gun separation (25 m)

Bottom figure equation:

$$\frac{\Delta d}{d} = \sqrt{\frac{2 + \left(\frac{x}{z}\right)^2\left[\left(\frac{\Delta x}{x} + 1\right)^2 + 1\right]}{\left(\frac{x}{z}\right)^2 + 1} - 2\sqrt{\frac{1 + \left(\frac{x}{z}\right)^2\left(\frac{\Delta x}{x} + 1\right)^2}{\left(\frac{x}{z}\right)^2 + 1}}}$$

x along-track offset from shot to receiver
z water depth (1600 m)
d full travel path

max. TWT difference ca. 0.3 ms

2.12 Travel time of reflections with two sources separated laterally. Top: relative horizontal offset difference. Bottom: relative travel time difference. With an acoustic velocity of 1500 m/s, the seafloor reflection using source MI (middle gun) arrives to the first receiver REC in a water depth of 1600 m about 0.3 ms before it does from the portside gun PORT, which is 25 m to the side. The effect decreases for larger channel offsets and water depths (as is the case at the Hongo area) and is thus negligible for our investigations.

Because of the relatively shallow signal penetration (ca. 700 ms sub-seafloor), a stacking velocity of 1500 m/s was deemed sufficiently accurate. Finally, missing cdps were padded (filled with zero traces) to retain correct geometry before a constant velocity Stolt fk migration. Interpretation was carried out with the help of the commercial Kingdom Suite software (copyright Seismic Micro-Technology, 1993-2003).

Quality and challenges of processing

As the above description shows, processing of these seismic data is far from perfect. Several methods may have helped further improve final image quality, such as deconvolution filters, manual noise editing, detailed velocity analysis, or prestack migration. A compromise was needed between processed data quality and quantity, in order to achieve a sufficient number of profiles to reach high spatial resolution. Some of the difficulties not described above include bird, shot time, and navigation errors, and missing data caused by buffer overflow. Guns occasionally failed (e.g. GeoB02-251), and shear boards were often overturned due to the bad sea conditions, causing an interruption of profiles or resetting of acquisition parameters. Permanently malfunctioning hydrophone channels decreased the theoretical coverage by 15-30%. Cdp locations can only be considered correct on the straight segment of profiles. Delay time step was found to differ from the theoretical value of 500 ms in several seismic lines (e.g. GeoB02-217, GeoB02-228, GeoB02-421, GeoB02-422). The large number of trigger jumps at Mount Culebra made it difficult to pick a correct absolute start time for traces, a predicament that was solved during the interpretation phase by the application of profile mistie shifts. Side arrivals are often present near abruptly varying topography, such as canyons, or the target mounds themselves.

However, numerous advantages can also be listed. For all profiles, the choice of bin radius of 30 m and separation of 10 m proved suitable for straight segments of seismic lines to bin more than 95% of all traces and achieve an initial coverage of 14-20 traces per cdp (see appendix for examples). As demonstrated earlier, it also allowed treating Hongo traces from sources with a lateral separation of less than twice the bin radius as one single profile. Because of the high signal frequency (50 - 150 Hz), shallow

sedimentary structures have been imaged on a 10 m scale, and sub-km profile separation warrants for high lateral resolution.

The data described above provide information of the upper few hundred meters of continental lower-middle slope. They do not image the entire sedimentary cover of the fore-arc, but in all cases penetrate as deep as the BSR and often to structures below. Through the morphology, continuity and relative amplitude of reflections, a description of local uplift/subsidence, of recent deformations, and of varying physical properties becomes possible. This in turn allows conclusions concerning fore-arc history, mound development, and dewatering patterns.

3

Structural observations in the vicinity of Mound Culebra mud dome, on the continental middle-slope of Pacific Costa Rica

(Fekete, Spiess, Reston)

3.1 Introduction

On the following pages, seismo-acoustic observations around Mound Culebra are described in detail. An extensive dataset of multibeam bathymetry, sediment echosounder and multichannel surface streamer seismic profiles is presented (see Fig. 2.2 in Chapter 2), in order to characterize the seafloor and the uppermost few hundred meters of middle-slope sediments underneath, with special attention to morphology, deposition patterns, styles of deformation, as well as recent and general tectonic behaviour. Qualitative analysis of acoustic facies (e.g. amplitude and continuity of layers, thickness variations etc.) provide insights to the origin, development, and internal structure of the area, and serve to broaden our understanding of the possible role of mud mounds in the fore-arc dewatering of Central America.

The northern Costa Rican fore-arc is dominantly formed by subduction erosion (Vannucchi et al., 2001). Oceanic material formed at the EPR is subducting steeply at a rate of 85 mm/a. A trench-parallel dextral displacement component of approximately 14 mm/a in earthquake slip indicates convergence partitioning (DeMets, 2001). The tectonic history of the margin displays periods of rapid subsidence at 6.5-5 Ma and 2.4 Ma ago (Vannucchi et al., 2003). The fore-arc wedge is established to consist of the relatively high-velocity ophiolitic material also exposed on land, covered by a sequence of slope sediments (Walther et al., 2000, Christeson et al., 1999). The boundary between the two is imaged as a regionally prominent seismic reflector often referred to as "rough surface". The narrow (< 10 km) frontal prism is largely thought to be made up of slumped slope sediment (von Huene et al., 2000, Morris et al., 2002). Recent deposition rates on the fore-arc are not well constrained (Kimura et al., 1997), ash stratigraphic investigations yield rates between 150-200 m/Ma (Kutterolf, pers. comm.). The anomalously low heat flow of the relevant portion of incoming plate is thought to be the cause for low and uniform values measured on the continental slope (Langseth and Silver, 1996). Local heat flow variations are strongly coupled to and often indicated by changes in the distribution of gas hydrates, which are widely present in the subsurface (Kimura et al., 1997). The influence of clathrates on pore space and other sediment properties affects the capability of material to ascend from depth. On the other hand, heat flow anomalies may mark locations of fluid escape from or inflow into the subsurface. Thus, both

heat flow and gas hydrates are intimately interrelated with the dewatering patterns of the fore-arc.

Data profiles presented in the following bear names of GeoB02-xxx, where the last three digits are a number between 415 and 455. The main dip lines are, from northwest to southeast, profiles GeoB02-425, GeoB02-427, GeoB02-424, GeoB02-428 and GeoB02-426, while the most relevant strike lines are, from trench towards the coast, GeoB02-418, GeoB02-416, GeoB02-430, and GeoB02-420. Profile locations are further specified in Figure 2.2.

3.2 Observations

Bathymetric dataset

The seafloor in the surroundings of Mound Culebra is topographically variable. Three regions can be distinguished in the area, oriented approximately along isobaths (Fig. 3.1). The first, landward-most region is divided by a large number of ridges and canyons up to a kilometer wide or more, with incised valleys between up to 200 m high canyon walls. In neighbouring territories offshore Nicaragua and northern Costa Rica, these tend to run normal to the trench (and parallel to one another), with smaller side gullies creating a fishbone pattern.

At the Mound Culebra segment of the margin, canyons and ridges are oriented in a fan-like way, converging and shallowing downslope, and seem to end at around 1700 m of water depth, at the edge of a locally flattened elliptical area of approximately 5 by 25 km. Here the continental slope, elsewhere characterized by an average slope angle of 4°-7° (cf. Shipley et al., 1992, Vannucchi et al., 2001), is almost entirely horizontal, with slopes less than about 2°. This basin makes up the second region. The ridges disappear at its rim, losing their topographic amplitude gradually without apparent abrupt steps (Fig. 3.2).

The third region is defined where a small number of the canyons seem to re-appear on the trenchward side of the basin. The continental slope regains its steepness here, and the seafloor is crossed by several trench-parallel topographic steps. These reach up to 50 m in height but can rarely be traced for more than 5 km laterally. They are parallel to one another (Fig. 3.3) and are oriented at an angle of 15° clockwise to the local

direction of the trench (which is WNW- ESE, azimuth 318°). The three regions are best visible in slope gradient maps (Fig. 3.4).

Naturally, the above-defined boundaries are somewhat arbitrary. Topographic steps do cross the flat area and are perhaps also present on the landward side of it. The apparent termination of canyons and ridges varies in water depth from northwest to southeast. One of the most prominent steps, preliminarily named "Culebra Fault", is located southeast of Mound Culebra and heads in its exact direction. It is laterally offset as it intersects a canyon and disappears entirely further to the northwest. A minor subset of steps is oriented normal to the trench, with the most prominent example 3 km northwest of the mound.

Mound Culebra is located towards the southeastern edge of the basin. From its base at about 1630 m water depth to the deepest part of the depression, roughly 12 km NW, there is a depth difference of almost 200 m. In ocean floor video observations, the mound displays a double summit, and appears elongated downslope rather than circular in shape (Weinrebe and Flueh, 2002). Its landward end connects through a small, crescent-shaped saddle to the trenchward end of a ridge.

A cluster of smaller mounds is found northwest of Culebra, near the deepest part of the basin. It consists of five circular 200-500 m diameter hills that rise less than 100 m high above the seafloor at 2000 m depth. Another circular topographic feature, named Culebrita, is situated about 5 km east of Mound Culebra, appearing crater-like with a central depression on its top. None of the mounds apart from Culebra has yet been surveyed for venting (Fig. 3.1).

Observations in the Parasound profiles

The following acoustic facies types are observed in the shallow sediment (Fig. 3.5): a) a closely-spaced succession of sharp reflectors, occurring on the order of 5-10 ms TWT (two-way travel time) one below another, b) transparent intervals of variable (5-50 ms TWT) thickness, c) indistinct but continuous prolonged seafloor echo without sub-bottom reflections, d) indistinct regular single hyperbolic bottom returns with conformable sub-bottom reflections and e) indistinct regular single hyperbolic bottom returns with no sub-bottom echoes (acoustic facies definitions modified after Damuth
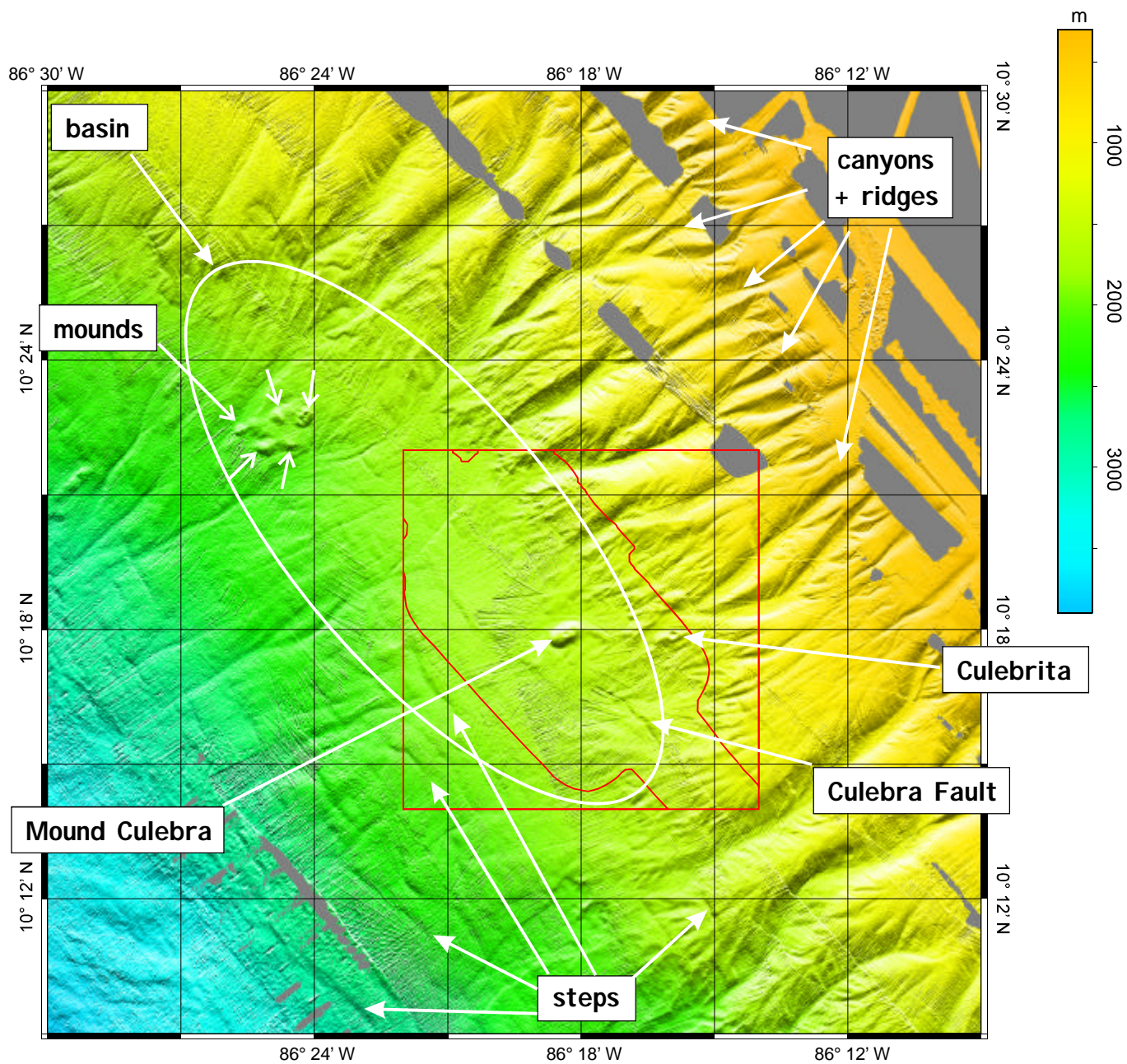
Figure 3.1 Bathymetric database of Mound Culebra and vicinity, showing morphological segmentation. The northeast is controlled by a canyon system. It is separated by a a flat middle region ("basin") from the trenchward part, which is crossed by several seafloor steps. Characteristic topographical objects are marked. Extent of figure 3.2 outlined in red.
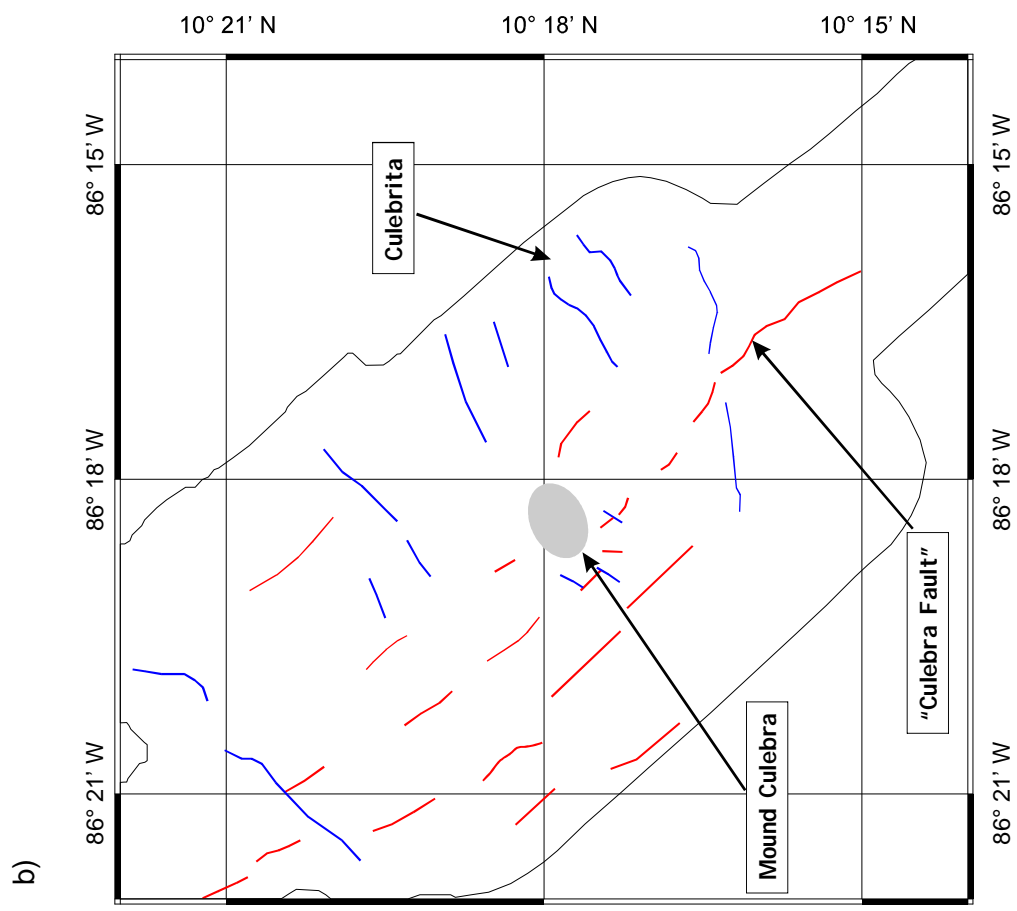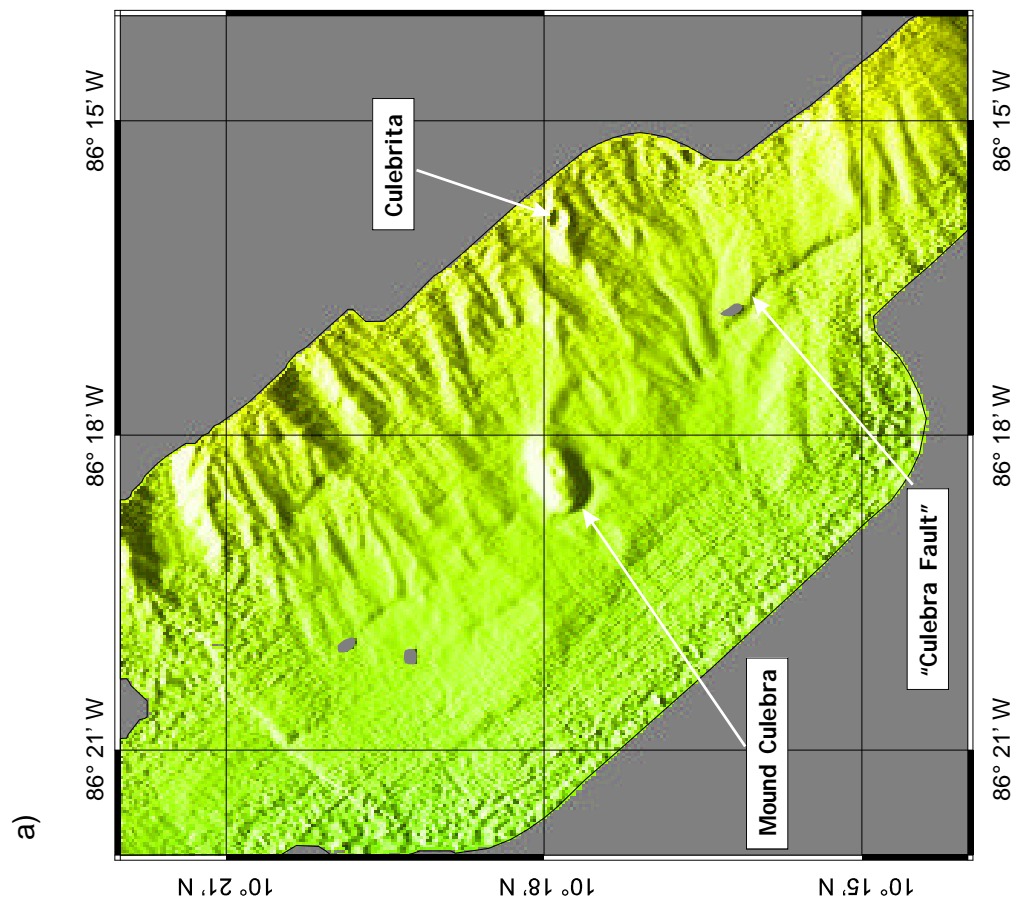
Figure 3.2 Hydrosweep bathymetry collected during R/V METEOR cruise M54-1 (extent shown in Fig. 3.1). Grey - no data. Note significant depth variations in the center and increasing noise towards the edges. Colour scale as in 3.1. b) close-up of line drawing in Fig. 3.3.
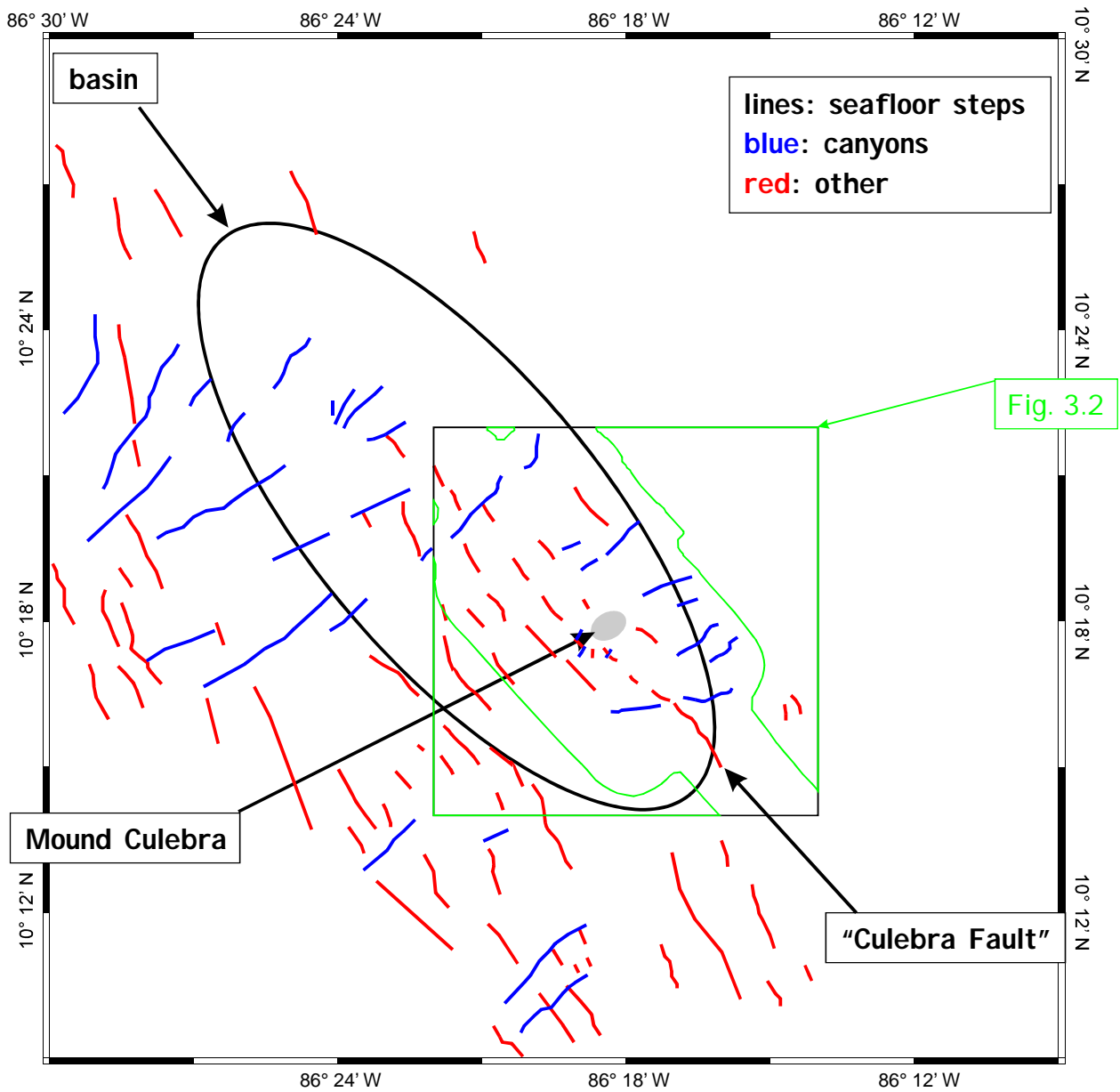
Figure 3.3 Line drawing of bathymetric steps, based on both bathymetric data sets and derived slope maps.
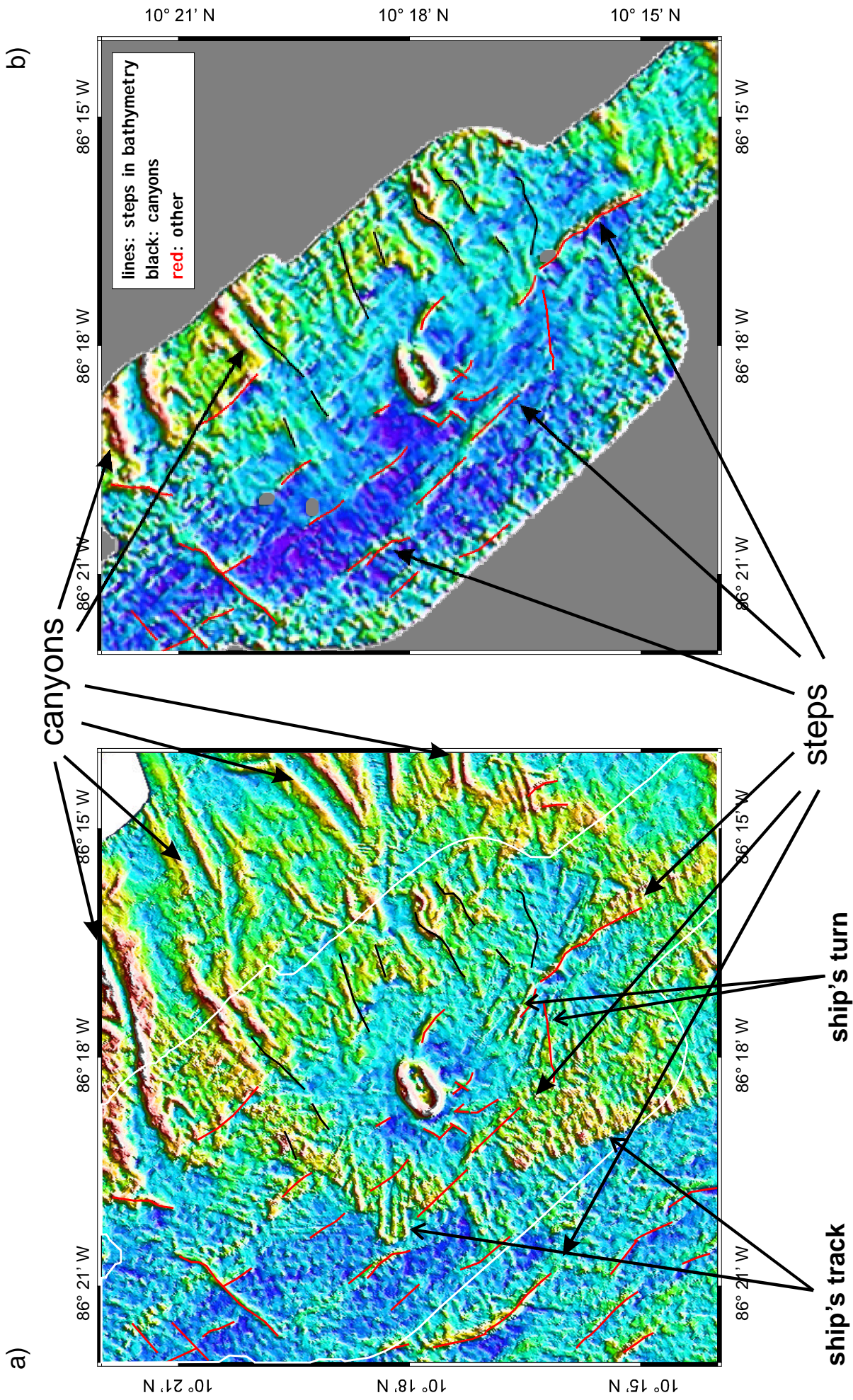
Figure 3.4 Maps of slope gradient: a) - calculated from the general database, b) - derived from Hydrosweep data. Purple and dark blue colours mark flat areas, yellow to red delineates abrupt changes. Topographic steps and canyon walls, as well as artifacts in the data, appear in bright colours (marked).

and Hayes, 1977, and Spiess, 1993). In the study area, type a) and b) often occur together, with typical package thicknesses significantly variable but on average decreasing away from the shelf edge in every dip line. Differences along trench are also present, however, less significant. Furthermore, layers exhibit both lateral and vertical variations of continuity and reflection strength. Type c) is primarily characteristic of Mound Culebra itself, while type d) is more typical in its close vicinity and e) further landwards. Because of the above-described distribution of acoustic facies, and Parasound's focussed signal energy and resulting incapability to image reflectors steeper than a few degrees (see Chapter 2 for further details), reflector tracing and investigation of their properties are mostly limited to the region around and trenchward of the mound.

Three characteristic horizons were traced in order to visualize changes in sediment thickness and horizon continuity. An example profile illustrates the features described below (Fig. 3.6). In the dip lines, all three show a series of typical, asymmetrical, wedge-shaped sediment bodies below seafloor trenchward of Mound Culebra, with a landward steeper and a trenchward less steep side of individual segments. Thickness decrease trenchward within the segments may reach 50% or more. Segment ends correlate with trench-parallel linear surface features described in the bathymetry section, but their orientation is difficult to determine even with sub-kilometer profile spacing. Horizons are vertically offset trenchward down at segment ends. The amount of relative offset in depth appears to change with distance from trench: in the example figure, all three reflectors deepen by about the same amount in TWT approximately west of the intersection point with profile GeoB02-418 (offset 3 km), while eastward of this, vertical offset increases with depth. At one location (offset 4.5 km), vertically offset reflectors curve upwards.

In strike lines, no similar pattern is observed, but a slight overall thinning of layers northwestward characterizes the region (Fig. 3.7), as far as a locality further northwest, where ~ 25% thickening of strata associated with a bathymetric step appears on several parallel profiles (Fig. 3.8) Exception from this observation is a small area west of Mound Culebra, which appears anomalously deepened.

Reflection amplitudes in Parasound data change with the steepness of seafloor. Therefore, only those amplitude variations are noted, which occur relatively abruptly (within a few hundred meters) and do not correspond to significant slope angle changes.

In several strike lines, locations of abrupt amplitude decrease occur either independently or associated with some of the downward steps of ocean floor (Fig. 3.8). They exhibit a shape and extent that makes them unlikely to be data artifacts. The anomalies have a narrow top close to the surface, get broader with increasing sub-bottom depth, and seem to continue beyond the penetration of echosounder data.

Parasound profiles reveal little about Mound Culebra itself. Its flanks are too steep to image. The relatively flat top is characterized mostly by densely spaced diffraction hyperbolae, and beneath that, no visible internal structures are shown (Fig. 3.8).

Multichannel streamer imaging

Seismic facies in MCS images of the target area can be divided into two regions vertically, showing distinctly different seismic properties. In an average penetration of 800 ms TWT, the upper 250 - 300 ms below the ocean floor appear relatively well-layered with subparallel bedding. Reflection polarity here is mostly positive, although a few cases of short intervals of polarity reversal are observed. Underneath, a mostly transparent seismic facies is seen, containing short segments of tilted reflectors of variable polarity. The only regionally prominent arrival in the lower part of profiles is a sharp, negative-polarity reflector at around 500-600 ms TWT below seafloor. Although it is characterized by moderate topography, significant amplitude variations, and several locations of disruption, it generally mimics the shape of ocean floor and is therefore termed bottom simulating reflector (BSR). The short reflector segments typical of this depth are still present 100-200 ms below the BSR, indicating a definite signal penetration to greater depths, and the fact that BSR amplitude variations are unlikely to be a result of insufficient imaging quality.

Marker horizons were selected both based on traceability, which favoured shallower reflections, and with the aim to achieve an even distribution of markers in depth (Fig. 3.9). Layer thickness variations are similar to those observed in the echosounder data:
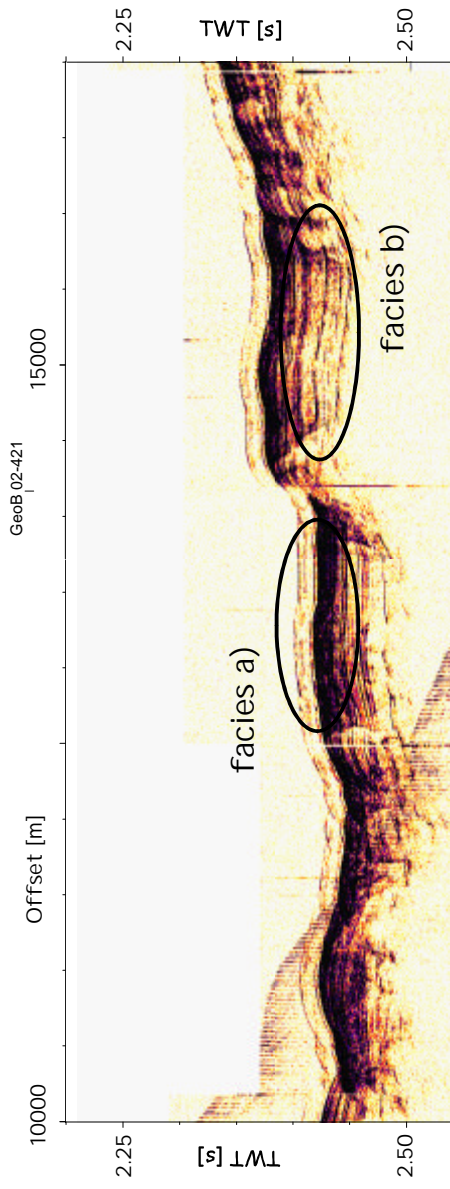
Figure 3.5 Typical acoustic facies seen in the Parasound images (VE ~ 10). a) closely-spaced succession of sharp reflectors, b) transparent intervals of variable thickness, c) indistinct but continuous prolonged seafloor echo without sub-bottom reflections, d) indistinct regular single hyberbolic bottom returns with conformable sub-bottom reflections and e) indistinct regular single hyperbolic bottom returns with no sub-bottom echoes.
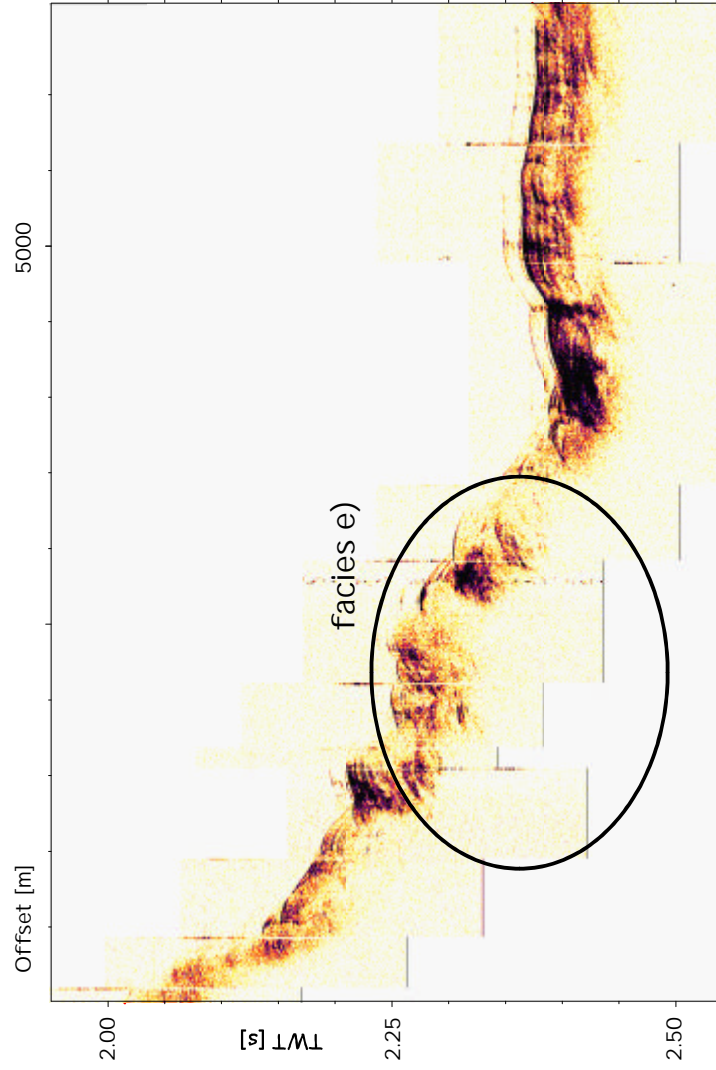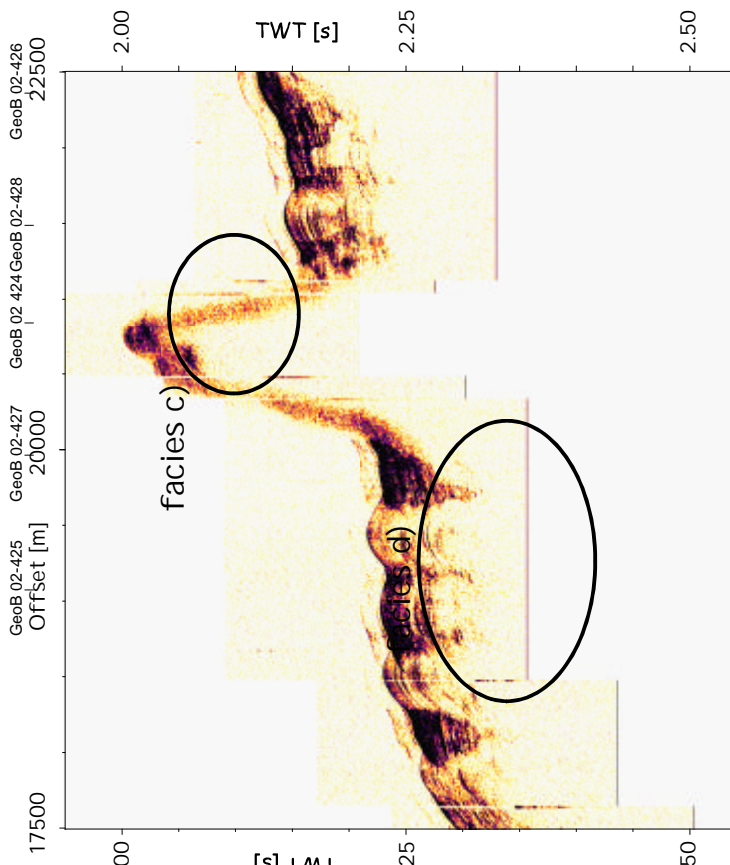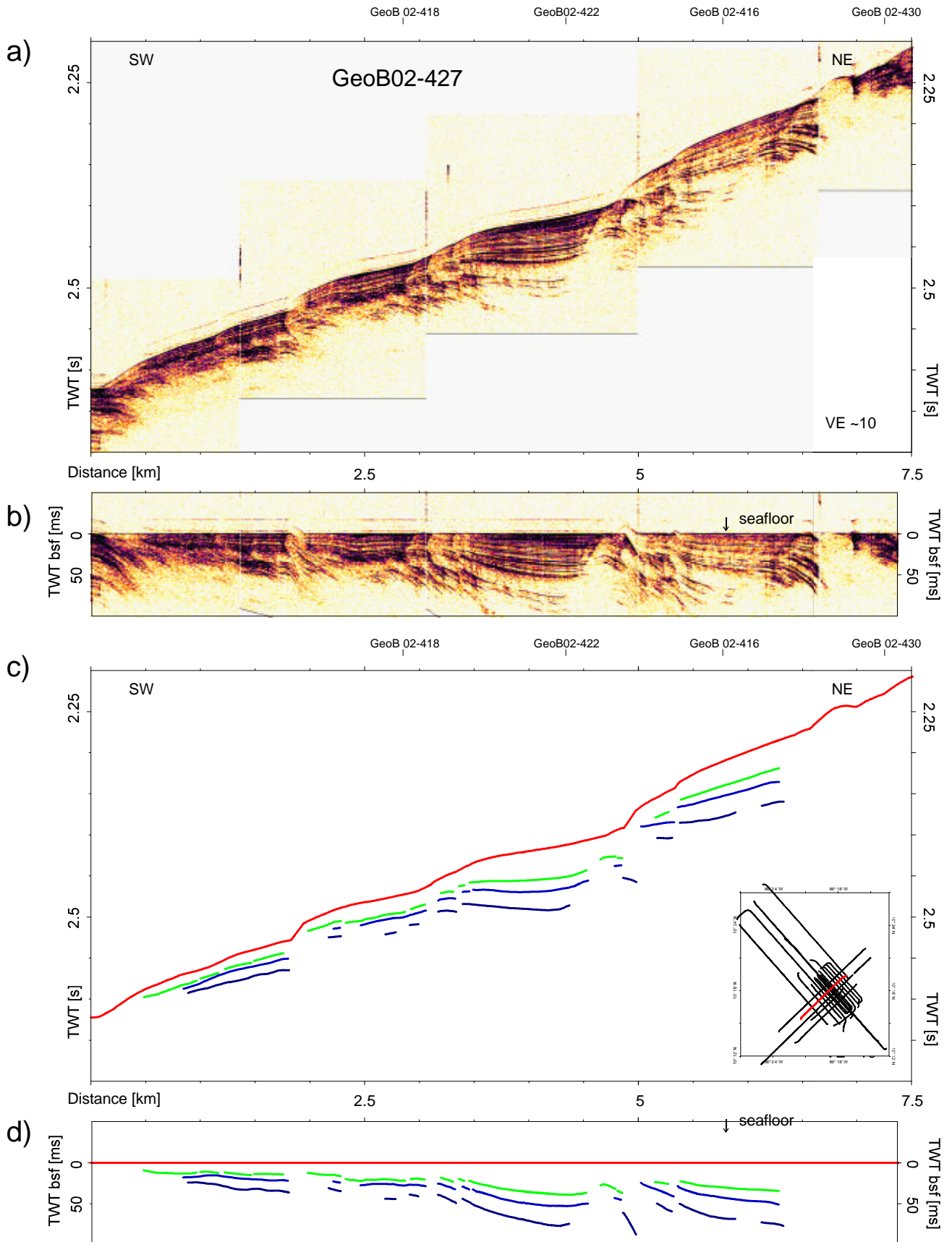
Figure 3.6 a) Example echosounder dip line GeoB02-427 showing typical, asymmetrical, wedge-shaped sediment bodies in the subsurface trenchward of Mound Culebra. b) Reflection time below a (flattened) seafloor. Tracer horizons as line drawing, displayed c) in two-way travel time and d) relative to the seafloor.
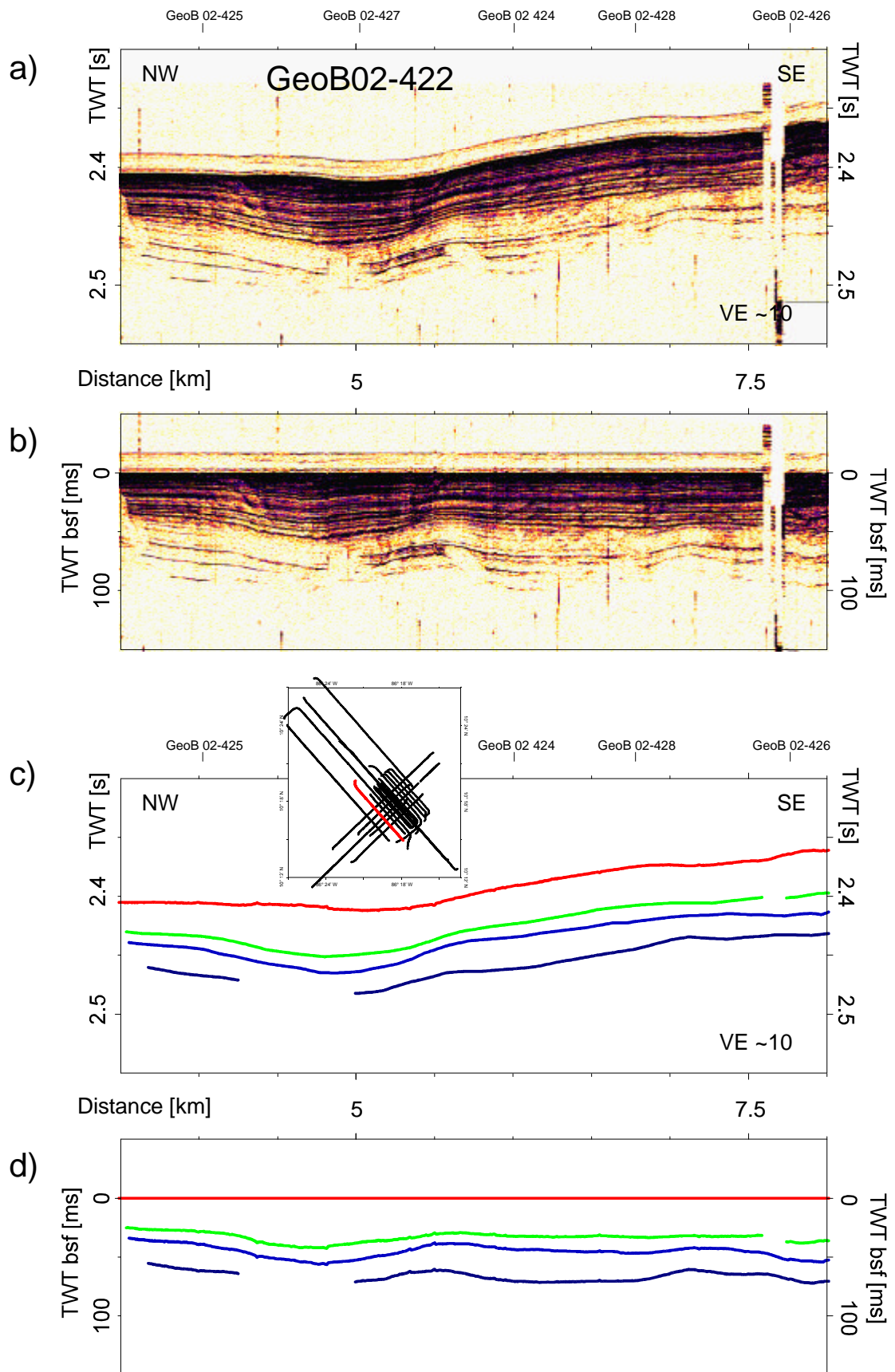
Figure 3.7 a) Example echosounder strike line GeoB02-422 showing slight northwestward thinning of strata. b) - d) as above.
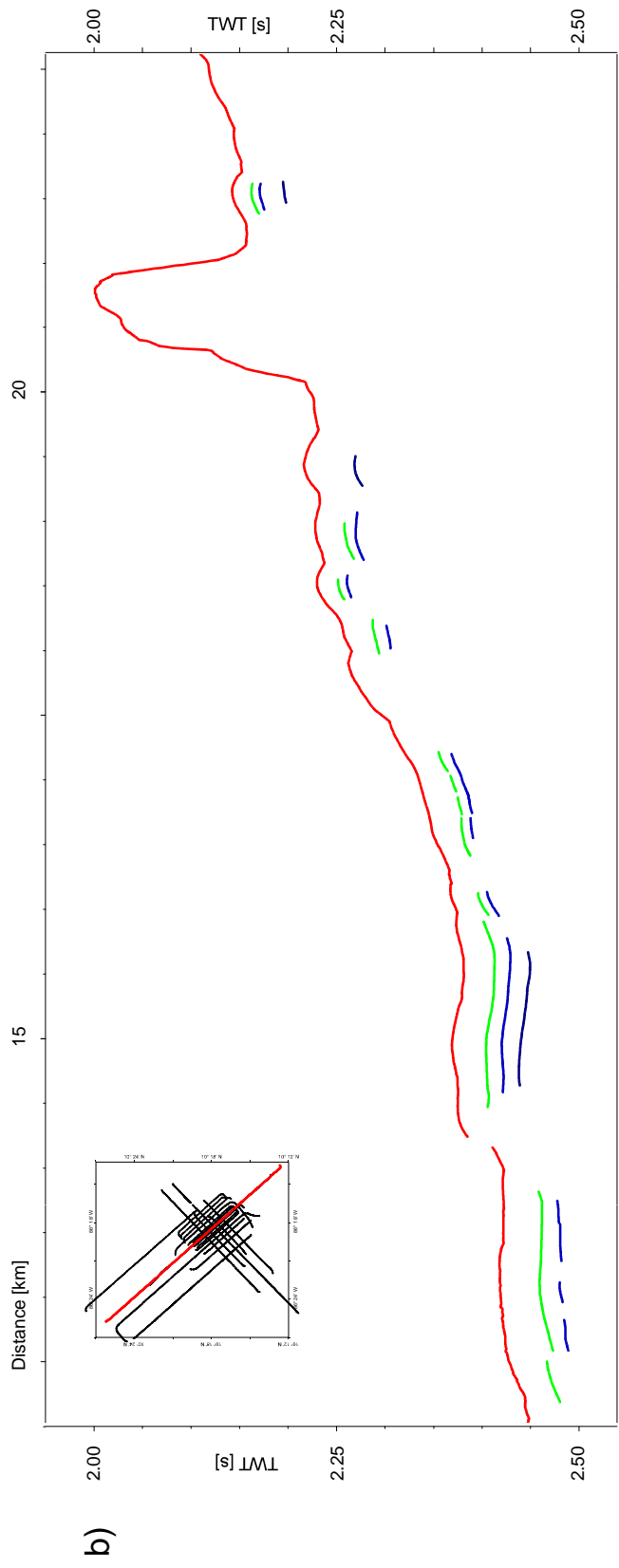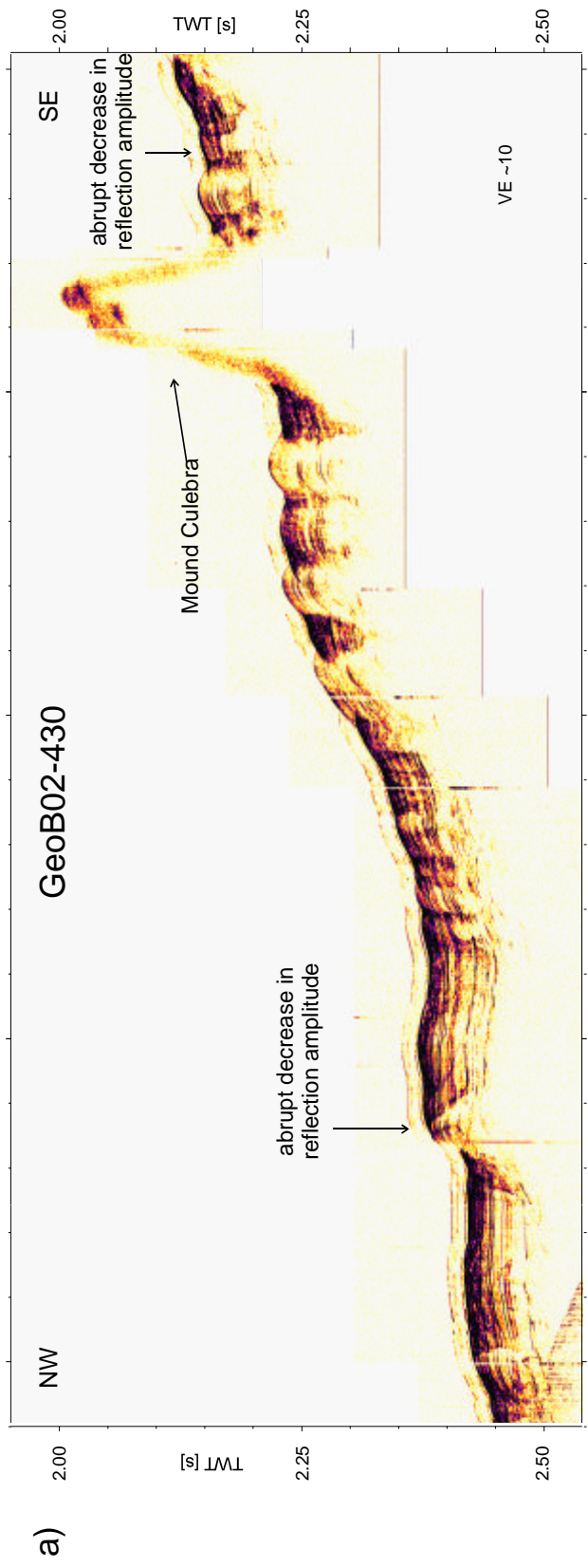
Figure 3.8 a) Main strike echosounder profile GeoB02-430 crossing Mound Culebra and b) line drawing of the same. Note locations of amplitude decrease, in cases coupled with vertical offset and abrupt thickening of strata (eg. northwest of Mound Culebra, offset 14 km).

layer thicknesses decrease gradually towards the trench. Wedge-shaped sediment bodies with vertical extent down to 150 ms TWT below seafloor characterize dip lines. Seismic horizons are observed to be bent upwards at several locations in association with being vertically offset.

Vertical discontinuities of seismic reflections are generally of larger vertical offsets than those seen in Parasound data. They are also fewer, but occur mostly at the same locations (Fig. 3.10). This implies that the difference is a direct consequence of the signal frequency difference: small-scale depositional processes, such as individual turbidity events, are unlikely to be imaged by the seismic technique, while they are possibly captured at echosounder resolutions. Apparent angles of downthrow vary from 11° to above 80°. Steep throws seem limited in penetration and reveal an arbitrary orientation. Low-angle discontinuities on the other hand appear to disrupt the entire reflecting sequence, and dip downslope. A major offset feature observed in trench-parallel profiles is the abrupt downthrow/thickening of strata northwest of the intersection point with profile GeoB02-421 (at 16 km offset), also seen in Parasound data. Seismic reflection amplitudes on its Mound Culebra side are significantly higher, especially at depth (Fig. 3.11).

Local amplitude variations are seen at several locations in strike lines (Fig. 3.11). These are marked by a low-amplitude zone of 70 - 200 ms TWT vertical extent, widening with depth to beyond 100 m. In some cases, internal seismic layering is visible. The feature is often accompanied by elevated amplitudes on its outside or at/above the top, in the latter case extending beyond its sides. These features occur at variable depth, in some cases close together. Shallow ones are marked by local highs in seafloor topography along the profile. A map view of the shallowest points of these features is shown in Fig. 3.12.
Individual reflection horizons also appear as segments of high amplitude that extend laterally over distances of a few tens to several thousands of meters (Fig. 3.9). This is often seen concurrently in horizons located above one another.

From a reflection characteristics point of view, Mound Culebra differs significantly from its vicinity. Beneath the high-amplitude reflections from its top, no further horizons are observed. The only exception is found towards its landward extension,

where short reflector segments are seen 200-250 ms TWT below the surface. Beneath the flanks of Mound Culebra, reflections appear to be bent upwards and then terminate abruptly. They remain parallel to one another. Anomalously high reflection amplitudes occur at depth northwest- and northeastward of the mound. The shape of seismically transparent interior widens towards the surface, reaching its largest lateral extent (1100 m measured parallel to the trench) about 1 ms TWT below the base of the mound.

3.3 Discussion

Mound Culebra

The properties of the most prominent object in the survey area, namely Mound Culebra, are derived from bathymetric and side scan sonar measurements, the results of non-geophysical investigations such as ocean floor video observations or gravity coring, and the characteristics and geometry of bordering reflectors.

The former indicate that the mound's high-amplitude surface echo is probably created by outcropping harder /rough material or a highly reflective surface cover. This is in agreement with the diffraction hyperbolae of Parasound recordings, which generally indicate topography below the spatial scale of its footprint (~100 m). Mound Culebra's reflection-free interior is most probably due to the absence of geological structures, destroyed by intense deformation and/or fluidization during a buoyant ascent from depth, as shown by structural sedimentological analyses (Soeding et al., 2003, Moerz et al., 2005). This is also supported by the abrupt termination and upward bending of seismic reflectors beneath Culebra's flanks. Alternatively, apparent upward bending in stacked or constant-velocity time-migrated sections may indicate a sound velocity increase above these reflectors, which would be a plausible consequence of rising, overconsolidated material within the mud dome. However, this effect does not occur consistently in parallel profiles, nor does it appear vertically within single profiles. Thus the explanation for bent layers as an artifact called "velocity pull-up", where the assumption of vertically unchanging velocity makes reflectors below high-velocity anomalies appear to lie shallower or bend upwards seems inadequate. Reflector geometry most likely indicates an upward drag by material rising in the center (Fig. 3.11).
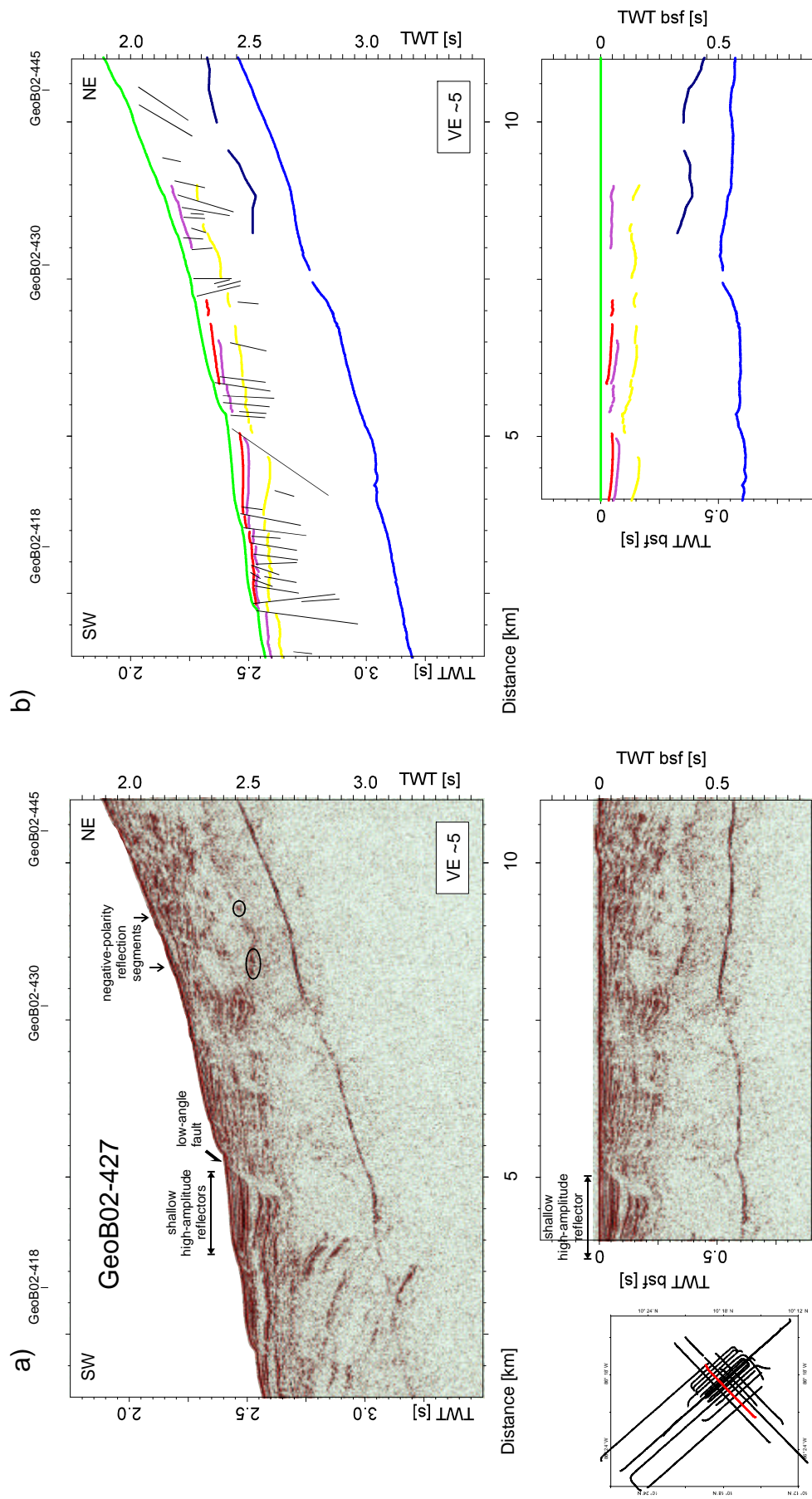
Figure 3.9 Example seismic dip line GeoB02-427. The upper well-layered interval of 250 ms is followed by mostly transparent seismic facies with a sharp, negative-polarity reflector at around 500-600 ms TWT below seafloor. Marker horizons are shown, as well as faults and fractures. Note shallow high-amplitude reflector segment between 3.5 - 5 km offset and examples of polarity reversal near 9 km offset. Also compare to Fig. 3.6. a) seismic profile, b) line drawing.
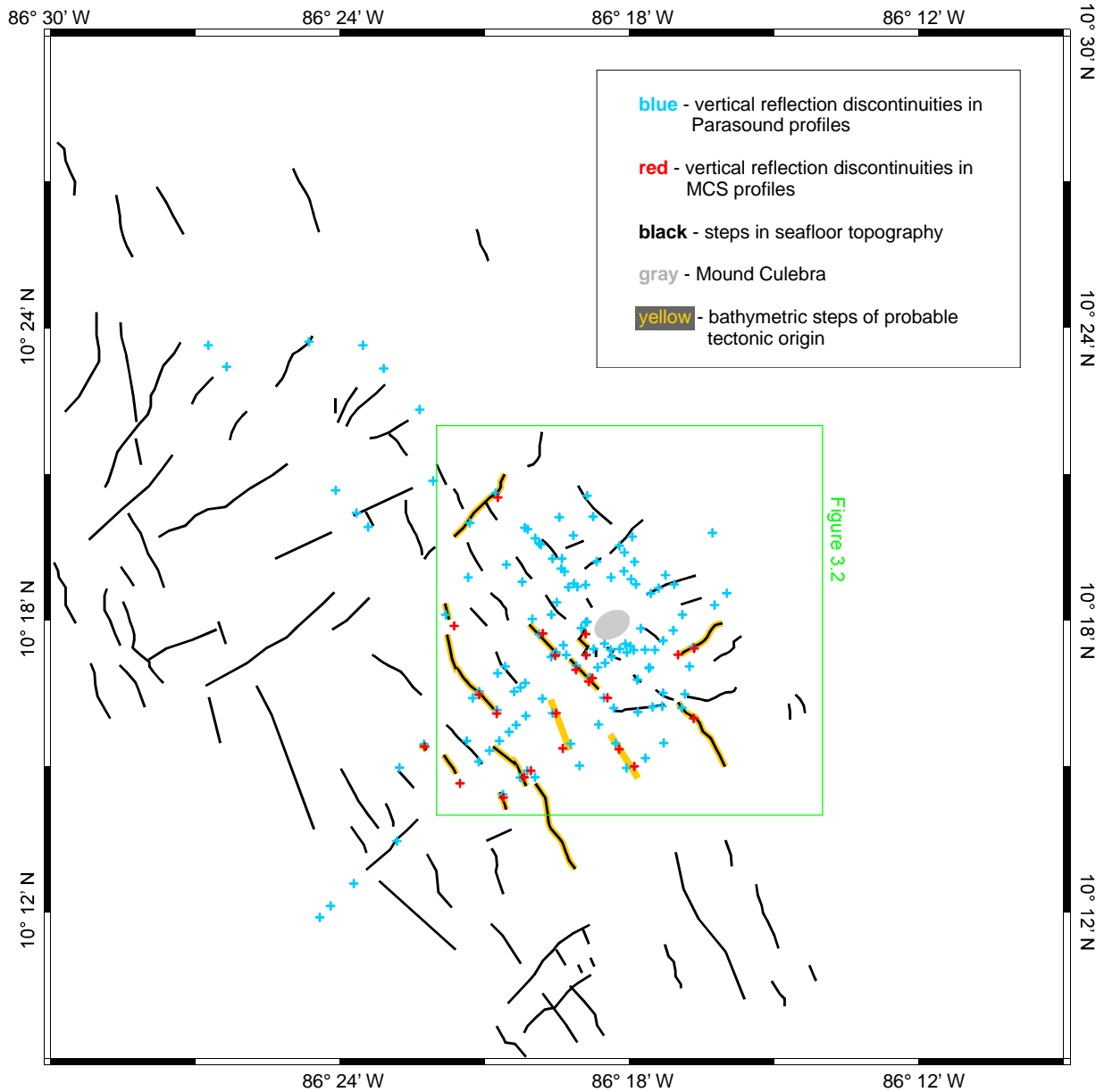
Figure 3.10 Map view of vertical reflection offsets in seismo-acoustic strata. Steps in seafloor topography (black lines, cf. Figure 3.3) are widely correlable with vertically offset reflectors observed in MCS (red crosses) and Parasound (blue crosses). This helps select offsets of probable tectonic origin (along steps underlain in yellow). Correlation of faults across profiles is also simplified, as well as predictions of fault locations which are not visible on the surface.
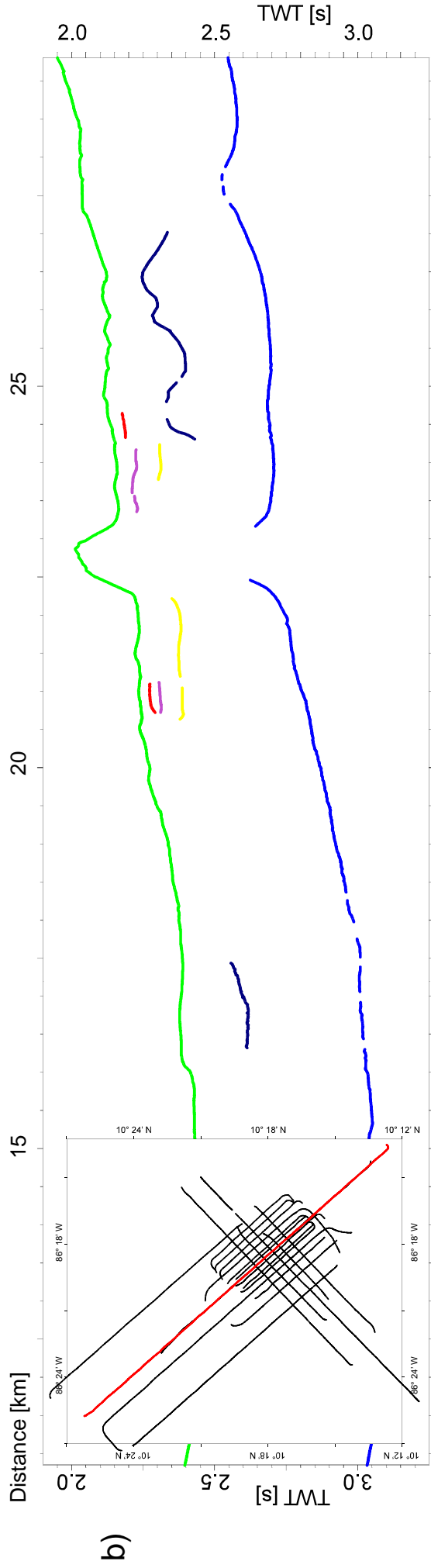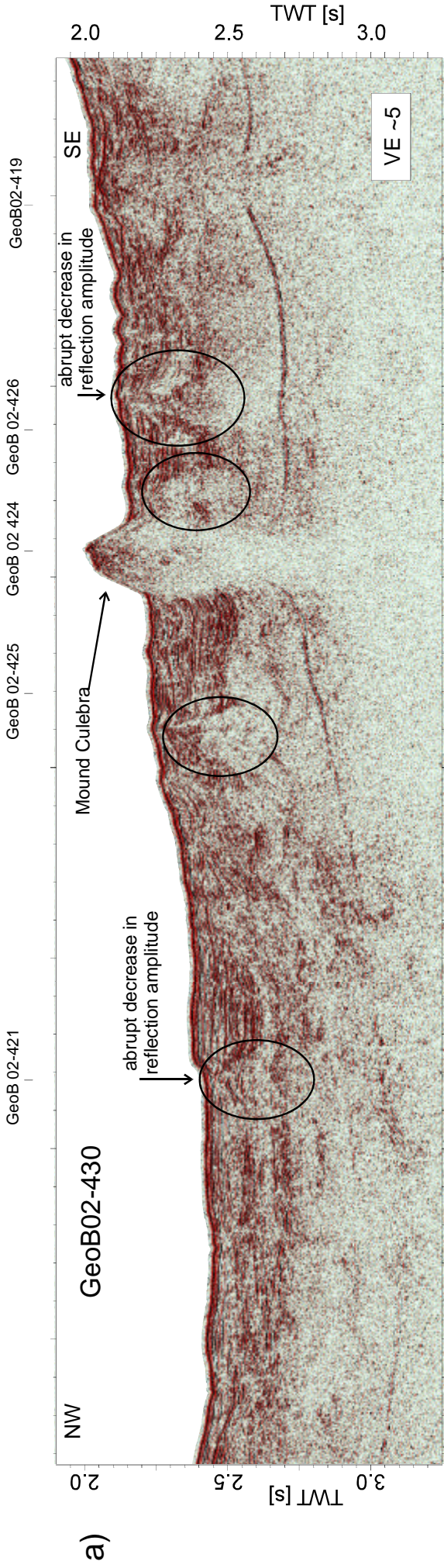
Figure 3.11 Main seismic strike profile GeoB02-430, crossing Mound Culebra. Reflections show apparent upward bending beneath the mound flanks, and are entirely missing in the centre. Locally elevated sediment deposition is seen at offset 16 km. Some low reflection amplitude zones broadening downwards are marked.
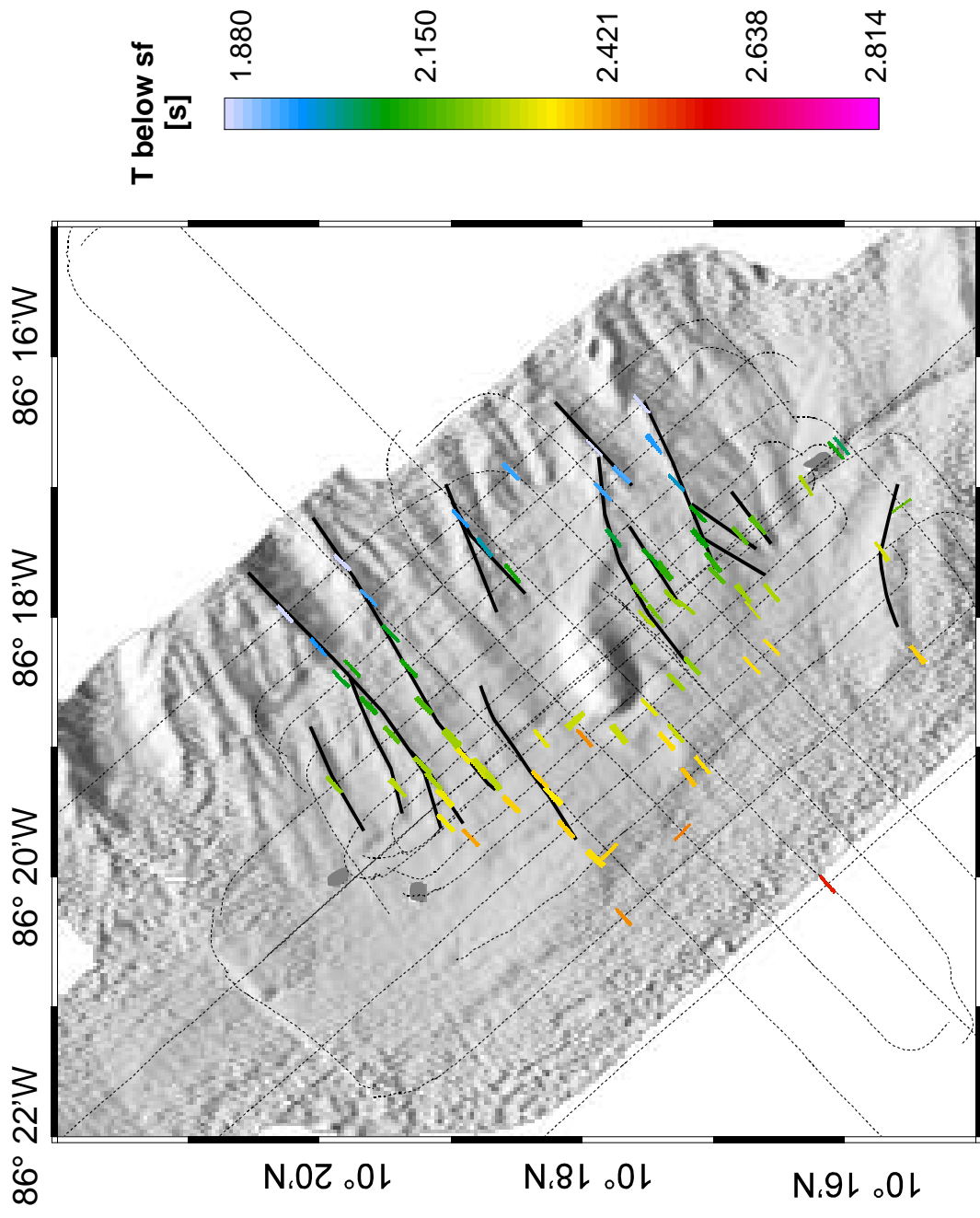
Figure 3.12 Map view of the shallowest points of triangular features in the subsurface which are characterized by anomalous reflection amplitudes. Colour coding shows travel time difference subsurface. Most of them correlate within picking accuracy to seafloor ridges (solid lines).

The shape of seismically transparent zone underneath the mound and the parallel geometry of reflectors beneath Mound Culebra's flanks implies active rather than reactive diapirism, the predominance of buoyancy over tectonically opening pathways (due to extension or faulting, e.g. van Rensbergen et al., 1999). This is in agreement with the generic model of Brown (1990), predicting a drop of the density and an increase of buoyancy of the diapir during the last stage of its ascent due to the decrease of ambient pressure, which allows gases in the pore space to expand.

Sedimentary features

As shown by several authors (e.g. Damuth and Hayes, 1977), echosounder facies worldwide can often be assigned to lithologic facies, being specific for characteristic sedimentation patterns. Well-layered returns such as described in the Parasound section imply either pelagic deposits or hemipelagic packages with cyclic compositional or grain size changes or graded bedding. In the light of slope morphology, specifically the presence of steep upper slope being divided by canyons and of sufficiently flat topography for deposition on the middle slope, a turbiditic origin of sediments is conceivable. Transparent zones and lenses generally mark strongly reworked structures, such as slump material or a debris flow. Prolonged and hyperbolic echoes in the echosounder profiles are controlled to a large extent by topographic variation and slope angle, such as mounds, lineaments, or in the case of acoustic facies type d), undulating surfaces (Damuth, 1975, Spiess, 1993). The characteristics of the shallowest seismic facies support the above explanation and extend its applicability down to a maximum of approximately 200 m below seafloor. A distinct change of seismic properties underneath may correspond to the lithological and structural boundary described for ODP drill site 1041 (units A1A and A1B, Kimura et al., 1997). Low seismic amplitudes in the lower interval may at least in part be caused by increased gas hydrate presence, but this theory is hard to evaluate because of a general lack of reflectors.

Lateral amplitude variations of seismo-acoustic horizons in sedimentary settings are most commonly a result of variable grain size and porosity. A set of such occurrences is discussed further in the *Canyons and ridges* Section. To a smaller extent, variable seismic amplitudes may also be caused by changes in the fluid or gas content in

connection with possible tectonically formed pathways, such as faults, as seems probable in the case of small-extent anomalies occurring simultaneously in subparallel reflectors (Fig. 3.9).

Fractures and faults

Vertical offset or concurrent termination of echosounder horizons can be attributed to various causes, the most important ones being faulting and depositional processes. These can best be convincingly separated by a joint evaluation of surface and seismically imaged features. In the target area, linear steps in topography are collocated with reflection offsets in both echosounder and seismic profiles (Fig. 3.10). This provides means to identify and correlate faults between profiles and in images of different frequencies and to determine their orientation. In the vicinity of Mound Culebra, such an analysis reveals that several bathymetric line segments, oriented trench-parallel, are the surface expressions of currently active low-angle (10-20°) normal faults. Their subsurface geometry implies a listric shape in depth, with individual blocks tilting landwards. The thickness of sediments thus deformed is at most a few hundred meters. A successive increase of the dip angle with depth of subsequent reflectors, as is the case near Mound Culebra, hints to syn-sedimentary faulting as the origin of the wedge-shaped sediment packages. Further trenchward, vertical offset remains constant with depth, indicating post-sedimentary movement, indicating that movement along the fault surface outweighs sediment deposition. A likely model of the role of these faults is shown in Fig. 3.13. The varying vertical offset of single faults gives control of the average speed at which the faults move: at an example fault in Parasound profile GeoB02-427, for 20 m average depth difference between two horizons, the downthrow difference is 3 m. Assuming for example a recent sedimentation rate of 20 cm/ka (Kutterolf, pers. comm.), the 20 m depth difference is equivalent to 100 ka of age difference of the two surfaces, and 3 m excess offset of the lower one yields a fault throw rate of 3 cm/ka. The net (in-)accuracy of this value depends on the quality of estimated deposition rate of the target area (it decreases proportionally in regions with lower sedimentation rates), the choice of location to measure average TWT difference between non-parallel reflectors, and the errors while determining times in the sections (+/- 3ms). A similar example from a fault further southeast in the same profile in seismic data (64 m / 320 ka age

difference between reflectors, 18 m excess offset in the lower) yields a throw rate of 5.7 cm/ka. Although these estimates are easily interpreted to show fault growth acceleration with depth and/or towards the trench, analysis of a fault which appears in several parallel profiles (Fig. 3.14) has shown variability on the scale of an order of magnitude, a primary result of local deposition rate variations and fault geometrical effects. Nonetheless, both an acceleration of movement along these faults and a decrease of local deposition rates trenchward are plausible reasons for the observed variation of vertical offset, and are thought to act simultaneously.
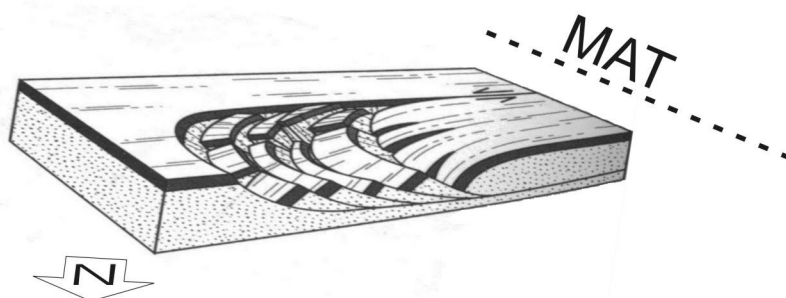

Figure 3.13 Inferred origin of trench-parallel faults. Due to oversteepening of the lower slope, unconsolidated shallow sediment creeps downslope towards the trench (MAT, dashed line) in blocks. At upper block ends, listric faults form, creating a characteristic wedge-shaped sediment pattern. Blocks are bound on either side by faults of strike-slip nature. Arrow shows north in the case of Costa Rica.

The local morphology may provide additional information about the timing of deformation relative to deposition. Topographical variations caused by low-angle faulting around Mound Culebra are not filled up by subsequent sedimentation. This may have a number of reasons. One possibility is topography-dependent sediment deposition, as in the case of turbidity flows, where material accumulated on lower-lying surfaces differs in volume, porosity, and grain size, consequently in consolidation capacity, from that covering elevated areas. Another possible explanation is episodical fault activity - average vertical movements stay low, while an "offset event" may need thousands of years to be evenly covered with new material. Topography-parallel bottom water currents may also contribute to the effect, since if they are fast enough, they can maintain or enhance surface elevation

differences. However, we have at present no appropriate measurements to assess the relative importance of these factors.

Small vertical offsets with high angles seen in the seismic profiles appear to reach the surface seldom (fewer than 10% of all occurrences), and in consequence to have no obvious surface expression (Fig. 3.9). Although they occur in large numbers, their correlation across even neighbouring profiles is not possible. They are tentatively interpreted as small-scale deformation locally compensating stresses caused by the regional tectonic movements.

Deep-reaching, regional faults were not imaged decisively in the presented dataset. These are expected to be present at a rapidly subsiding margin with retreating coastline. They have been imaged to occur offshore Central Costa Rica where they are characterized by a landward dip (Ranero and von Huene, 2000). The only example in our data set is from the southeastern rim of the study area (Fig. 3.15). The feature is associated with a prominent surface lineament and has a trenchward dip of 55° in the subsurface. The interpretation that this fault is directly or indirectly connected to significant depths is supported by several indirect observations. These include an updoming of the BSR, high backscatter values and extensive chemosynthetic fauna on the surface (Soeding et al., 2004), and, above it, a prominent methane plume in the water column with a bottom source (Mau et al., 2006), which together point to the outflow of warmer-than-background, possibly deep-sourced fluids at this location.

Canyons and ridges

Subsurface structures of a different origin are revealed by trench-parallel oriented profiles. They are mostly characterized by triangular low-amplitude anomalies observed in seismo-acoustic images. In the MCS data, their vicinity is often characterized by locally elevated reflection amplitudes.

In map view, the structures seem to follow the canyon and ridge system of the landward portion of the study area, more specifically, to mark the continuation of ridges (Fig. 3.12). Such amplitude anomalies could be related to locations of anomalous fluid content, such as upflow regions. However, their great number of
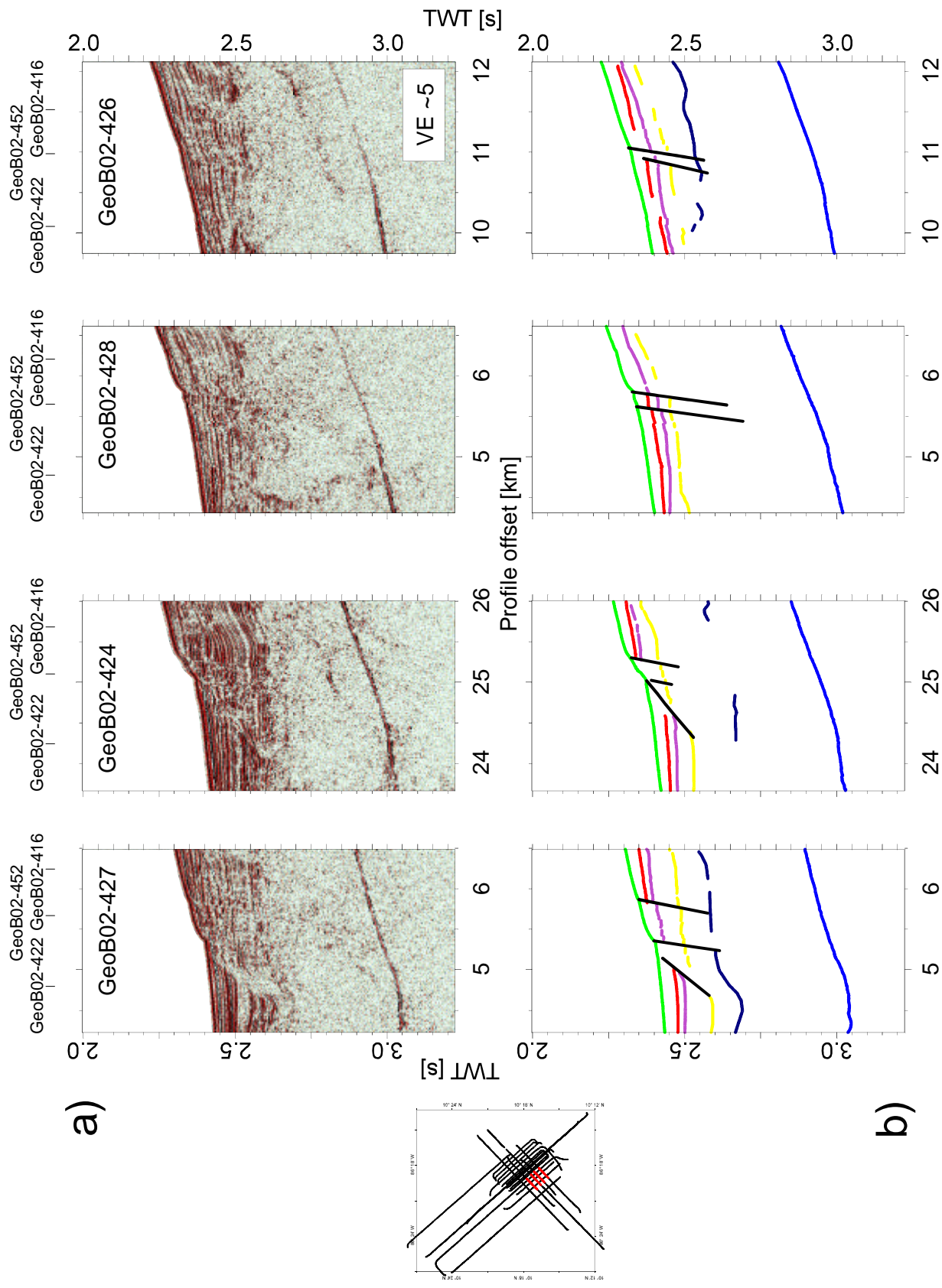
Figure 3.14 Example of fault correlated through four adjacent dip lines, in seismic profile (a) and in line drawing (b). While it looks similar in pairs of adjacent profiles, correlation would be difficult without surface information beyond a lateral distance of 1 km due to changing offset and dip angle.
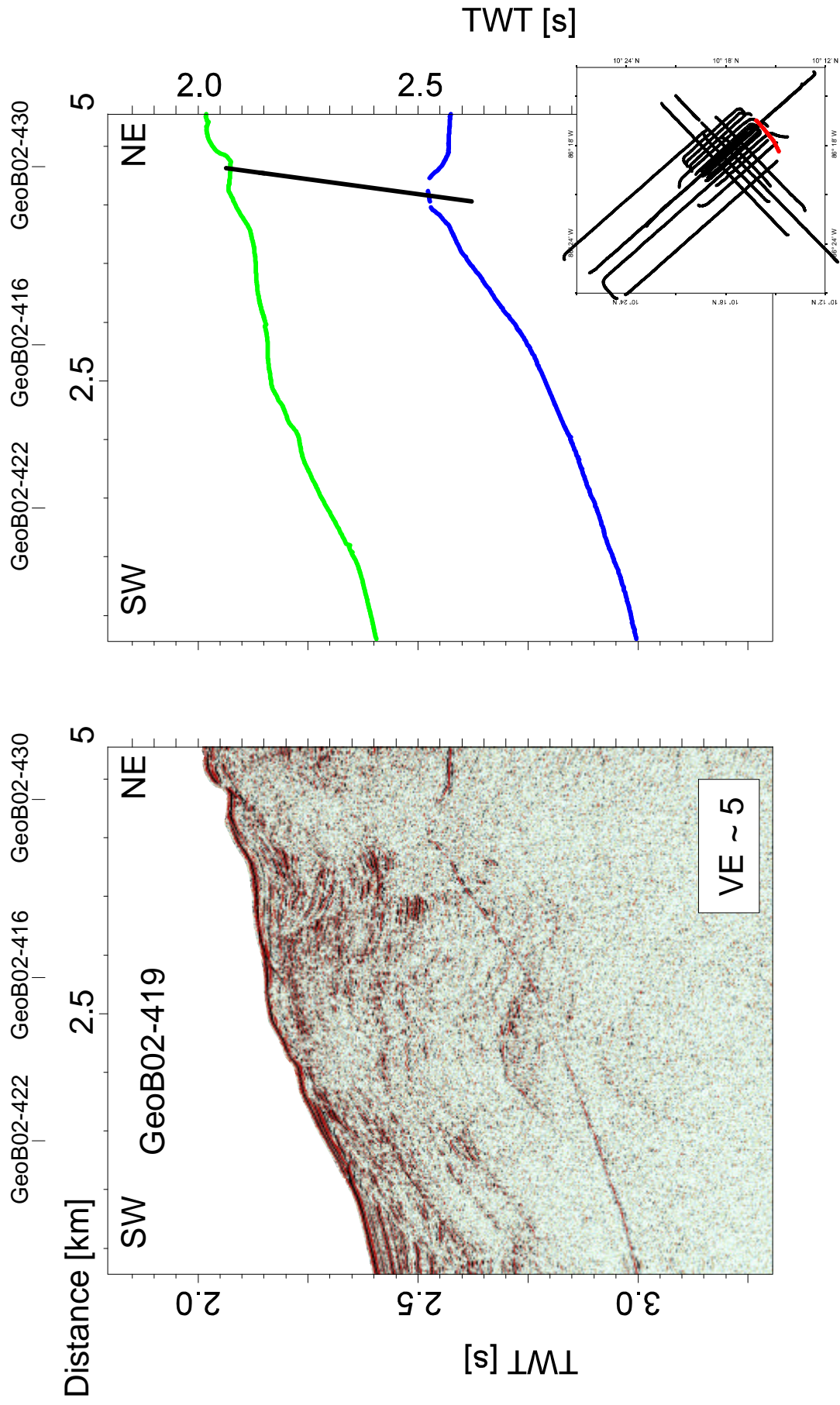
Figure 3.15 Short seismic dip line from the southeastern rim of the study area, revealing the only example of fault with a probable connection to greater subsurface depths.

occurrence and spatial distribution suggests another explanation. The amplitude anomalies are arranged in the continuation of every major ridge, and are correlable between strike lines. Therefore, we interpret these anomalies to be canyon walls. Beneath the basin, they are imaged to be buried by a few to tens of meters of sediments. Low reflection amplitudes within the ridges as well as patchy layering may be explained by fine-grained overspill sediments from constrained suspension flows being deposited at the canyon flanks. Space between buried ridges may have been subsequently filled by sediments of similar properties as material deposited on top of them, creating "background" seismic reflection strength. Alternatively, if the canyons became clogged by some obstacle, it probably caused sediment movement to stop abruptly. In this case, canyon fill may include larger grain size fractions, which create enhanced amplitudes, as is possibly the case in profile GeoB02-430 between offsets 16 - 17 km (Fig. 3.11). This location also reveals asymmetrical sediment thicknesses on either side, with a 35 m step-down in seafloor topography and an obviously offset and possibly slightly thicker subsurface sedimentary succession towards the northwest, implying a tectonic control of ridge location. This is in agreement with the implied tectonic origin of the surface lineament, shown in Figure 3.12.

Ridges and canyons reoccur on the surface on the trenchward side of the basin. They are few, shallow, and run parallel to one another downslope. The slope regains its steepness here and a number of trench-parallel, low-angle normal fault segments are found to cut the shallow subsurface. Although individual segments are only a few kilometers long, they are often arranged collinearly, and probably indicate the occurrence of an alternative way of transporting material down the slope with respect to turbidites, namely by gravity-driven mass creep (Fig 3.13).

3.4 Interpretation

Sediment transport on the continental slope

The continental slope of Middle America is provided with abundant supply of sediment. Its fate is primarily controlled by slope morphology, while transported or deposited material also shapes the seafloor. Canyons typically form where large amounts of material are transported downslope, for example in the form of turbidites.

The steep upper slope provides gravitational energy to sediment masses that carve valleys into the surface and form ridges in between, which in turn steer and confine downslope transport. When the volume of suspended material conveyed is greater than the capacity of the valley, overspill structures at the sides may be built from fine-grained fractions, building the flanks higher.

Deposition centers are generally areas with adequately small slope angles and sufficient accommodation space, for example created by subsidence. The basin around Mound Culebra is a likely candidate. Where ridges are less high, confinement of the sediment flow is absent, therefore flow speed decreases and the cross section of moving mass widens. This effect is here corroborated by the loss of gravitational energy, and results in an abrupt reduction in the transport capacity of the flow, associated with the deposition of larger grain fractions and resulting amplitude contrast of seismic reflections. Deposition primarily concentrates on areas close to the mouth of canyons, building up a depositional lobe.

The process results in a filling of canyons where their gradient is reduced, i.e. in the vicinity of the basin. It also causes the basin to extend upslope at a slow speed, which maybe accelerated by simultaneous tectonic subsidence, possibly at the landward rim. The fact that ridges as high as 200 m above the canyon floor are identified in the subsurface of the basin being covered with several tens of meters of sediments just a few kilometers trenchward suggests that the role of basin subsidence is significant.

Trenchward of the basin, gravity-driven material creep and channelized downslope sediment movement occur simultaneously. Canyons remain shallow and few, indicating that they are no longer the dominant form of trenchward material transport in this region. The significance of mass creep cannot be assessed from observations limited to the study area.

The tectonic regime of the Mound Culebra area

The regional tectonic settings at the Middle America Trench imply the following processes to act on the continental slope: frontal erosion at the deformation front, basal erosion of the margin wedge, and frictional coupling to the downgoing slab.

These have been established to result in coastal retreat and margin subsidence. In light of the above-discussed observations, we propose the following model to describe the local tectonic context around Mound Culebra (Fig. 3.16).
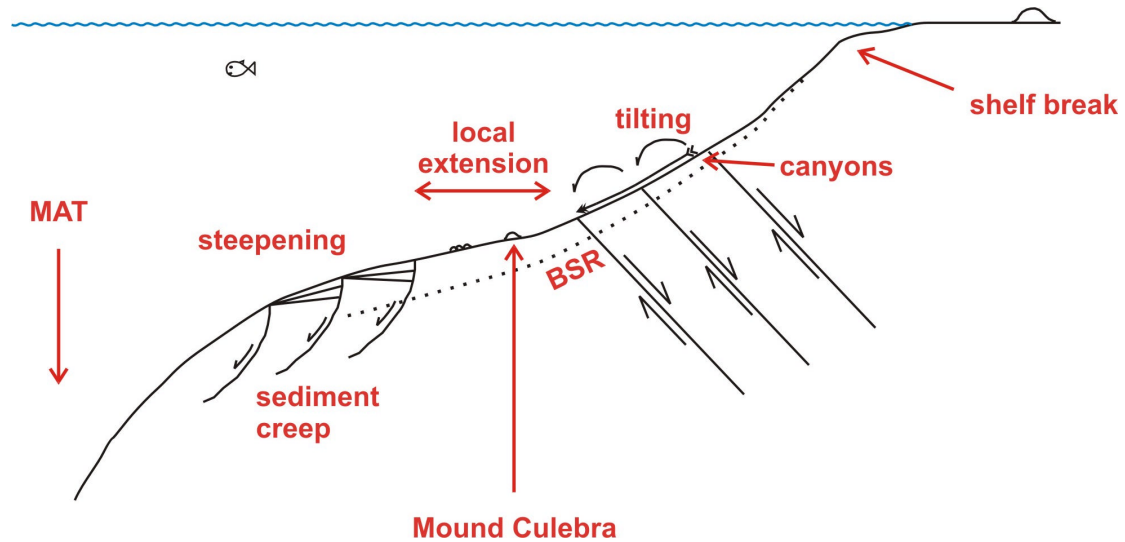

Figure 3.16 Conceptual tectonic model of the margin wedge. Near the trench, the upper plate is eroding both frontally and from its base. The wedge gets thinner and can thus possibly bend due to frictional coupling with the subducting slab, generating a lower slope steepening trenchward. Consequently, the sediment cover becomes remobilized. Downslope sediment migration occurs in the form of gravitational creep, in association with listric faults and bathymetric steps oriented trench-parallelly. BSR as well as seismic layering of the subsurface disappears. The middle slope undergoes extension, creating flat topography and a location of elevated deposition of sediments coming from the upper regions. Upward fluid flow may be enhanced by the opening of pathways, and mud diapirism maybe triggered or promoted by the relatively higher sediment load. The structure of upper slope is formed primarily by the continuously eroding trenchward support and the rigidity of the ophiolitic wedge. The slope steepens, producing a region of mainly erosive downslope sediment transport in canyons, in the form of turbidites. Landward-dipping faults are expected to develop in response to the margin subsidence.

Near the MAT, material is continuously removed both from the frontal prism and the base of the upper plate. This results in the thinning of the wedge. In this area, it is probably thin enough to respond to frictional coupling elastically, that is, by bending. The lower slope steepens, destabilizing the sediment cover, which starts to move into

the trench in form of slumps, or as mass creep along trenchward oriented listric growth faults. The nearer to the trench, the more this movement dominates relative to deposition: slip along the fault planes accelerates, and sediment accumulation rates decrease concurrently.

Due to the bending of margin wedge and a net movement of both wedge and sediment material towards the MAT, local extension is created further upslope. The seafloor is characterized by moderate angles in this region, providing favourable depositional circumstances. It may be this enhanced sediment accumulation which provides the solid component of source material for the forming of mud diapirs. The margin wedge may undergo normal faulting due to the combined effect of its increased thickness and continuing basal erosion. Elevated subsidence with respect to the vicinity is possible. Sediments will respond to extension and mechanical stress by small-scale fracturing. This is the setting where Mound Culebra and the smaller mounds to the northwest of it are located.

Local extension results in a lack of support for material further landwards. Landward dipping faults, imaged offshore central Costa Rica (Ranero and von Huene, 2000) to cut the margin wedge as well as the sediments, probably segment the continental upper slope, allowing fault blocks to tilt trenchward On the surface, canyon systems develop due to high slope angles and transport sediments efficiently from the shelf.

The model is in good agreement with observed seismic stratifications. Both sedimentary layers, largely absent beneath the canyon system and distinctly present on the middle slope, and the BSR, traceable continuously in the vicinity of Mound Culebra, lose their distinctness and disappear altogether trenchward of the study area, probably as a consequence of sediment destabilization.

The location of Mound Culebra

Mud diapirs are generally thought to form in compressional settings with high deposition rates (e.g. Kopf, 2002), the latter supplying potentially overpressured material while the former triggering its buoyant rise towards the surface. Although this is not the case in Middle America, numerous mounds created by mud extrusion have been found on the Costa Rican - Nicaraguan continental fore-arc.

Their presence has been explained invoking two-phase diapirism. Mud and fluids are thought to originate from different source regions (e.g. Hensen et al., 2004, Moerz et al. 2005). According to these authors, fluids are likely to rise from the plate boundary through the entire margin wedge and gather at the base of the low-permeability sediment column. Diapiric processes are triggered and material remobilized upon reaching a critical overpressure. Moerz et al. (2005) estimate the source depth of diapiric mud constituting Mound Culebra to 600 - 800 m below seafloor. For these depths, sedimentation at the given rates (~200 m/Ma) is unlikely to provide necessary overpressure alone via insufficient dewatering and undercompaction. Additional fluid input from below eliminates this difficulty. Dissociation of gas hydrates due to margin subsidence and basal heating may also contribute, especially if free gas from dissociating hydrates is subsequently trapped under the stability zone. This is a process that takes place at comparable depths (down to 500 m at Mound Culebra).

The previously described tectonic model is adequate to explain the location of Mound Culebra. A strong relationship between the location and existence of the mound and the presence of the basin around it is assumed. Sediment thickness and resulting buoyancy differences above the wedge are likely to reach a critical amount easiest in an extensionally evolving area, and any faults within the margin wedge will potentially focus fluids also here. However, the spatial extent of the model's validity is uncertain and should therefore be investigated further.

One possibility is that it accurately describes the entire continental slope. In this case, the presence of a middle slope basin would be a direct consequence of the mechanics of margin subsidence and subduction erosion. This explanation implies a causal relationship between the extensional regime and the occurrence of mud diapirs, which we have not decisively established. However, with this assumption, the model would plausibly elucidate why Costa Rican mounds seem to be confined to a belt around the middle slope (Sahling et al., in prep.)

A difficulty with this hypothesis is that it predicts a continuous belt of low seafloor angle on the middle slope. Local flattening of the middle slope has been noticed at different locations by other authors (von Huene et al., 2004). Randomly selected bathymetric shelf-edge-to-trench profiles (Fig. 3.17) also suggest that such flat areas
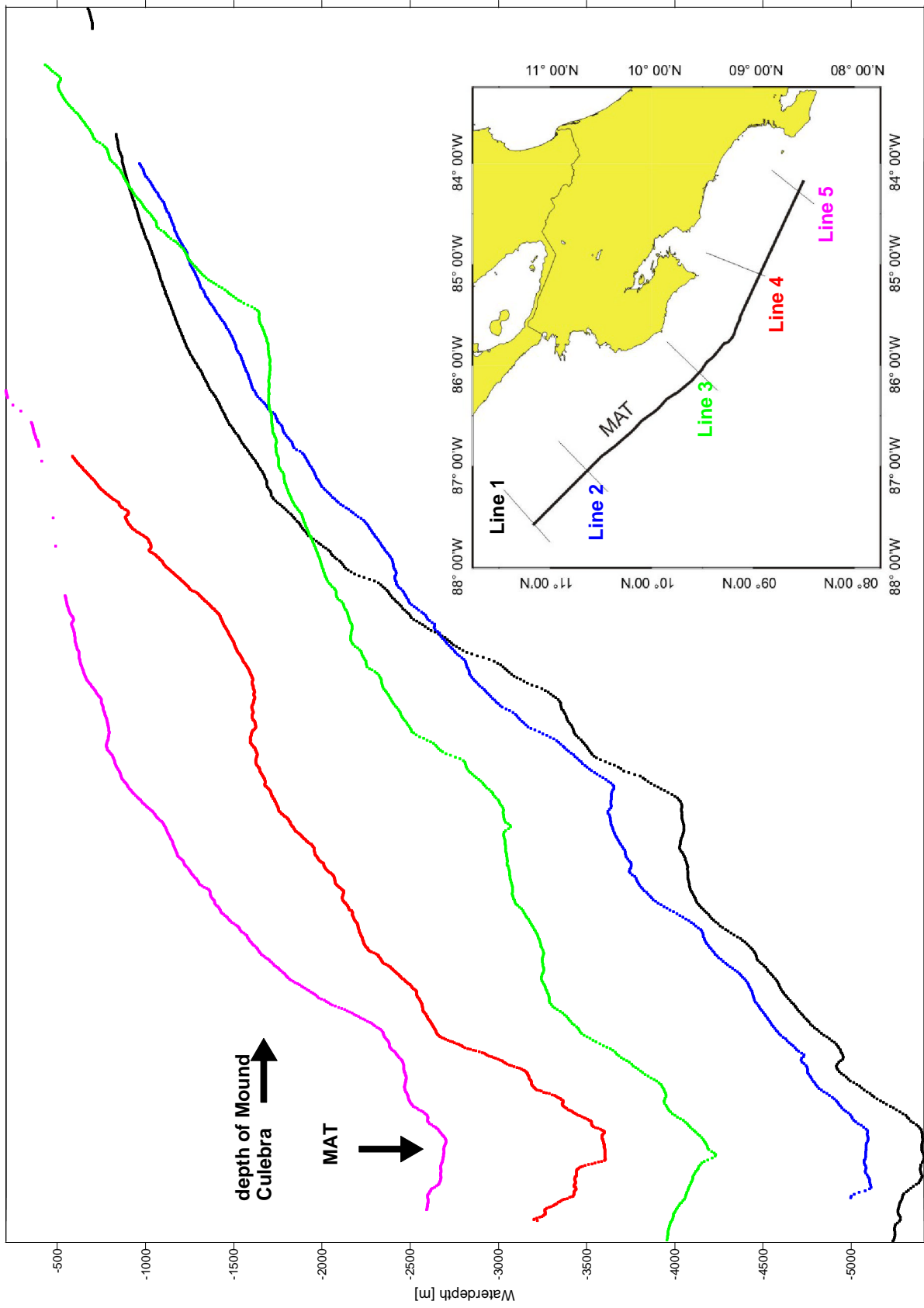
Figure 3.17 Five randomly selected bathymetric profiles offshore Costa Rica, covering depths from 500 m to trench depth. Insert shows location of profiles. Profiles off Nicoya peninsula (lines 3 and 4) display a local flattening around 1650 m water depth. "MAT": Middle America Trench. Approximate depth of Mound Culebra is marked.

are seen south of Nicoya peninsula, they are not a unique feature in the Mound Culebra vicinity. However, they still remain far from being a general phenomenon. Nonetheless, the constraint may be an unnecessary one. In their reconstruction of Costa Rica's subsidence history, Vannucchi et al. (2002) present a figure showing inferred water depths for the last ~16 Ma (Fig. 3.18). Rather than water depths through time, this curve can be viewed as a present hypothetical bathymetric profile from the near-shore regions (where the carbonate-cemented breccia was deposited) to the drill site location near the trench. The profile closely resembles the actual bathymetric cross-section through the Mound Culebra area, in that two steep segments bracket a flat interval of water depth similar to that of the mound. The drill site itself however is located at a portion of the trench that, at least at present, displays no middle slope basin in the bathymetry. It is therefore possible that mounds would exist at locations where the slope angle between the shelf edge and the trench stays relatively stable.
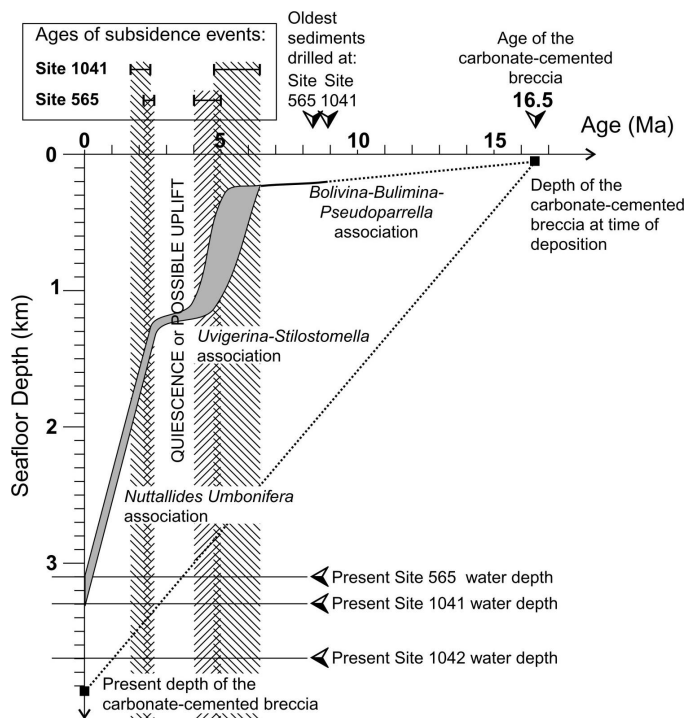

Figure 3.18 Subsidence history of the continental margin. Sediment age versus inferred water depth, from ODP Sites 1041, 1042 and DSDP Site 565 (from Vannucchi et al., 2002).

Another interpretation is one that suggests the presence of a topographic feature on the subducting slab beneath Mound Culebra. This considers the basin to be an anomaly, possibly caused by subsidence / collapse behind a subducting seamount or

similar object. However, an appropriate instrument is not easy to find. Seamount tunnelling appears to create long, narrow valleys elongated downslope rather than broad, and short ones. In addition, no large topographic feature is presently visible on the oceanic side of the trench opposite the study area.

Nonetheless, this hypothesis is able to explain several aspects of mud diapirism as seen at Mound Culebra. It implies extensive faulting of the entire margin wedge beneath the sediments, providing both pathways for the upflow of deep fluids and, due to rugged wedge topography, a variable sediment thickness. Changes in the stress field as the subduction of seafloor object continues could probably trigger the remobilization of mud on the upper plate. It would make a scenario plausible where deep fluids allowed upwards along faults through the margin wedge gather on the wedge-sediment boundary. Here they may create a density contrast in the low-permeability sediments, which are triggered to start rising buoyantly to the surface by changes in the pressure distribution.

However, this hypothesis does not explain the presence of mounds at locations where no basin is seen on the seafloor. It also fails to determine why Mound Culebra is so close to the edge of the deposition center, rather than being near its deepest point.

A third possibility is conceivable to explain the location of mud domes. Since our direct observations are limited to the sediment cover of the upper plate, we can regard its properties as primarily determined by the topography of the margin wedge. From this viewpoint, diapirs are likely to occur where the basement provides extra depositional space, for instance due to faulting. This appears to be the case near Mound Culebra, as suggested by the deep seismic profile BGR99-39 (Ranero et al., 2003) crossing the area outside of the basin, approximately 10 km southeast of the mound (Fig. 3.19). Near the intersection point with our main high-resolution strike line GeoB02-430, this image reveals a trenchward step down in wedge topography of approximately 500 ms TWT (at offset 41 km). Downslope from this step, the sediment cover appears anomalously thick for about 15 km, increasing the potential to produce overpressured mud at its base.

An indirect consequence and advantage of this explanation is that it does not connect the existence of mud mounds to the presence of locally flattened seafloor. Instead, it emphasizes the influence of deep faulting in the upper plate, which promotes the dewatering of the subducting slab.
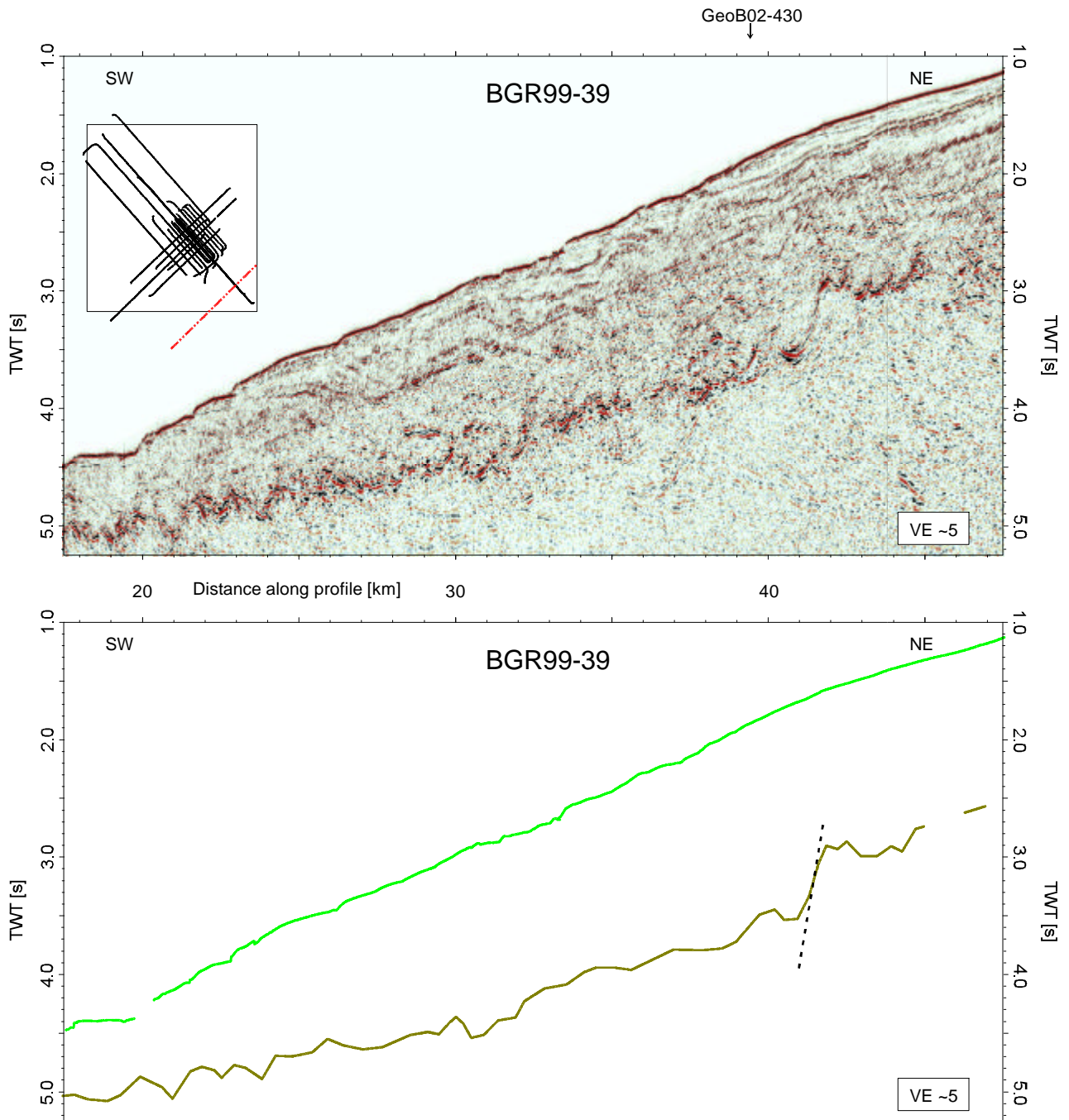
Figure 3.19 a) Deep seismic dip line crossing the study area from Ranero et al. (2003). b) Line drawing of the relevant horizons (seafloor - light green, top of margin wedge - olive green) and probable fault offsetting the wedge surface. Note extra depositional space trenchward of the fault. See text for discussion.

Seismo-acoustic indications of dewatering

One of the important scientific goals of our investigations was to identify and locate subsurface structures that are related to the dewatering and devolatilization of the subduction system.

Seismo-acoustic observations support the interpretation that the most prominent feature in the study area, namely Mound Culebra, is of diapiric origin. Based on their similar morphology and internal structure, - seismic transparence, the truncation of reflectors beneath the flanks, and the disruption of BSR, - the small mounds further northwest are also considered to be mud diapirs. The contribution of these mounds to dewatering is thought to be relatively small, since fluid upflow in diapirs is generally a subsidiary process to mud upwell (Brown, 1990). Further investigations to the role of Mound Culebra in specific are described in the Chapter 4.

Potential locations of focussed outflow in the region are faults that reach the seafloor. Of the different types imaged in our dataset, the one of greatest significance is probably the fault shown in Figure 3.15. It was referred to as "Culebra Fault" based on geochemical - geological observations, which documented fluid expulsion at its surface. The seismic structure of this object suggests that it possibly reaches considerable depth. The importance of other fractures, including the low-angle faults observed in the trenchward portion of the study area, is possibly limited to providing potential pathways to fluids that have penetrated most of the sedimentary column already.

Short intervals of reflection polarity reversals are widespread in the data (e.g. Fig. 3.9). Apart from a few exceptions, their location does not correlate with other subsurface structures or one another, and are interpreted to be independent of dewatering. At one occasion, a polarity reversal caps a buried ridge (Fig. 3.11, offset 16 km), and a structural connection to a nearby fault is possible.

3.5 Conclusions

We have presented structural investigations of a mud dome on the continental middle slope of Pacific Costa Rica. Data included bathymetric, narrow-beam sediment echosounder, and high-resolution streamer seismic profiles.

Derived from observations of surface morphology, reflector topography, seismo-acoustic amplitudes and continuity, specific subsurface features were described and explained. The nature of Mound Culebra was proposed to be diapiric. Characteristic reflection amplitude anomalies in the subsurface were verified to be caused by variations in the style of deposition, due to the filling of canyons and burial of ridges. The types, orientation, and role of deformation were determined, and the rate of movement along low-angle faults estimated.

Based on the above, the fate of sediment in the study area was outlined. It undergoes three distinct processes on different parts of the continental margin: downslope transport in canyons on the steep upper slope; accumulation in a local deposition center around Mound Culebra; and finally, destabilization and gravity-driven creep towards the trench further downslope.

Based on the above, a local tectonic model of the region was portrayed. A distribution of the region from the shelf edge towards the trench, into domains characterized primarily by 1) faulting and tilting, 2) local extension and relative subsidence, and 3) oversteepening and the presence of low-angle listric faults, was presented.

Several hypotheses were confronted in order to evaluate the spatial extent of validity of the tectonic model and its consequences regarding the potential location of mud diapirs. These included a "rule" view and an "exception" view, depending on whether the existence of an extensional regime was deemed a general, margin-wide feature or the result of anomalous circumstances. A third, minimalist explanation was proposed to overcome some of the difficulties of the previous theories.

Finally, the relevance of observed features in terms of fore-arc dewatering was briefly discussed. In the next chapter, this last item is further elaborated through a detailed analysis of the role of Mound Culebra and its vicinity in the fluid output of the Costa Rican margin.

4

Gas Hydrates, Heat and Fluid Flow on the Continental Fore-arc - Seismic Observations in the vicinity of Mound Culebra mud dome, Costa Rica

(Fekete, Grevemeyer, Spiess, Reston)

4.1 Introduction

On the following pages, observations of a reversed-polarity bottom simulating seismic reflector (BSR) in the Costa Rican fore-arc are presented. In settings with gas hydrate-bearing sediments, such horizons are interpreted to mark the bottom of the hydrate stability zone. Since gas hydrate stability is primarily a function of temperature and pressure, BSR topography can be used to reach conclusions about the thermal state of subsurface. This is achieved through the calibration of subsurface thermal parameters with *in situ* heat flow measurements. In regions of high deformation rates and active fluid flow, BSR-derived heat flow helps localize and quantify these processes. In addition, the effects of gas hydrate presence and stability, fluid / heat advection, and ongoing deformation are discussed in detail.

Gas hydrates are found abundantly within continental margin sediments (Kvenvolden, 1988). They are crystalline substances composed of cages of water molecules that host molecules of gas (Dickens and Quinby-Hunt, 1994) and, where present, generally occupy the shallow subsurface down to a few hundred meters below seafloor. The occurrence of gas hydrates is controlled by a number of factors, including gas abundance and composition as well as the chemical properties of both pore fluid and host material, but potential gas hydrate volume is found to be primarily determined by subsurface temperature and pressure (Dickens, 2001).

Hydrates are stable in cold, high-pressured settings (Fig. 4.1). This phase diagram defines their subsurface location: in offshore environments, gas hydrates occur where water depths provide enough pressure (> 250 - 300 m, Ganguly et al., 2000), but subsurface temperatures do not exceed stability values (< ~ 2000 m below seafloor, Kvenvolden, 1988). Should conditions leave the stability interval, gas hydrates dissociate, releasing significant amounts of free gas.

Seismic images of hydrate-bearing sediments often display a distinct reflector several hundred milliseconds of two-way travel time below seafloor (TWT bsf). It is characterized by reversed polarity compared to the seafloor arrival, and approximately mimics its topography across geological layering. While the BSR is generally interpreted to mark the base of hydrate stability zone (HSZ) (e.g. Hyndman and Davis, 1992), it is thought to be primarily caused by the seismic impedance drop at
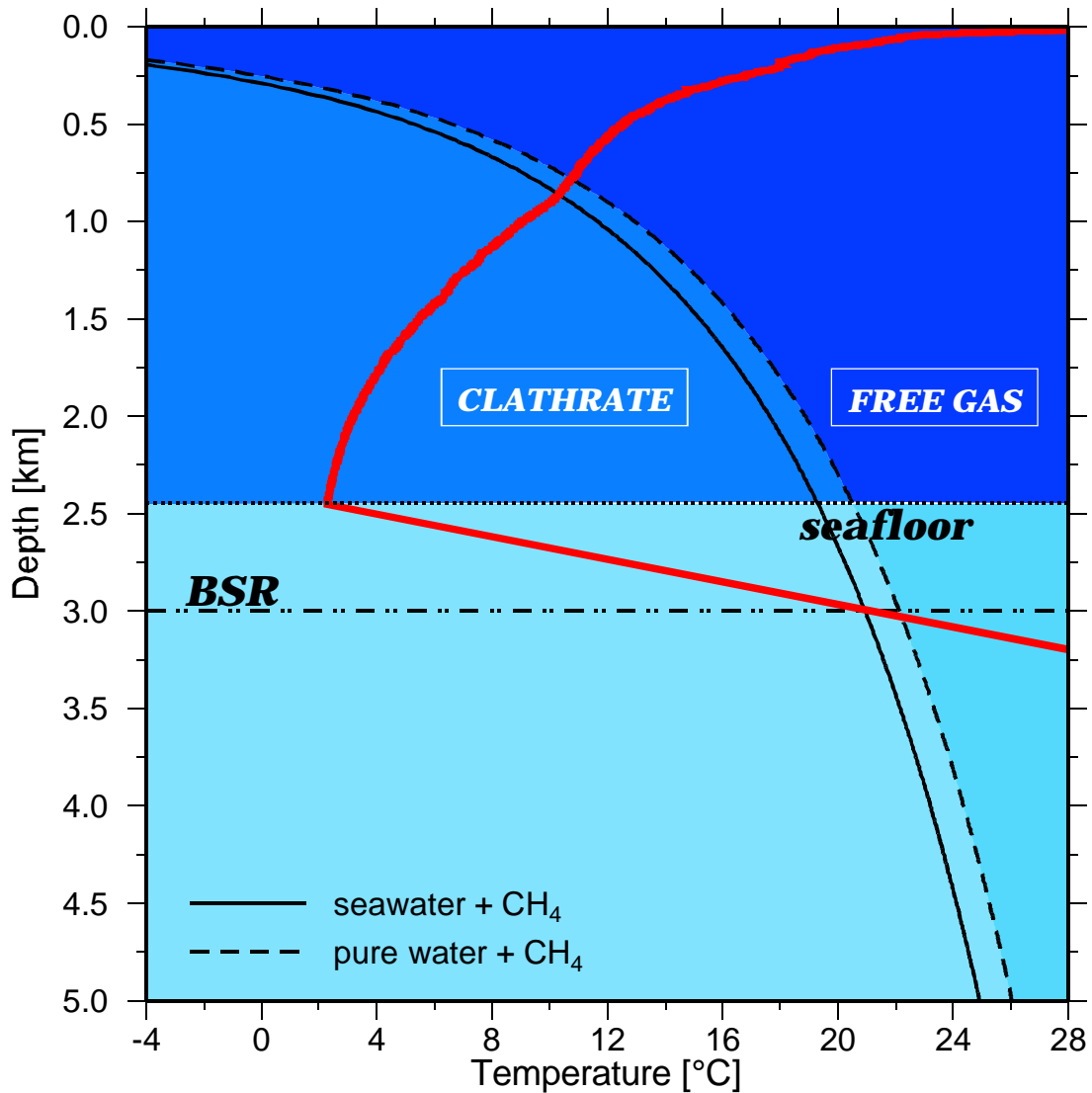
Figure 4.1 Phase diagram of methane hydrates in fresh (dashed line) and seawater (solid line) environments. Left of the two curves, methane is stable in hydrate form, while on the right, it dissolves into free gas and water. Temperature (marked red) above and below the seafloor defines the hydrate stability zone, at the lower boundary of which a characteristic seismic reflector, the BSR, may form.

the transition from the upper, hydrate-bearing strata to the sediments with pore space containing free gas (eg. Bangs et al., 1993). Therefore, a BSR is not necessarily imaged everywhere where gas hydrates are present in the subsurface: its reflection strength is at least in part controlled by the amount of free gas in the pore space.

The sedimentary effect of gas hydrate presence is not entirely understood. Gas hydrates are often assumed to increase the cementation of sediments and decrease their permeability. In consequence, hydrates are thought to clog fluid pathways, thereby preventing consolidation or trapping mobile material. They may also cause major landslides upon regional dissociation (e.g. Mienert et al., 2005). Alternatively, hydrates may form part of the pore fluid, or of the sediment matrix (Eckert, 2001).

In any case, the presence of gas hydrates in the pore space is thought to affect material migration conditions, and is therefore relevant in fluid flow investigations. This also implies an indirect effect of gas hydrate presence on the thermal state of sediments, since fluid advection may transport excess heat from depth. On the other hand, because of their sensitivity to thermal variations, hydrates are excellent and fast indicators through their dissociation of temperature increasing beyond the stability range.

In the reverse case, when sediment enters the HSZ, adjustment to the new conditions is probably much slower, and necessarily controlled by additional factors such as the availability of hydrate constituents, namely free gas and water. That again is strongly related to the spatial distribution and rate of fluid migration.

Where a BSR is present in the subsurface, these variations cause its properties - for example its reflection amplitude, its depth below seafloor, or its continuity - to change significantly. Thus, with some assumptions listed below, the thermal regime of the subsurface can be imaged seismically.

From a thermal point of view, the subducting lithosphere in Central America consists of two domains. The northern domain of EPR (East Pacific Rise) crust, approximately 24 Ma old at the trench, has been reported to be anomalously cold compared to both global mean values and CNS (Cocos-Nazca Spreading Center) crust subducting further south. Heat flow is about 70 % less than predicted by normal convection models for oceanic plates of similar age. The deficit is thought to be caused by a complex and vigorous hydrothermal circulation, aided by the presence of basement

outcrops and enhanced lateral permeability (Fisher et al., 2003). The thermal state of the oceanic plate also reveals profound changes parallel to the trench axis (Soeding et al., 2003).

The continental fore-arc is necessarily influenced by the thermal properties of downgoing slab. Unusually low and constant background values are attributed to gradual reheating of the lower plate as well as dewatering along the plate boundary and through the margin wedge (e.g. Langseth and Silver, 1996, Kahn et al., 1996, Silver, 2000). Of these two factors, the first one - burial reheating and frictional heating of the oceanic lithosphere - determines the regional heat flow pattern landward of the trench, while dewatering and its small-scale lateral variations are expected to affect heat flow more on a local scale.

Gas hydrates have been recovered from core samples in several locations in the fore-arc of the Middle American Trench (MAT) (Coulbourn et al., 1982, Kimura et al., 1997, Soeding et al. 2003). Widespread occurrence of the BSR has been documented by Pecher et al. (1998), and is observed extensively in the high-resolution seismic data set presented here. In this paper, variations in BSR position and properties are portrayed, together with the modelling procedure used to estimate heat flow values from seismic data. Finally, an interpretation of observed variations is attempted, in particular in the context of deformation and fluid advection through the fore-arc.

4.2 BSR-derived heat flow

Thermal structure of the subsurface

The assessment of the vertical thermal structure of margins is generally derived from heat flow measurements carried out on the seafloor. Heat loss q is not recorded directly, but calculated from the thermal conductivity, k, of the near-surface material and the geothermal gradient, dT/dz: $q = k * dT/dz$.

The vertical temperature gradient and the thermal conductivity can be measured *in situ* in the shallow subsurface at selected locations. Between and beyond measurement points, predictions about the thermal field may be produced using temperature-dependent processes, such as gas hydrate dissociation at the base of HSZ. Where a BSR is imaged, local heat flux can be estimated from its depth (e.g. Grevemeyer and

Villinger, 2001). Input parameters for this analysis are seismic velocities within the subsurface, seafloor temperature, and the thermal conductivity of material between seafloor and BSR.

Velocity analysis

Velocity analysis was carried out at ten CDPs on the relevant (mound-near) portions of two main seismic lines crossing Mound Culebra, one parallel and one normal to the trench. CDP gathers, stacks, and semblance images were used to find the most likely acoustic velocity values at each location. Apart from the BSR, reflectors suitable for velocity analysis were generally restricted to the upper 250 ms TWT bsf. Beneath that region, reflectors are scarce and reflection amplitudes too weak for conclusive analysis. Estimates in the lower part of profiles are therefore less well constrained. While coherent reflectors are absent beneath the mud mound, reflection segments are well enough imaged in CDP gathers at several bins to yield velocity estimates of similar accuracy to the surrounding analysis locations. Results were subsequently compared to and found to be in good agreement with laboratory acoustic velocity measurements on core material (Soeding et al., 2003, Flueh et al., 2004, Moerz et al. 2005b) and expected values from literature (e.g. Grevemeyer and Villinger, 2001, Kimura et al., 1997). An example of a final velocity profile is shown in Figure 4.2.

Thermal parameters

The thermal parameters of shallow sediments are based on *in situ* measurements in the area, carried out in the summer of 2002. Data were recorded at several stations along two profiles, one collocated with the seismic line BGR99-39 for assessing regional background values, and one along the main high-resolution MCS strike line GeoB02-430 across Mound Culebra (Fig. 4.3). Geothermal gradients were measured with outriggers mounted on a gravity corer and with a Lister probe. Thermal conductivities were taken both *in situ* and in laboratory settings by needle probes, which were inserted into undisturbed areas of split cores recovered from the seafloor. Measured values were inverted jointly to yield surface heat flow (Soeding et al., 2003, Grevemeyer et al., 2004). These measurements provided a means of calibration for
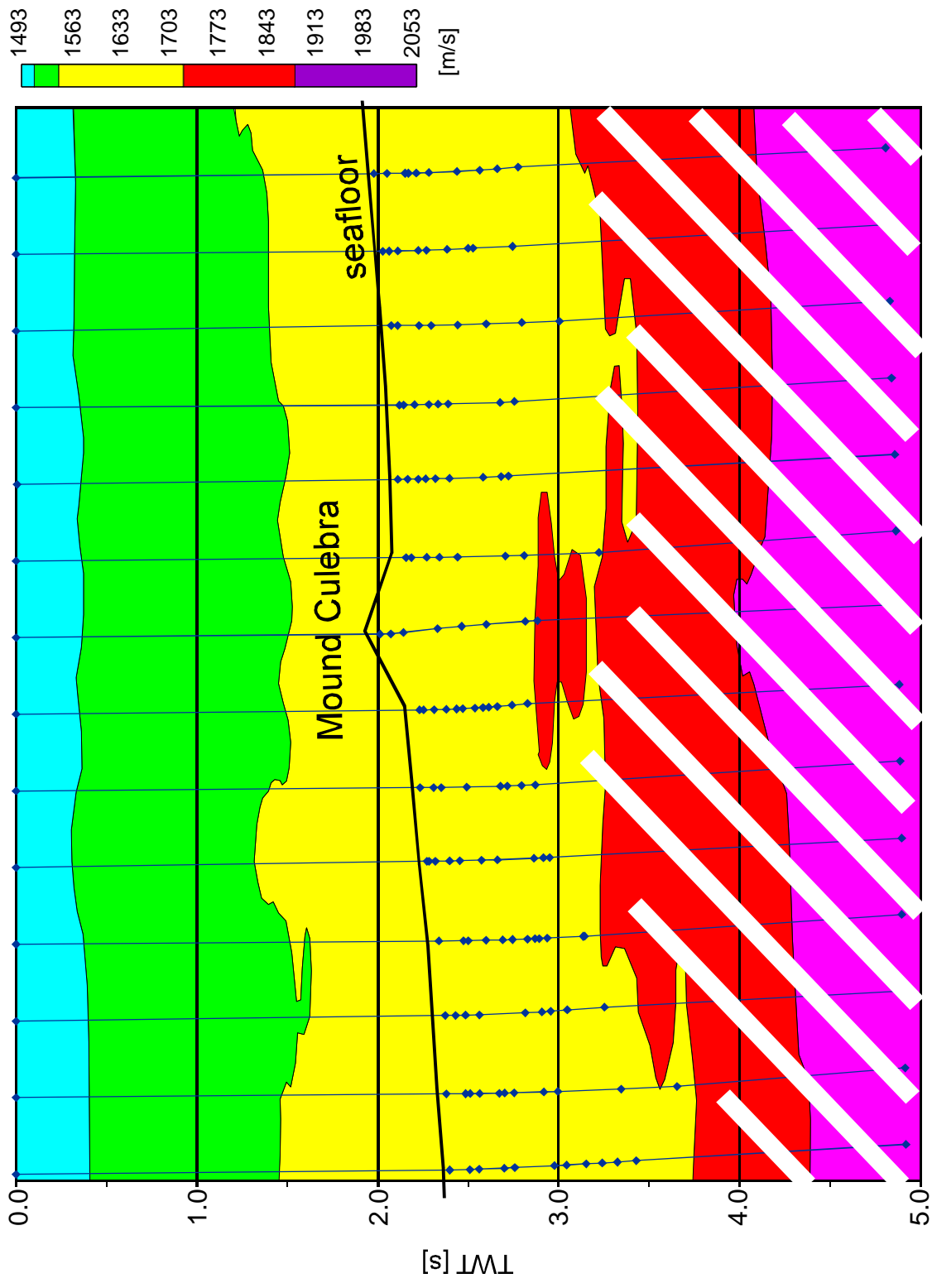
Figure 4.2 Velocity distribution along the main strike profile GeoB02-430 above Mound Culebra. Analysis locations are 1 km apart. Colour code shows interpolated velocities. Measurement points are marked (blue dots). Velocities of 1500 m/s and 2000 m/s are assumed on the surface and at the lower profile end, respectively. The lowermost portion (hashed white) is not well constrained. Seafloor and Mound Culebra are shown. Although not obvious with the rough colour coding, Mound Culebra is revealed to have elevated acoustic velocities with respect to its surroundings.
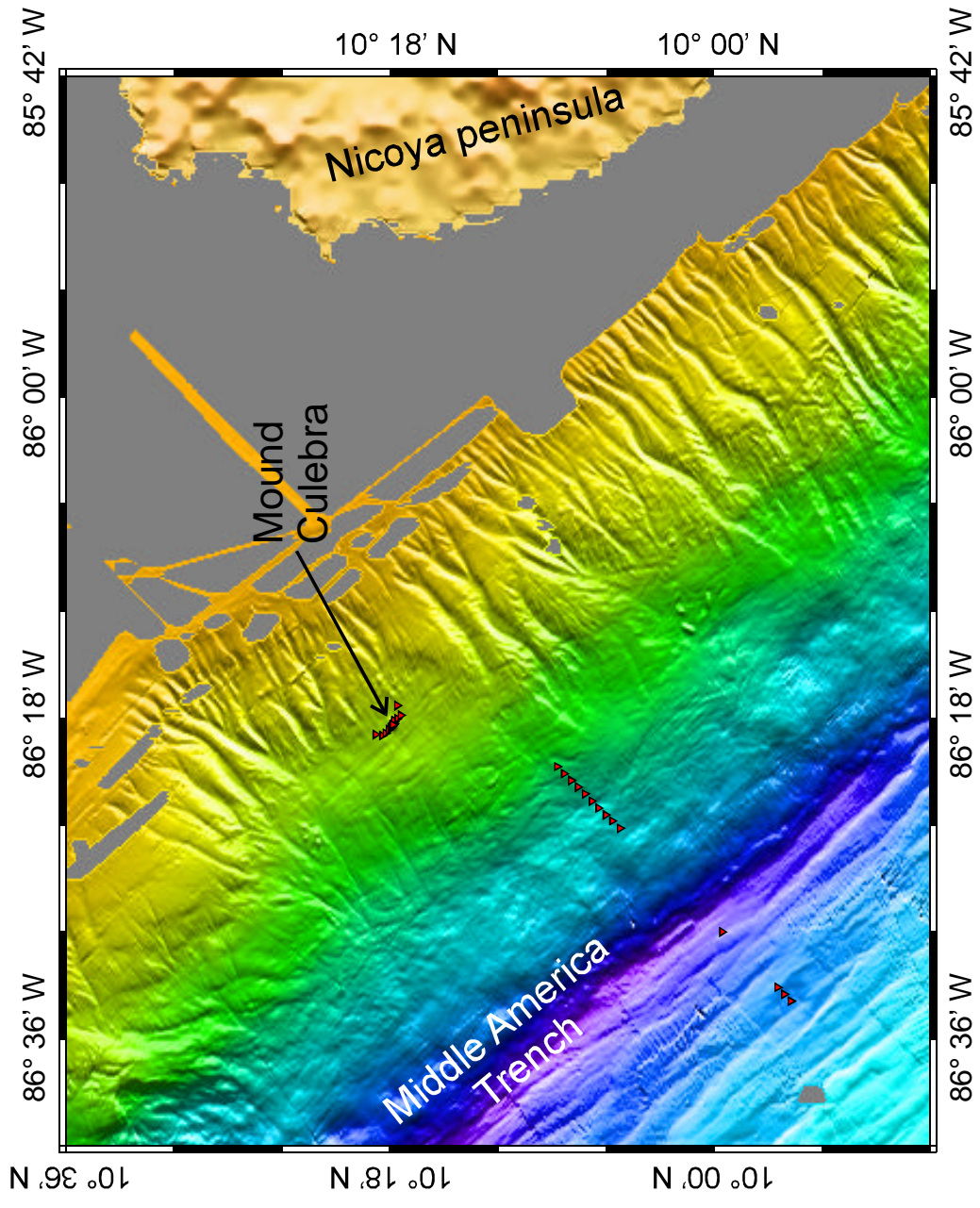
Figure 4.3 Location of in situ surface heat flow measurements (triangles): background profile across the Middle America Trench along the deep seismic line BGR99-39, and 16 stations above and near Mound Culebra.

heat flow estimates from BSR depths, such that where both types are available, they should agree within accuracy limits (Fig. 4.4).
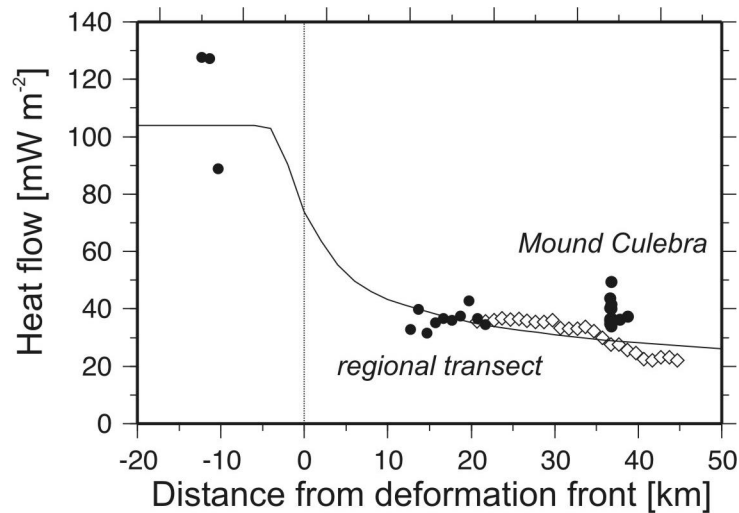

Figure 4.4 Comparison of directly measured surface heat flow to values derived from BSR depths and to a conductive model. Solid circles - in situ heat flow values, open diamonds - BSR-derived data. Background conductive heat flow is shown (solid line). After Grevemeyer et al., 2004.

Variable topography influences heat flow measurements. Thermal refraction results in elevated heat flow near concave-up morphology and low heat flow values for example on mound summits. The effect can and should be corrected around larger topographical features (e.g. Grevemeyer et al., 2004). Fig. 4.5 shows the correction of directly measured values.

Heat flux estimated from BSR depth was not corrected for the effect of thermal refraction. On one hand, perturbations in the temperature field decrease exponentially with distance. Therefore, distortion should be much smaller for data at depth than for surface heat measurements. On the other hand, only two features are significant enough to noticeably influence results in the study area. Below one of them, Mound Culebra, BSR is not imaged; therefore, heat flow estimates cannot be calculated. The other location only concerns one profile above the canyon system on the landward edge of the area, and is not the focus of our investigations.
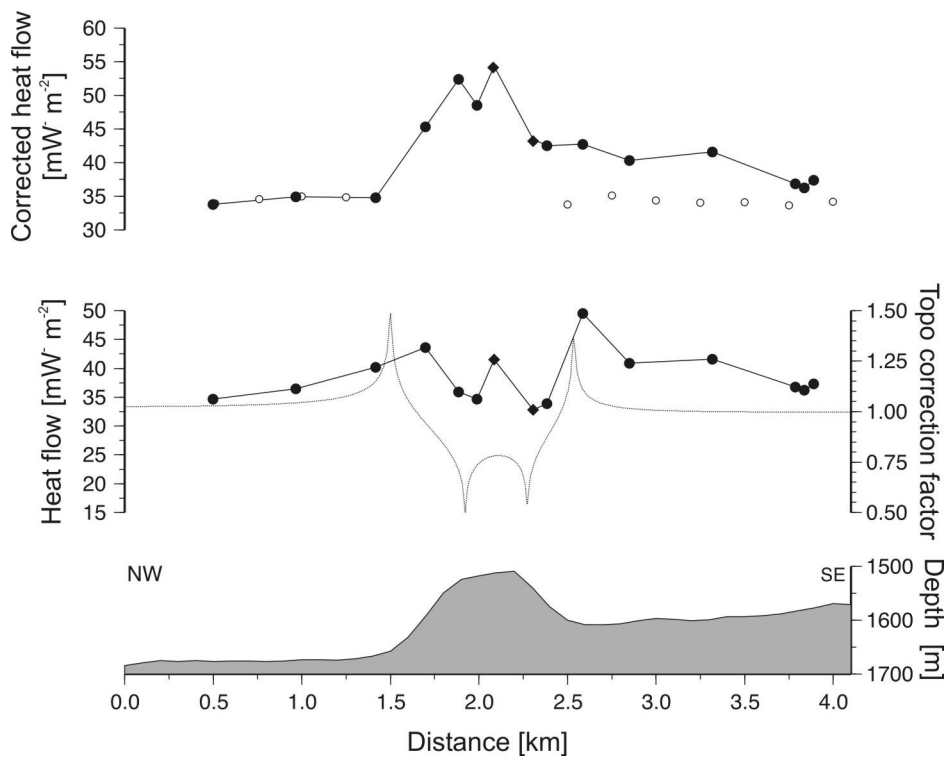
91

Figure 4.5 Effect of topographical heat refraction. Bottom: topography, middle: observed heat flow values (solid circles) and normalized effect of heat refraction (dashed line), top: corrected data. Note discrepancy relative to BSR-derived values (empty circles) southeast of Mound Culebra. After Grevemeyer et al., 2004.

While the accuracy of estimated heat flow is highly dependent on the assumed input parameters (primarily *v* and *k*), the existence of relative variations is not. Localized anomalies, especially those associated with potentially dewatering-related structures, should be considered real.

4.3 Observations and model calculations

Seafloor temperature

Seafloor temperature in the modelling is approximated by that of bottom water. This was acquired by vertical CTD profiling in the vicinity and is assumed to be laterally uniform, only a function of water depth. Typical values range between 2.7 - 3.1°C.

The accuracy of approximation is affected by temporal as well as spatial variability of bottom water temperatures. Seasonal changes are likely to increase errors, since temperature measured by the CTD in a matter of hours may not reflect yearly average values. A one-degree difference in ambient temperature would correspond to a BSR depth shift on the order of 25 m. Another source of error is the assumption of lateral uniformity. While the target area is relatively small in size, strong topographical variations (e.g. near Mound Culebra) probably induce strongly localized surface temperature anomalies. However, since temperature variations are strongly attenuated with depth, it is unlikely that they attain dimensions where they significantly influence BSR position.

Geothermal gradient

Geothermal gradients were calculated from the temperature difference between seafloor and BSR, and the reflector depth. A linear gradient, although a simple approach, is thought to be appropriate to describe subsurface temperature distribution in the area. According to an error analysis by Grevemeyer and Villinger (2001), deviations from this model would be hard to resolve even with downhole tools. Active fluid advection at rates of a few cm/yr would generate non-linear temperature gradients, however, even direct gradient measurements at a probable discharge site failed to detect such an effect (Grevemeyer et al., 2004). Values between 23 and 42 K km^{-1} were derived from the BSR depth, which correspond well within accuracy limits to thermal gradients measured *in situ* on the mound (28.7, 38.6, 47.7 K/km, Soeding et al., 2003).

Thermal conductivity

Thermal conductivity in the first few meters below seafloor was measured to be approximately 0.85 W m^{-1} K^{-1}. Since thermal conductivity is influenced by porosity, it increases with depth. Following the argument of Grevemeyer et al. (2004), a mean value of 0.95 W m^{-1} K^{-1} has been taken to be representative of the subsurface down to BSR depths in subsequent calculations.

Model calculation

Figure 4.6 shows the time delay of BSR arrivals in ms TWT with respect to seafloor return. A general trend of landward shoaling is modified by deviations of limited lateral extent. Heat flow values are estimated from BSR depth following the empirical relationship determined in a system of methane hydrate and seawater by Dickens and Quinby-Hunt (1994): $T^{1} = 3.79 * 10^{-3} - 2.83 * 10^{-4} * log(P)$, where T and P are temperature (K) and pressure (MPa) values at the BSR depth. To calculate pressure, an average acoustic velocity of 1750 m s^{-1}, a density of seawater of 1035 kg m^{-3} (assuming hydrostatic pressure in the sediments) and a constant of gravity of 9.782 m s^{-2} (corrected for latitude) were used. Figure 4.7 displays estimated heat flow. Values are between 22 and 40 mW m^{-2}. Based on the accuracy of input data and on an error assessment of Grevemeyer and Villinger (2001), final heat flow estimates are erroneous up to 10 - 25 %.

4.4 Discussion

Regional trends in BSR-derived heat flow

BSR-derived heat flow shows a gradual decrease away from the trench at a rate of approximately 0.7 mW m^{-2} / km (Fig. 4.7). A (slower) decrease is predicted by subduction zone heat flow models for the first few tens of km arcward: increasing vertical distance between surface and subducting plate - the heat source - is mainly responsible for this phenomenon. However, as several authors have shown, the case of Northern Costa Rica is more complex.

Surface heat flow of the incoming crust has been measured to be about 30 % of values predicted by conductive models (Langseth and Silver, 1996). Values are sometimes lower than above the continental fore-arc, documented for instance along several profiles crossing the trench from the M54-2 cruise in 2002 (Soeding et al., 2003). To explain the thermal state of the continental side, burial reheating and frictional heating during subduction have been proposed.

The heat flow of EPR crust appears to vary significantly along the MAT (cf. Fisher et al., 2003). In this perspective, the presence of any regional trend on the fore-arc is somewhat unexpected, and is possibly only characteristic of an area of limited extent.
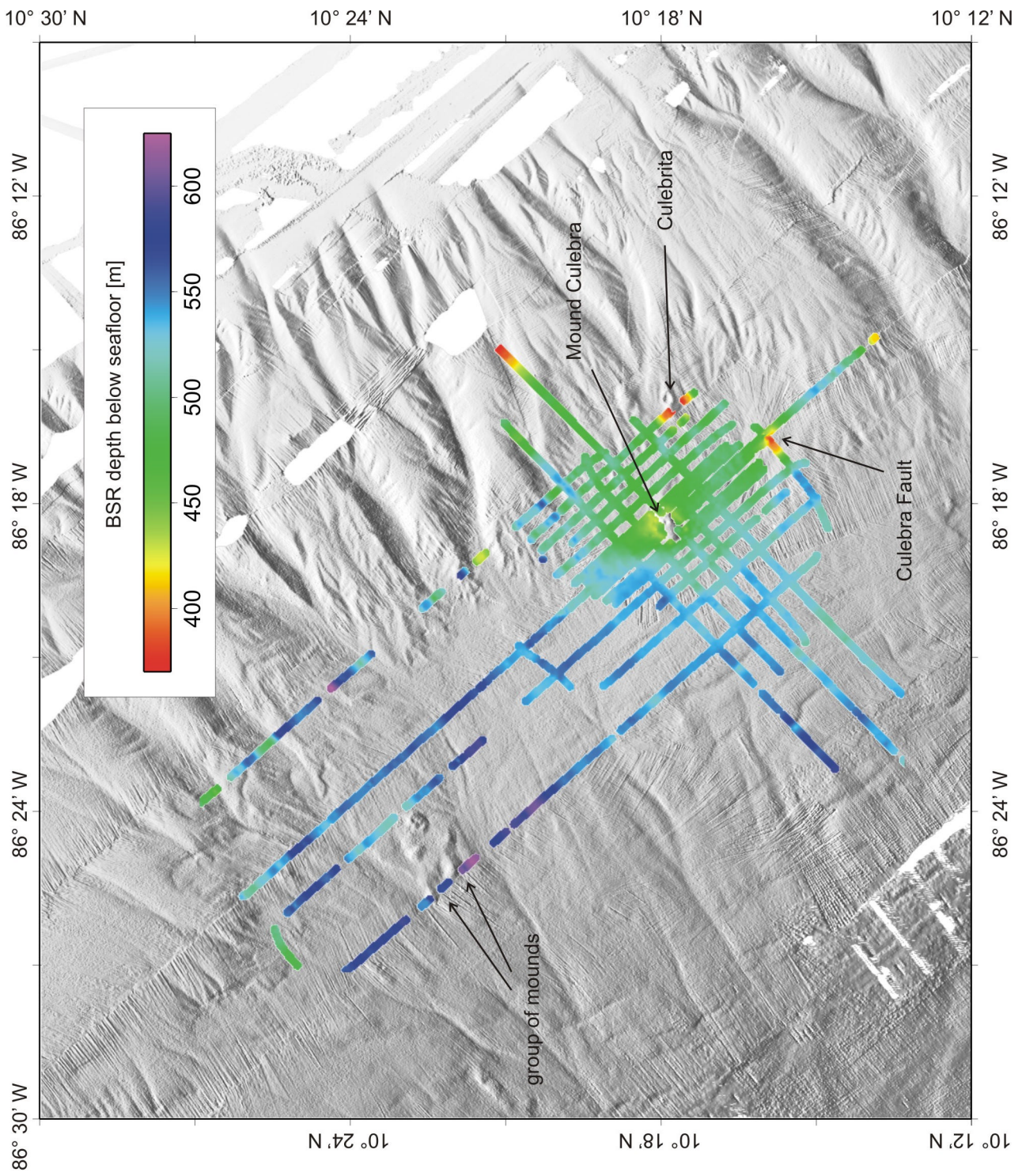
Figure 4.6 Map of BSR depth below seafloor reveals a shallowing away from the deformation front, several locations where the BSR was not observed (eg. beneath Mound Culebra, or near the group of smaller mounds in the northwest), and significant local variation.
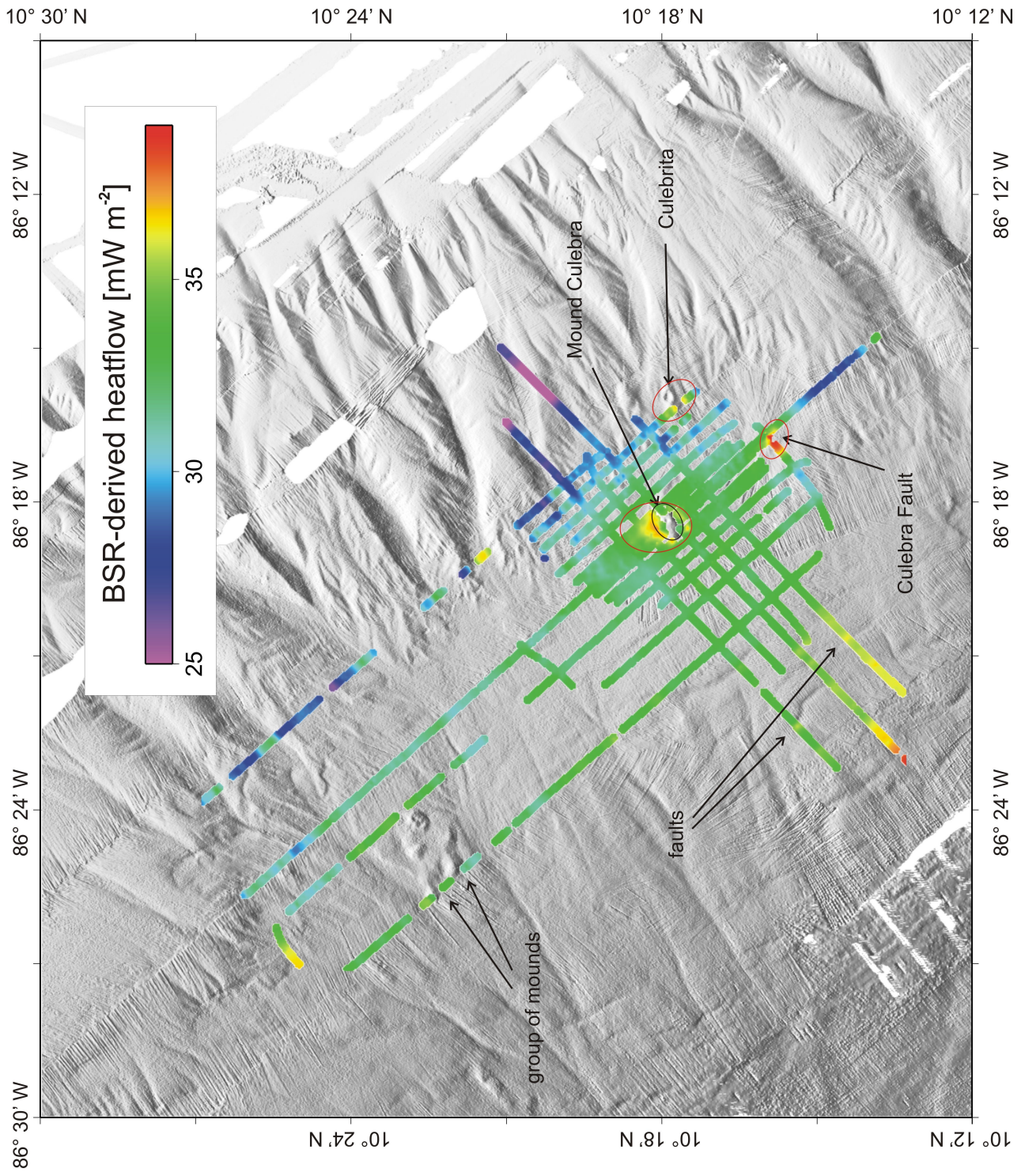
Figure 4.7 BSR-derived heat flow data. Arrows mark characteristic seafloor features, red ellipses highlight locations of anomalously high heat flow. Mound Culebra is outlined in black. See text for discussion.

The M54-2 study has acquired a heat flux profile above the EPR crust approximately opposite Mound Culebra with values which do not show any significant deviation from those predicted by the conductive model (Soeding et al., 2003, Grevemeyer et al., 2004).

A generally accepted explanation of the heat flow deficit above the incoming plate is heat mining via complex and vigorous hydrothermal circulation in the shallow crust. Vertical cell sizes of 100 to 1000 m have been suggested (Langseth and Silver 1996, Fisher et al. 2003). Harris and Wang (2002) have modelled the thermal behaviour of Northern Costa Rican fore-arc and estimated surface heat flow trends for heat mining limited to 500, 1000, or 2000 m below the surface, respectively. In each of their models, heat flow above the lower and middle continental slope increases towards the volcanic arc. Their only curve showing a trend with decreasing heat flow values is that without any hydrothermal cooling on the oceanic plate. It is this latter trend that the pattern revealed by our BSR-derived heat flow values corresponds to (Fig. 4.8).

No regional tendency is observed parallel to the MAT (Fig. 4.9). Unlike in dip profiles, these data are relatively constant, showing only small-scale perturbations that we mostly attribute to variability inherent in the modelled parameters (esp. k and v). In the assessment of local anomalies below, incorrelable variations smaller than ~ 2 mW m^{-2} are therefore not included.

Local variation of modelled heat flow

BSR depth and calculated heat flow values reveal several distinct, localized thermal anomalies in the shallow subsurface. The most prominent of these is near Mound Culebra. Estimated heat flux reaches 38 mW m^{-2} at the northern flank, about 5 mW m^{-2} higher than the average along strike lines. In map view, the anomaly is elliptical, elongated in a trench-parallel direction, and appears not centered above the mound itself (Fig. 4.7), but further north, collocated with observations of chemosynthetic organisms as well as of elevated methane content in the seawater (e.g. Mau et al., 2006).

This lateral offset was not confirmed by *in situ* measurements (Grevemeyer et al., 2004). Directly measured heat flow appears approximately symmetric around the mud dome. Assuming fluid advection as the means of transferring heat, a lateral flow

component southeastward beneath Mound Culebra was proposed to explain the difference (Grevemeyer et al., 2004).

Two other locations of excess apparent heat flux are seen in the data, both related to seafloor morphological features. Southeast of the mound, a segment of a fault scarp has been found to host vent fauna and identified as the source of a methane plume in the water column (Flueh et al., 2004, "Culebra Fault" in Fig. 4.7). The BSR rises steeply in the vicinity of the feature, by about 150 m in 1500 m of lateral distance, and displays a significant drop of reflection amplitude (Fig. 4.10). This indicates the partial escape of free gas from beneath the HSZ, and a thermal influence associated with the fault.

The other site is found east of Mound Culebra ("Culebrita" in Fig. 4.7). Although the circular, crater-like bathymetric feature of 1 km diameter (Fig. 4.11) itself was not crossed by seismic lines, the 4 mW m^{-2} heat flow anomaly in the nearby profile appears to be related to it. The exact nature of this structure remains yet to be examined.

A different type of heat flux irregularities is observed trenchward of Mound Culebra. Several of these are identified in the map of estimated heat flow ("faults" in Fig. 4.7). These anomalies are abrupt, exceed 2 mW m^{-2} in amplitude, and are easy to correlate between neighbouring profiles. They are apparently related to faults offsetting the seafloor, and are located beneath bathymetric steps with no associated variation in the BSR depth below sea surface (Fig. 4.12). An apparent heat flow anomaly in the estimated values here is a consequence of the modelling technique[3] and is not related to thermal processes.

On the other hand, a causal relationship possibly exists at these sites between the faults and the BSR's amplitude decrease. A lack of BSR upwelling indicates that the thermal field in the subsurface remains stable, while the amount of free gas is locally reduced.

---

[3] Seafloor temperature is approximated to be a function of only water depth, and is thus allowed to change in the model from one point to the next. However, any temperature perturbations at the surface would be spatially filtered over the distance to the BSR, the reflector will normally not show abrupt topography. This creates artifacts near bathymetric steps.
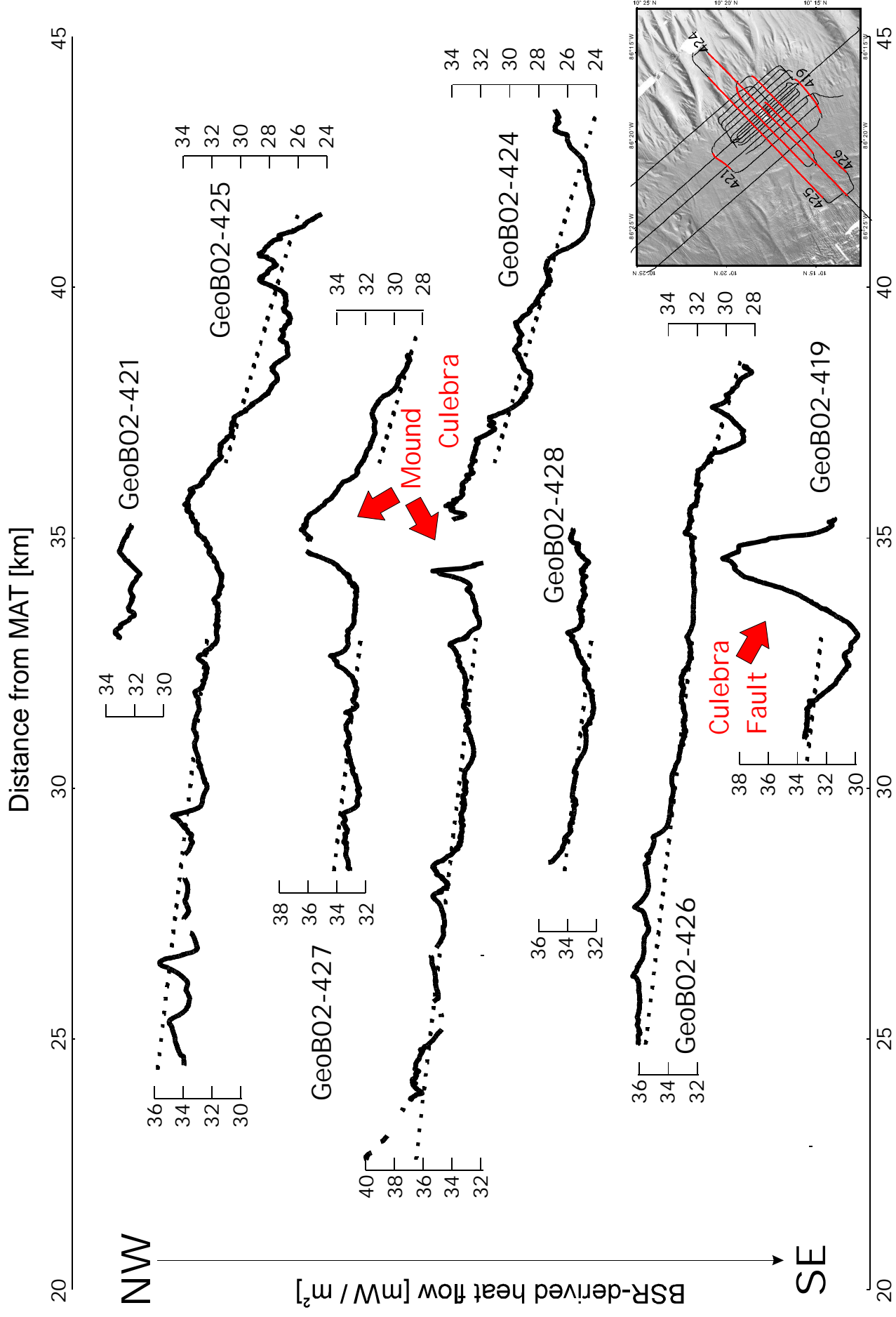
Figure 4.8 Heat flow profiles in dip direction. Values plotted against distance from the trench. Stippled lines display linear trend in two segments: rate of decrease trenchward of Mound Culebra is - 0.4 mW m-2 /km, landwards - 1.1 mW m-2 / km. Insert shows profile locations. Red arrows mark relevant anomaly. For discussion, see text.
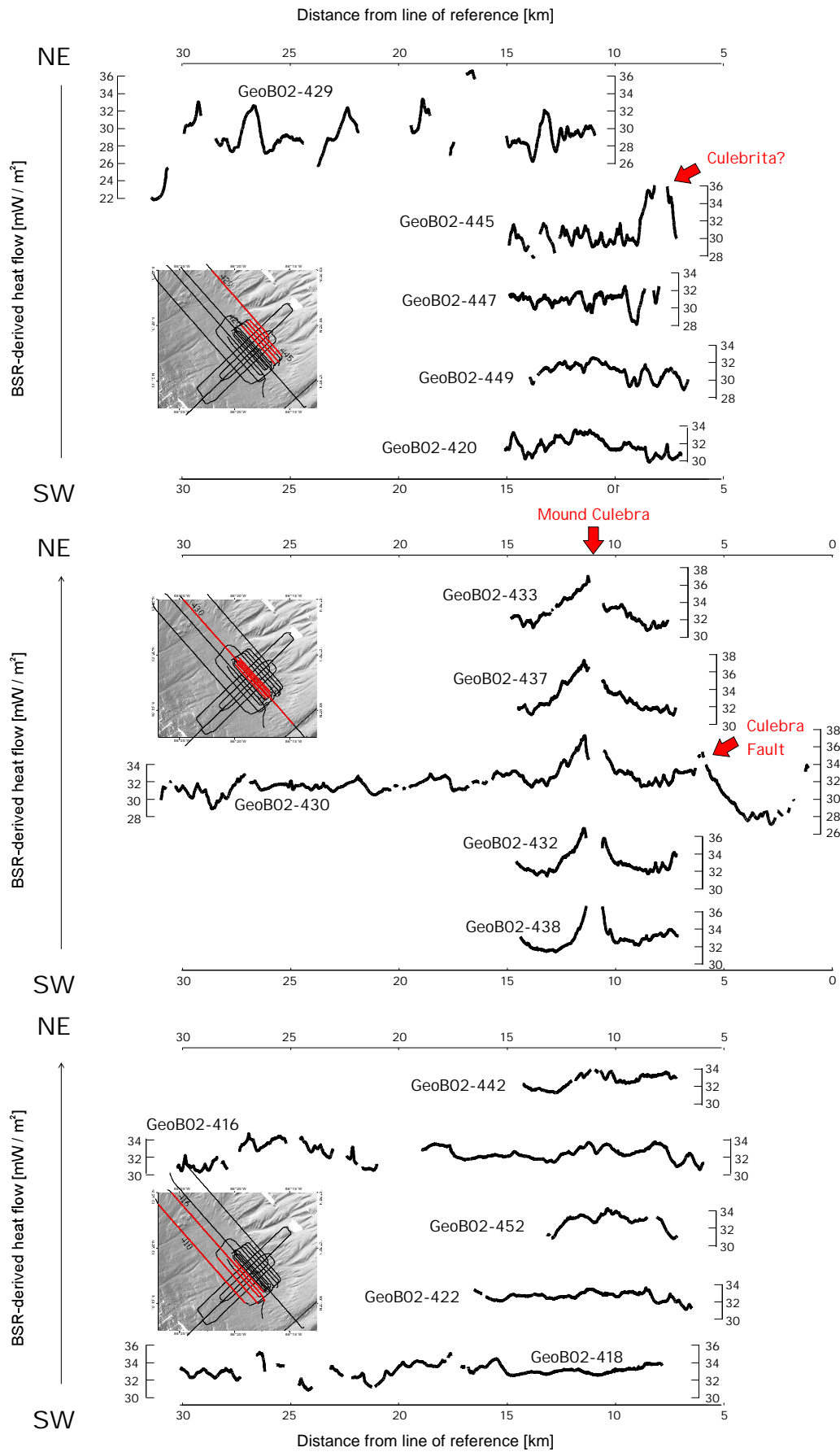
Figure 4.9 Heat flow profiles in strike direction. From bottom to top: trenchward-most, Mound Culebra-near, and landward lines. Values plotted against distance from intersection with deep seismic profile BGR99_39 (stippled line in inserts). Inserts show profile locations. Red arrows show relevant anomalies. No regional trend in the heat flux is seen parallel to the trench.
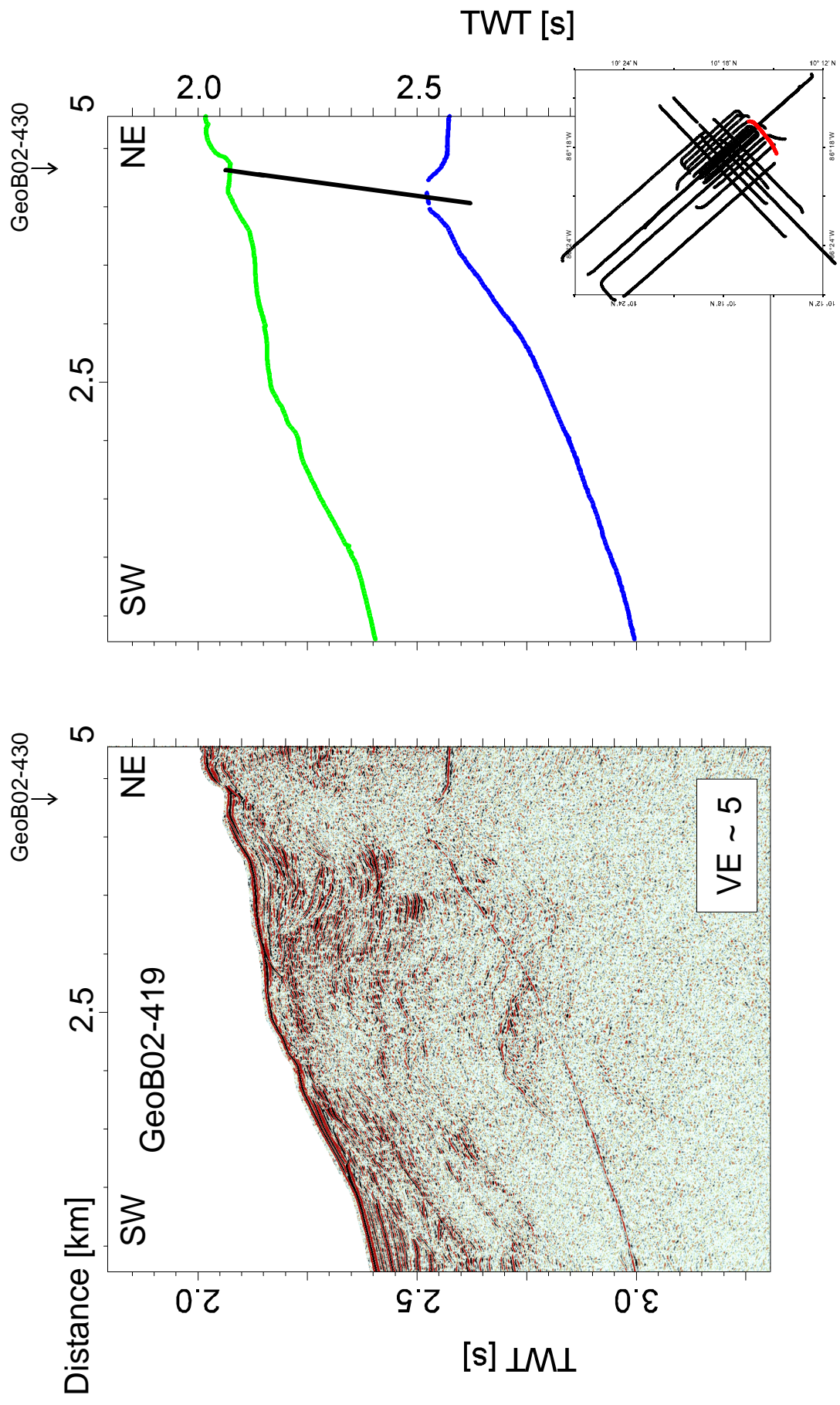
Figure 4.10 Seismic profile GeoB02-419 across Culebra Fault. BSR depth below seafloor decreases by ca. 150 m in just 1.5 km laterally near the structure, and also its reflection amplitude weakens significantly, implying elevated permeability in association with thermal variation.
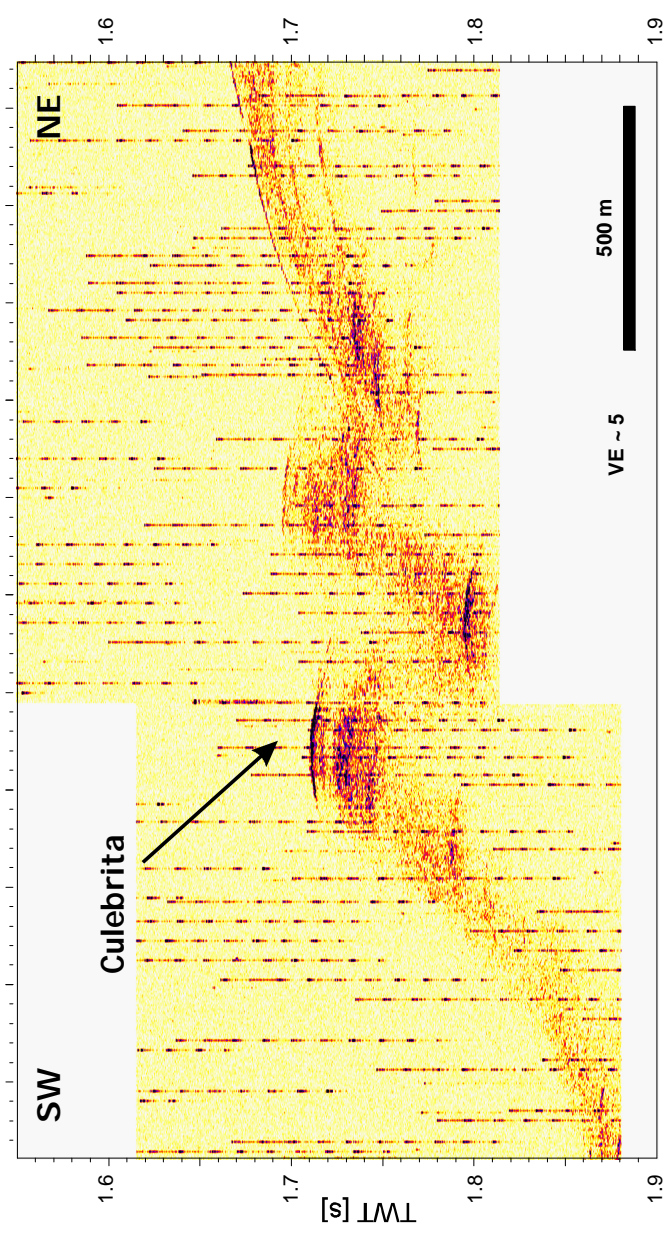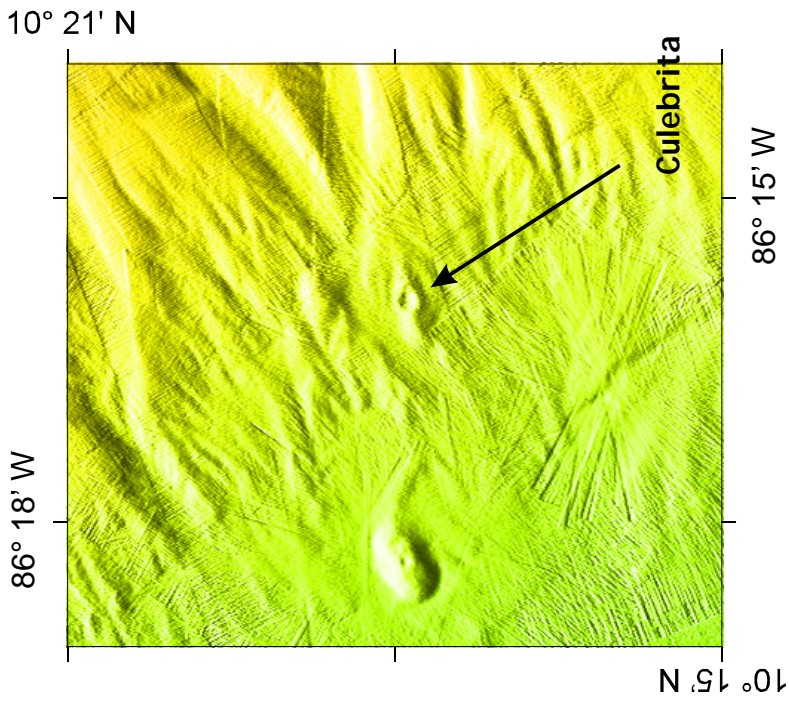
Figure 4.11 Bathymetry and Parasound profile of a crater-like seafloor structure east of Mound Culebra, which is probably associated with a local decrease of BSR depth.

Locations of BSR disruption

One of the most obvious limitations of the seismic method to estimate heat flow is that it can only be done where a BSR is imaged. Although the reflector is widely observed in the study area around Mound Culebra, it is absent at several locations. Some of these are associated with a gradual lateral amplitude decrease (e.g. Fig. 4.13, offset 10 - 12 km), and the presence of these intervals may be explained by reduced free gas content beneath the HSZ as well as by insufficient signal-to-noise ratio. In at least three cases, however, BSR disruption seems abrupt, occurring within a few tens of meters. This is the case beneath Mound Culebra, near Culebrita (Fig. 4.14), at a short segment of the Culebra Fault in the southeast, and beneath each of the smaller mounds in the northwest. (Compare also to Fig. 3.11.)

Several explanations may be given for the unexpected lack of the seismic reflector. One is data acquisition limitations, either in the form of low S/N ratio, or the occurrence of reflections that are too steep to image with a surface-towed short streamer system. Decreasing S/N values during acquisition will generally result in a gradual degradation of imaging quality, while in the observed cases, this transition happened within just a few CDPs. Beneath Mound Culebra, stacked sections display seismic diffracted energy on both sides of the disruption, which is a clear indication of actual BSR termination. As for reflector geometry, since on small scales BSR mimics seafloor topography, it is unlikely that the seafloor reflection would be perceived while the BSR is beyond equipment capacity.

Another possibility is that reflections are masked by high-amplitude arrivals in the shallower subsurface. However, such abrupt amplitude anomalies, stretching laterally to the same extent as the absent BSR, are not seen in the data.

A complete lack of gas hydrates above the missing reflector segments would possibly also result in BSR disruptions. Should this be the case, it would require enough excess heat to dissociate all hydrates in the stability zone. This would cause significant shoaling of the reflector outside the interval of disruption. There is no indication for such a strong thermal anomaly in the area.

The remaining plausible alternative is an absence of free gas below the HSZ. For the small lateral extents in question, this appears most likely if gas is either used up or has

moved away from some locations. The first possibility may occur if the temperature-pressure distribution of subsurface is presently changing such that gas hydrates are forming at a faster rate than gas can be created at or transported to the stability zone. Since the continental fore-arc is undergoing regional subsidence, gas hydrates are likely to be forming, at least away from positive heat flow anomalies. Sediment permeability may be locally low enough to prevent the formation of a BSR. Alternatively, free gas may escape either laterally, within permeable strata below a stratigraphic seal (such as the base of HSZ itself may be), or vertically along structural pathways. A combination of all three processes is the most likely to take place at the sites of abrupt BSR disruption.

4.5 Interpretation

Heat flux above the EPR crust and on the continental side of the trench

In situ observations of low heat flow on the oceanic plate opposite Nicaragua as well as central Nicoya peninsula (Langseth and Silver, 1996, Soeding et al., 2003, Fisher et al., 2003) indicate an anomalously cold oceanic plate segment. In contrast, our model calculations and direct measurements across the trench near Mound Culebra seem to reveal heat flow values close to those expected from a simple conductive model. Several ways are possible to reconcile this contradiction. Fisher et al. (2003) put forward the presence of basement outcrops, coupled with significant lateral permeability, as most plausible explanation for observed low heat flux. This would allow a patchiness in EPR heat flow patterns, and the presence of regions away from basement outcrops with values close to predicted. The plate segment subducting beneath Mound Culebra possibly represent such a region. Alternatively, lower plate thermal properties may return to "normal" faster with the shutting off of circulation after burial than predicted by Harris and Wang in their study (2002). The possibility of an additional heat source also has to be considered.

From this perspective, the lack of trench-parallel variation in our data is attributed for the most part to the small size of the surveyed area.

Relationship to structural observations
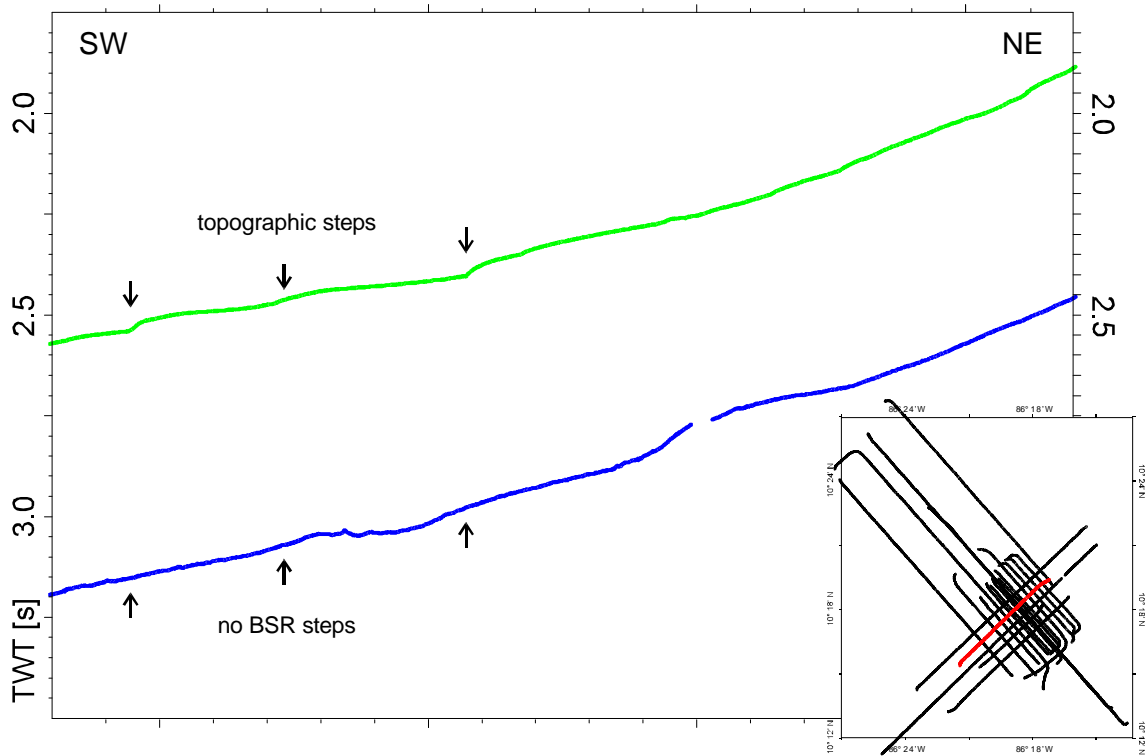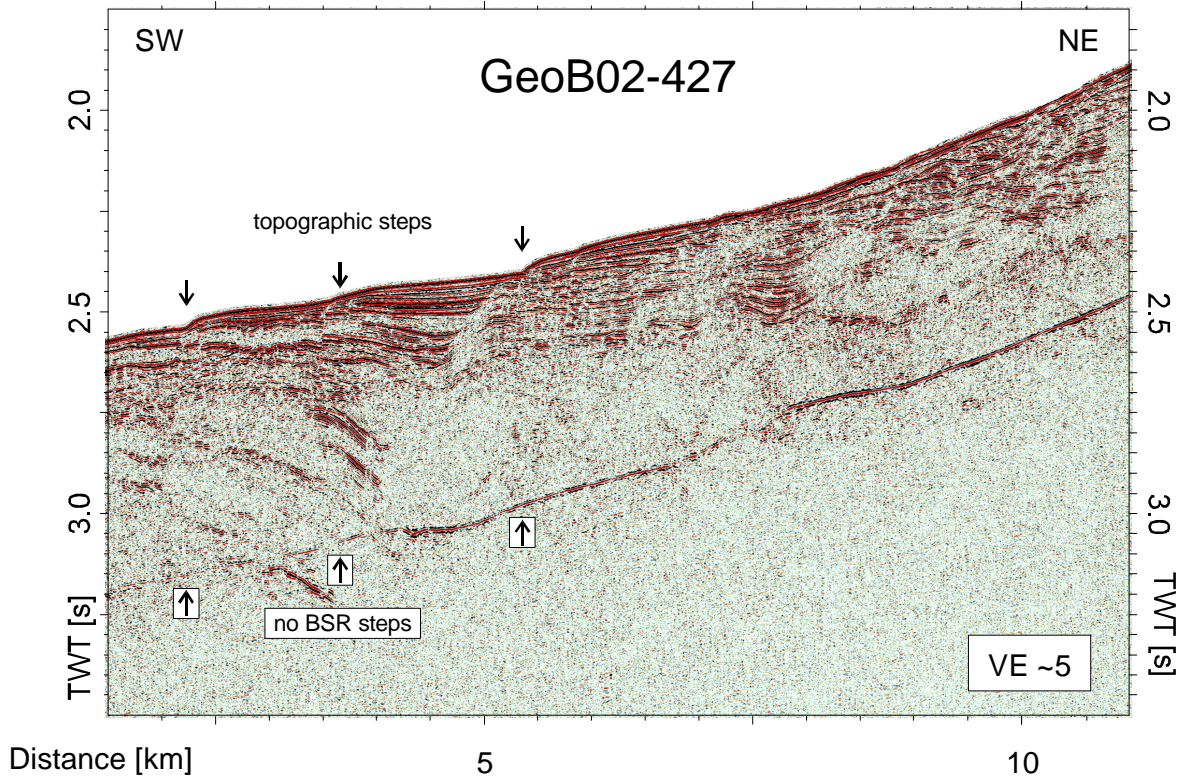
Figure 4.12 Seismic profile GeoB02-427, showing seafloor and BSR topography at the locations of several faults. Apparent anomalies in calculated heat flow, associated with these structures, is a consequence of the modelling technique and is probably not related to thermal processes.

Figure 4.13 Seismic profile GeoB02-416, showing the BSR to weaken and disappear towards the northwest. This gradual reflection amplitude decrease may be explained equally well by a decreasing signal-to-noise ratio of the data and by a gradual decrease of gas content beneath the HSZ.

Figure 4.14 Seismic profile GeoB02-445, showing abrupt BSR to shoal and disrupt near Culebrita.

The rate of landward heat flow decrease appears to change approximately 35 km from the MAT, beneath Mound Culebra (Fig. 4.8). Although the relatively small amount of data 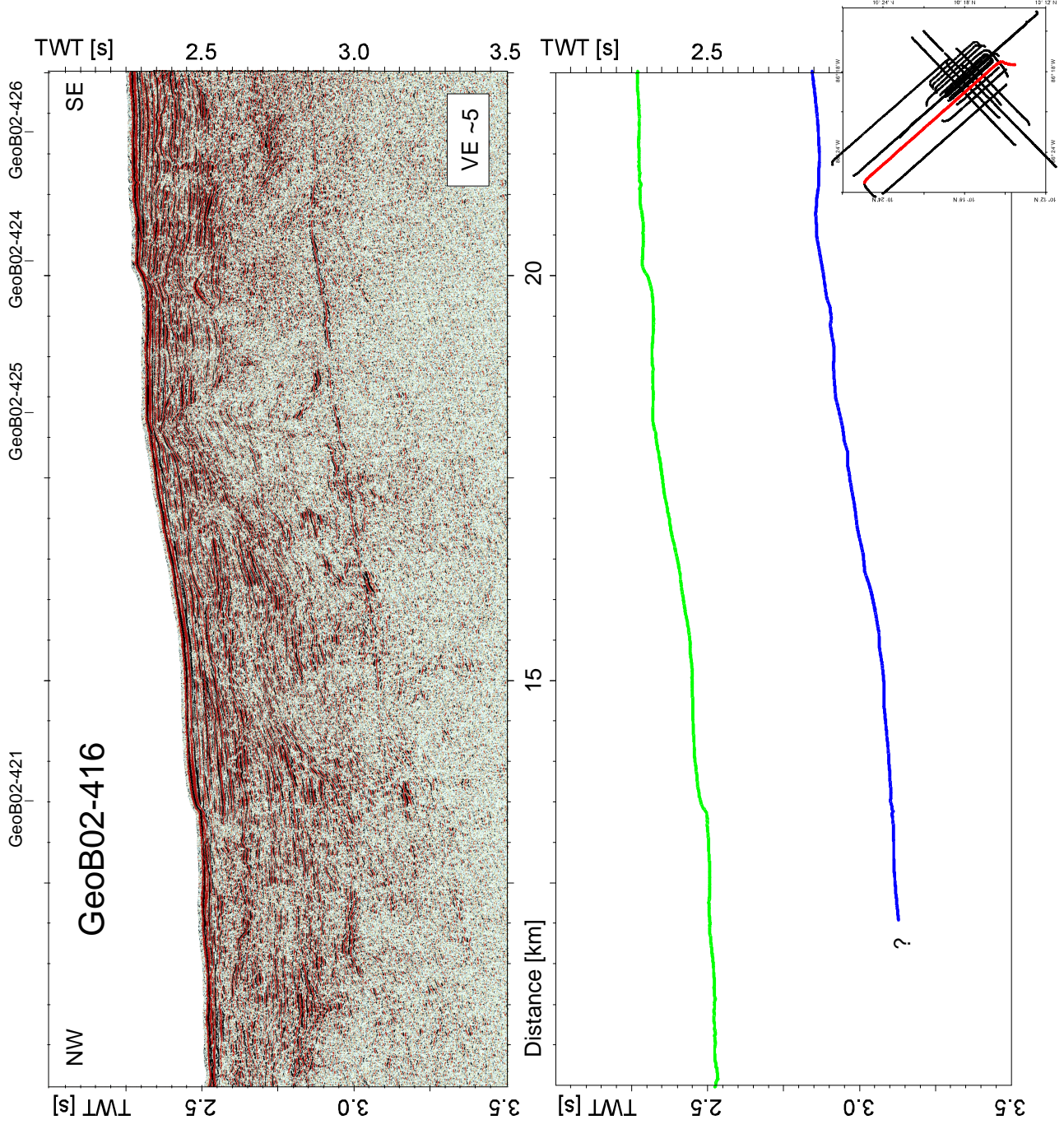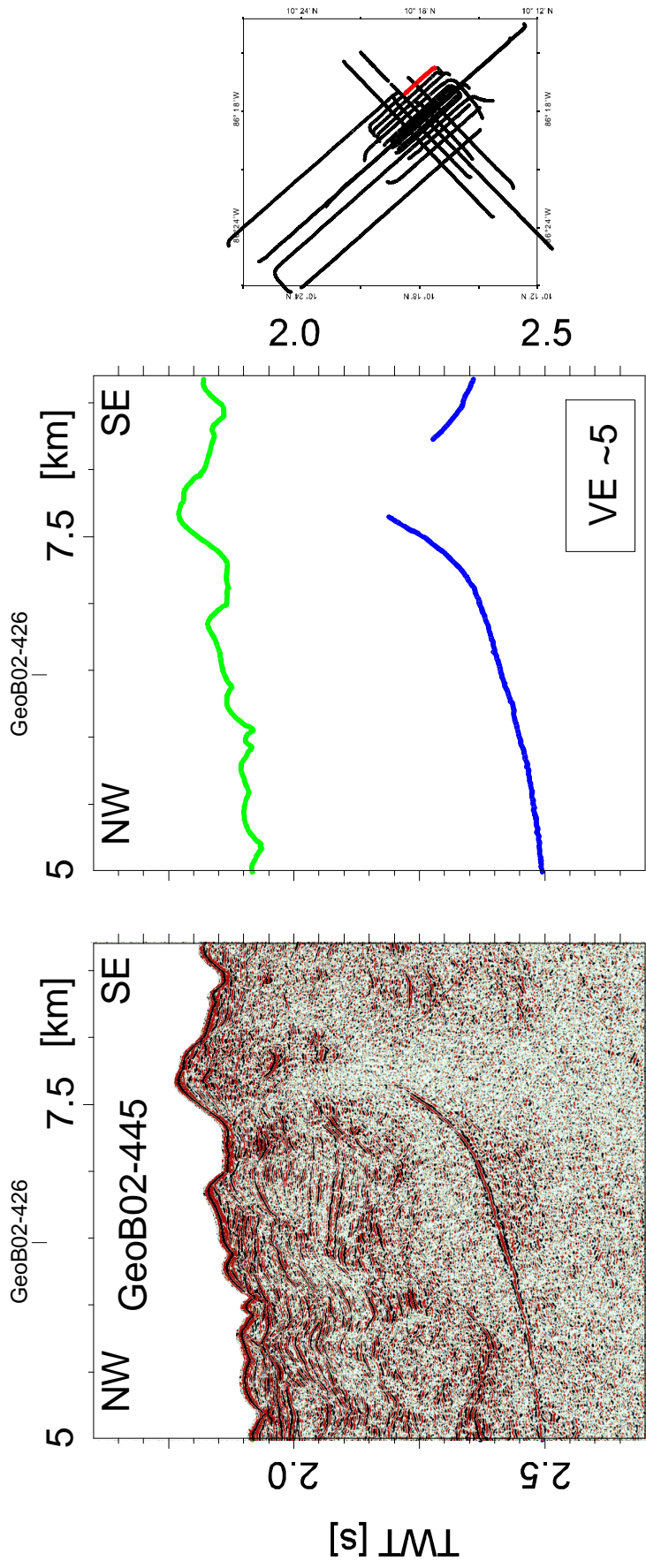available limits the statistical significance to derive robust conclusions, it seems that the rate of decrease rises from 0.4 mW m^{-2} per km, trenchward of the mound, to 1.1 mW m^{-2} per km upslope of it. The location of this apparent change coincides with the change in regional structural setting to local extension described in Chapter 3, and supports the tectonic model presented there. It may ultimately be related to an increase of dip angle of the subducting plate from 6° within the first 30 km of subduction to 13° in the next 30 km (Christeson et al., 1999).

The absence of heat flow anomalies associated with trench-parallel faults downslope of Mound Culebra is also in good agreement with their interpretation as being of low-angle listric nature. Examples of decreased BSR amplitude in their vicinity point to sufficient permeability along the fault planes for the migration of gas, and the constant depth of the reflector indicates that their role in the upward transport of deep-sourced warm fluids remains indirect.

Indications of dewatering

Within the studied area, estimated heat flux indicates probable dewatering related to several bathymetric features. These include a fault scarp, a mud diapir, and possibly a small, crater-like seafloor structure. All three sites are associated with a local decrease of the BSR depth below seafloor as well as its disruption. For the most prominent anomaly, that above Mound Culebra, a rough estimate of flow rates was attempted based on the amplitude of the heat flux deviation. Using the formula
$\Delta q = \rho * c * v * \Delta T$, where $\Delta q = 5$ mW m^{-2} is the heat flow anomaly, $\rho = 1035$ kg m^{-3} and $c = 4000$ J kg^{-1} K^{-1} are the density and specific heat of seawater, respectively, ΔT = 3 K is the temperature difference at the BSR depth (approximated to be 500 m bsf) causing the anomaly, and v is advection rate, a flow speed of $0.4 * 10^{-10}$ m s^{-1}, or 1.3 cm a^{-1} was obtained. This value is in good agreement with constraints from direct heat flow measurements (flow rates more than 1 cm a^{-1} would result in non-linear geothermal gradients, Grevemeyer et al. 2004) as well as geochemical investigations of pore fluids (flow rates are between 0.5 - 1.5 cm a^{-1}, C. Hensen, pers. comm.).

This simple estimate provides no constraints about the volume of material output over time. The extreme case of uniform flow of 1 cm a^{-1} through the entire horizontal cross-section of the seismically transparent region beneath Mound Culebra (625 m * 500 m * 3.14), although probably a substantial overestimation, yields a throughput of 9800 m^3 a^{-1}. Diapirs however exhibit large variations in their permeability, as the consequence of strain-induced anisotropy. Vertical fluid migration is often found to be focussed along the sides of the diapiric body (Brown, 1990). With such a flow geometry, a yearly discharge two order of magnitudes lower would still be sufficient to maintain the observed heat flow anomaly. Nonetheless, this scenario fails to yield sufficient explanation for the presence of carbonate precipitates, vent fauna, and methane enrichment in the water column near the summit of Mound Culebra.

An interesting phenomenon is revealed by the discrepancy of direct heat flow measurements and BSR-derived values up to 2 km southeast of Mound Culebra (Fig. 4.5). While Grevemeyer et al. (2004) suggest the occurrence of a lateral flux between seafloor and BSR to explain this anomaly, evidence of outflow has been found neither in the form of methane plumes in the water column, nor as patches of high backscatter or chemosynthetic life forms on the seafloor above the southeastern flank of the mound. The nearest of such indications are documented further away at the Culebra Fault, where no *in situ* thermal measurements were carried out. It is conceivable that a portion of the advecting fluids is redirected laterally along stratigraphical horizons or fault planes from Mound Culebra, and migrates within in the subsurface for at least as long as 4 km.

4.6 Conclusions

A sharp, negative-polarity BSR is observed in the high-resolution seismic data set acquired in the vicinity of Mound Culebra. Interpreted as the bottom of HSZ, the reflector's depth was used to estimate heat flow in the shallow subsurface. The calibration of model parameters was carried out with the help of *in situ* temperature and thermal conductivity measurements.

Observations regarding regional trends in the heat flux field reveal a gradual decrease away from the trench. On one hand, this is consistent with values predicted for the continental middle slope at subduction zones, and in accordance with directly acquired background thermal data across the trench. However, it contradicts the widely documented coldness of oceanic crust offshore northern Costa Rica and Nicaragua and consequently expected landward heat flux increase due to the shutting off of hydrothermal circulation in the downgoing slab. Possible explanations for the discrepancy include an irregular heat flow pattern of the EPR crust, faster than assumed reheating of the downgoing slab, or an additional heat source at depth.

Localized anomalies up to 6 mW m^{-2} emerge from background values of 22 - 40 mW m^{-2} in association with various seafloor structures. At two sites, above Mound Culebra and at the Culebra Fault, these are accompanied by the presence of extensive chemosynthetic fauna and elevated methane content in the water column. This is not the case near trench-parallel bathymetric steps southwest of the mound: the apparent heat flux variation they exhibit can be explained by the limitations of the modelling technique.

A rough estimate of fluid flow rates at Mound Culebra, based on the amplitude of observed heat flux anomaly yields values of 1. 3 cm a^{-1}. This is in good agreement with constraints from other investigations.

BSR disruptions of both gradual and abrupt character are observed in the study area. The former one is possibly related to reduced free gas content beneath the HSZ as well as insufficient signal-to-noise ratio. Abrupt terminations of the reflector are attributed to structural or stratigraphic escape paths for the free gas content of the sub-HSZ sediments.

Finally, an attempt to relate these results to the main tectonic structures of the Mound Culebra area, described in Chapter 3, was undertaken. Low-angle faults associated with gravity-driven material creep were found by thermal investigations not to play a direct role in fore-arc dewatering. In contrast, Culebra Fault, interpreted as a possibly deep-rooted normal fault, reveals significant heat flux variations, supporting its proposed relevance as fluid pathway. A possible change in the regional heat flow

trend with distance from the trench appears to correlate with the shift to locally extensive tectonic setting in the close vicinity of Mound Culebra.

The following chapter presents investigation of a different locality, in order to compare tectonic as well as thermal characteristics associated with mud mounds on the Costa Rican fore-arc.

5

Sediment Structures and Fluid Venting near a Subducting Plate Segment Boundary - Seismic Observations at the Hongo mounds

(Fekete, Spiess, Grevemeyer, Reston)

5.1 Introduction

The area offshore central Nicoya peninsula has been of considerable scientific interest for the last decades (e.g. Shipley et al., 1992, Kahn et al., 1996, Kimura et al., 1997, Fisher et al., 2003). One of the reasons is its special tectonic setting: the Cocos plate subducting at this segment of the Middle American Trench is produced at two origins. Material from the EPR on the northwestern side differs significantly from CNS lithosphere in its geological - geophysical properties (cf. Chapter 1). The tectonic boundary separating the two domains appears to be located beneath a small ridge named "Fracture Zone Trace" (FZT, Barckhausen et al., 2001).

On the continental slope, approximately opposite the subducting boundary of oceanic plate segments, a group of seafloor structures similar to the mound described in Chapters 3 and 4 was found. They appear in sidescan sonar data as high backscatter areas, indicating a hard surface, and some host chemosynthetic fauna, providing direct evidence of actively ongoing fluid and gas venting (Weinrebe and Flueh, 2002). Based on bathymetric and high-resolution MCS data, a comparison to Mound Culebra is given on the following pages, with a focus on similarities and differences in surface morphology, seismic, and thermal characteristics. The main purpose of our investigations is to find out whether the origin of these mounds is independent of that of Mound Culebra, or typical for this part of the Costa Rican margin and a consequence of certain regional geological settings, and, if so, what these may be.

5.2. Observations

Seafloor morphology

The Hongo mounds are a group of six mounds situated about 20 km east of the ODP Leg 170 sites, in water depths of about 2000 m. (Fig. 5.1). Their diameters range from a few hundred meters to a kilometer and their heights above seafloor remain below 90 m, with typical values of a few tens of meters. Their shapes vary from approximately circular to elongated. Several other seafloor features appear in their vicinity, which show even more pronounced elongation and rise to heights comparable to the smaller mounds. They are randomly oriented, and only up to a kilometer long.
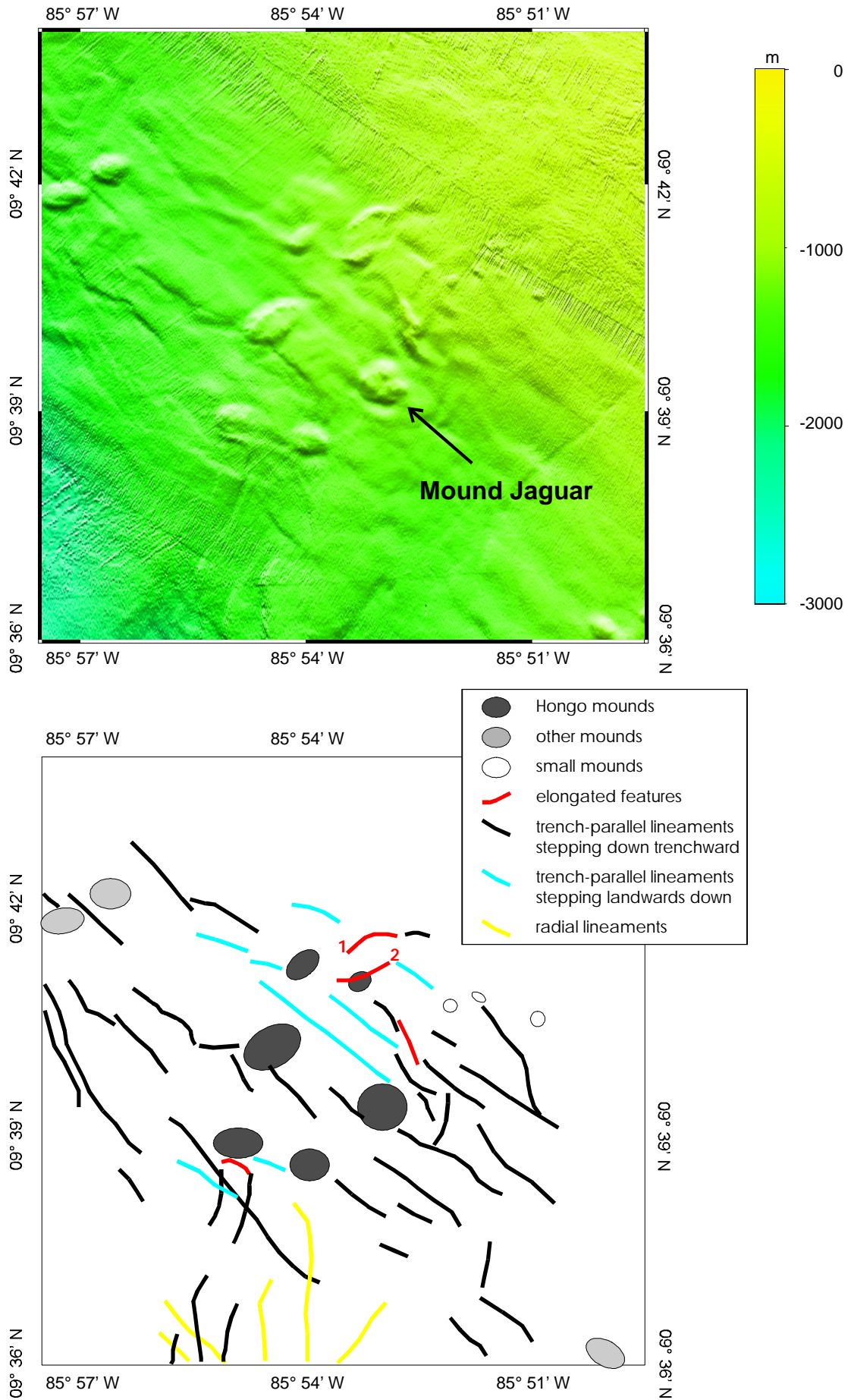
Figure 5.1 Bathymetry of Hongo mounds and their vicinity (top). Six domes and several other elongated seafloor features occur among numerous trench-parallel lineaments of comparable heights. Bottom: line drawing of characteristic bathymetric features.
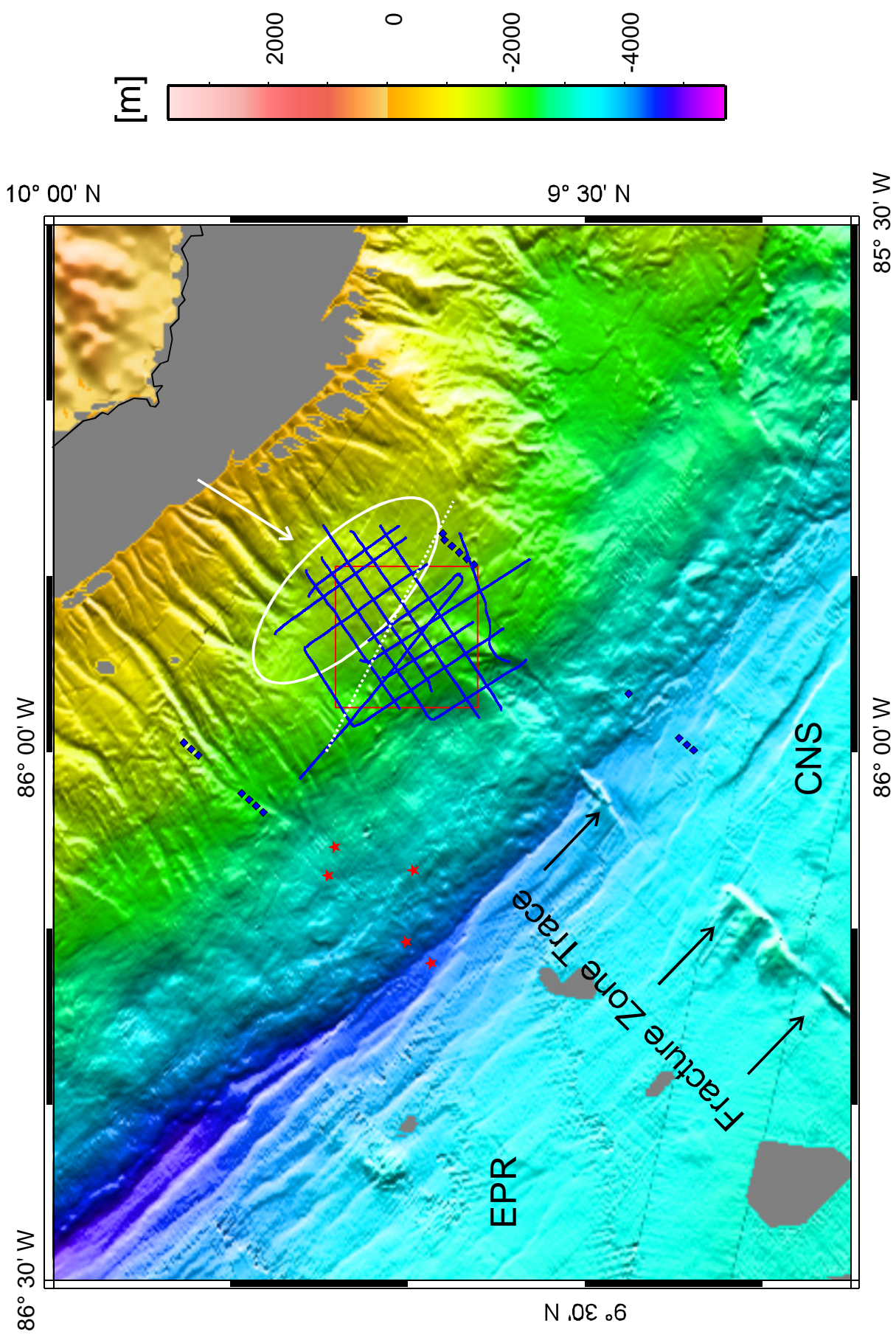
Figure 5.2 Bathymetric map above the oceanic plate segment boundary, with location of processed multichannel seismic profiles (blue lines) and of in situ heat flow measurements (blue diamonds) on the continental slope. Dotted line divides domain with coherent shallow reflectors - landwards - from that characterized mainly by disperse seismic energy - southwestwards. White arrow marks region of updoming on the middle and lower slopes. Outline of Fig. 5.1 and ODP site locations are shown for orientation. EPR, CNS: lithosphere produced at the East Pacific Rise and Cocos-Nazca Spreading Center, respectively.

Another group of typical seafloor structures in the area are lineaments, with vertical offsets up to several tens of meters, oriented approximately parallel to the trench, and extending laterally over several kilometers. Their majority is marked by a trenchward step down, while others have a landward throw. The lineaments occur throughout the entire study area near and downslope from the mounds, as close as 1 km apart from one another. They are however not seen upslope of the Hongos. Their orientation differs in the southwestern corner of the study area, where they strike radially away from the landward end of an embayment.

The embayment is a feature on the trenchward edge of the area, a valley of about 5 km width and 200 m depth, elongated landwards, and with an uneven floor. It appears to be collinear with the subducting FZT on the continental side of the trench (Fig. 5.2).

Upslope of the study area, an elliptical region of smaller slope angles is visible in the bathymetry, extending about 15 x 10 km. The canyon system located further upslope terminates abruptly at its landward edge. The basin appears slightly domed in the center along its shorter axis, approximately in the direction of plate convergence from the Hongo mounds.

Seismic characteristics

High-resolution multichannel profiles (Fig. 5.2) reveal the subsurface to be of variable properties. The survey area, comprising approximately 20 x 20 km, shows two distinct lateral domains. The landward and northern part is characterized by coherent reflectors down to 150 - 200 ms TWT bsf (two-way travel time below seafloor), with a seismically transparent interval beneath, and the widespread presence of a sharp negative-polarity BSR around 550 - 650 ms TWT bsf. In this domain, mounds and other topographically elevated structures appear to be related to low reflection energy and the interruption of coherent reflectors beneath (Fig. 5.3).

The well-layered upper facies thins towards the center of the area and disappears fully in the southern and trenchward regions (Fig. 5.4). Along with this change, the amplitude and distinctness of the BSR deteriorate, although its presence can still be

inferred at several locations in the southern parts from seismic attributes such as polarity and instantaneous phase. The transition between the domains is generally gradual, with a few exceptions where reflectors terminate abruptly (e.g. the BSR at offset 16 km).

Despite the limited occurrence of coherent reflectors, vertically displaced horizons are observed at several locations. Small-scale vertical offsets occur in dip lines (e.g. 5.4). These mostly represent a few tens of ms TWT and are closely spaced, often just a few hundred meters apart, in the upper 200 ms TWT bsf.

A more striking feature is seen at offset 17 km. A BSR disruption of 500 m is associated with its vertical offset by as much as 90 ms TWT. Elevated amplitudes of a shallow reflector package appear to be related to this phenomenon.

Additional BSR disruptions occur beneath mounds (GeoB02-208 at 7.8 km) and other sites of locally elevated seafloor (e.g. Fig. 5.5, between 9.8 - 11 km).

Anomalous amplitudes of variable characteristics are found throughout the entire study area. Near the northern end of GeoB02-251, a strike line landward of the mounds, several downward widening triangular structures with low reflection amplitudes are displayed in the shallow subsurface (Fig. 5.6). Some of them are associated with elevated seafloor topography. Seismic layers show enhanced reflection amplitudes and an upward bending geometry on the southeastern side of one example (offset 4.7 km). No similar structures are recognized in other profiles.

Reflector segments with anomalously high amplitudes are observed in the same profile at 460, 510, 560, and 720 ms TWT bsf between offsets 4.5 - 4.8 km. They exhibit a clear negative polarity, extend less than 300 m laterally, and are arranged subvertically.

In line GeoB02-219 (Fig. 5.4) at offset 17 km, approximately 25 m thick and 1 km long reflector package reveals amplitudes that are on average 5 times higher than in the vicinity. The polarity of individual reflectors cannot be determined. The anomalous amplitudes extend northward for as much as 5 km (see insert in Figure 5.4). Other examples of locally elevated amplitudes are observed beneath mound flanks.

The trenchward edge of the study area is characterized by chaotic reflectors, side arrivals, and scattered seismic energy in the subsurface (Fig. 5.7).
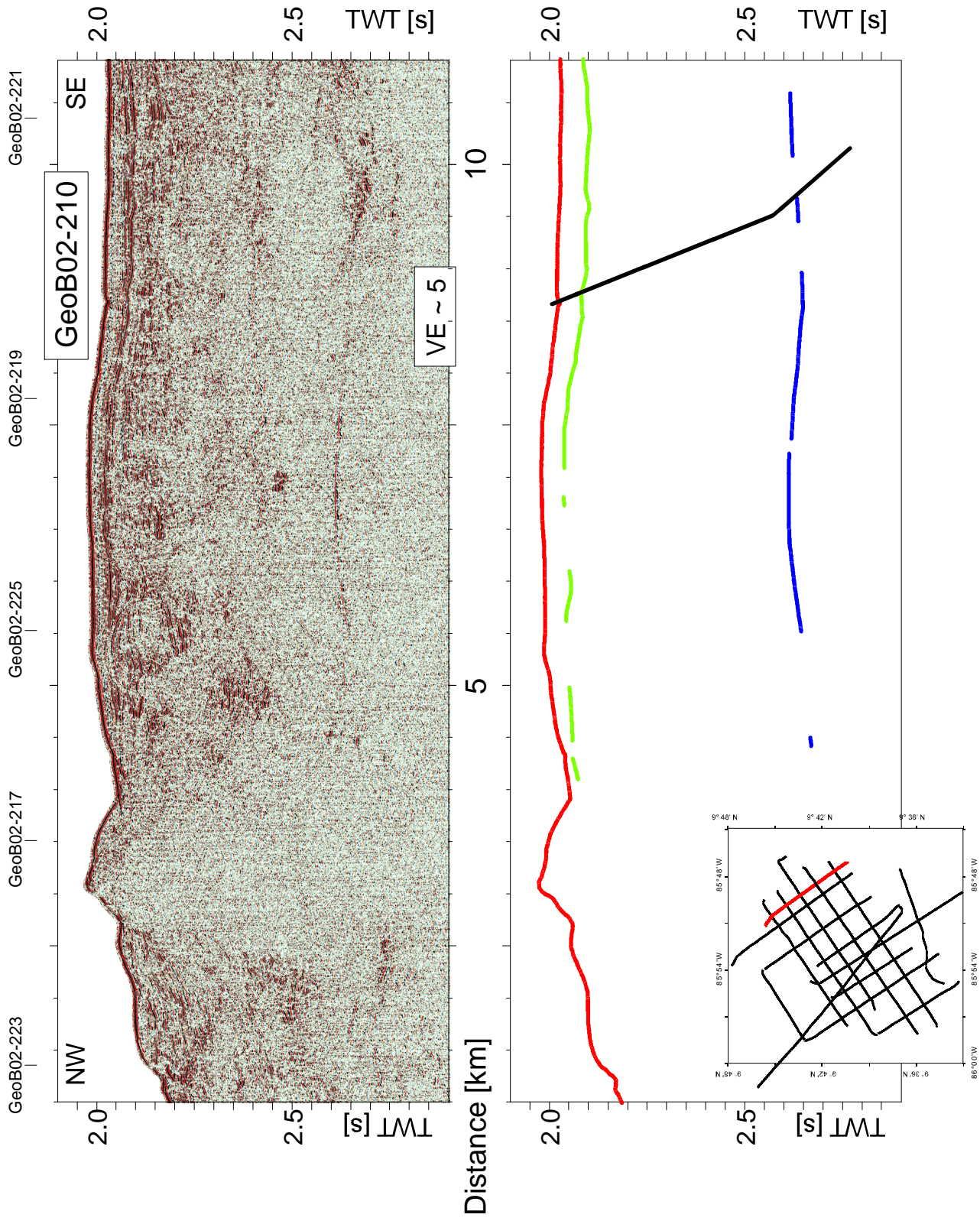
Figure 5.3 Seismic profile GeoB02-210. The landward part of the study area shows similar seismic facies distribution to those see near Mound Culebra: a shallow interval of coherent reflectors (150 - 200 ms) is followed by a seismically tranparent zone. A distinct BSR is also visible. Beneath a mound at offset 2.5 - 4 km, subsurface layering is interrupted. Insert shows location.
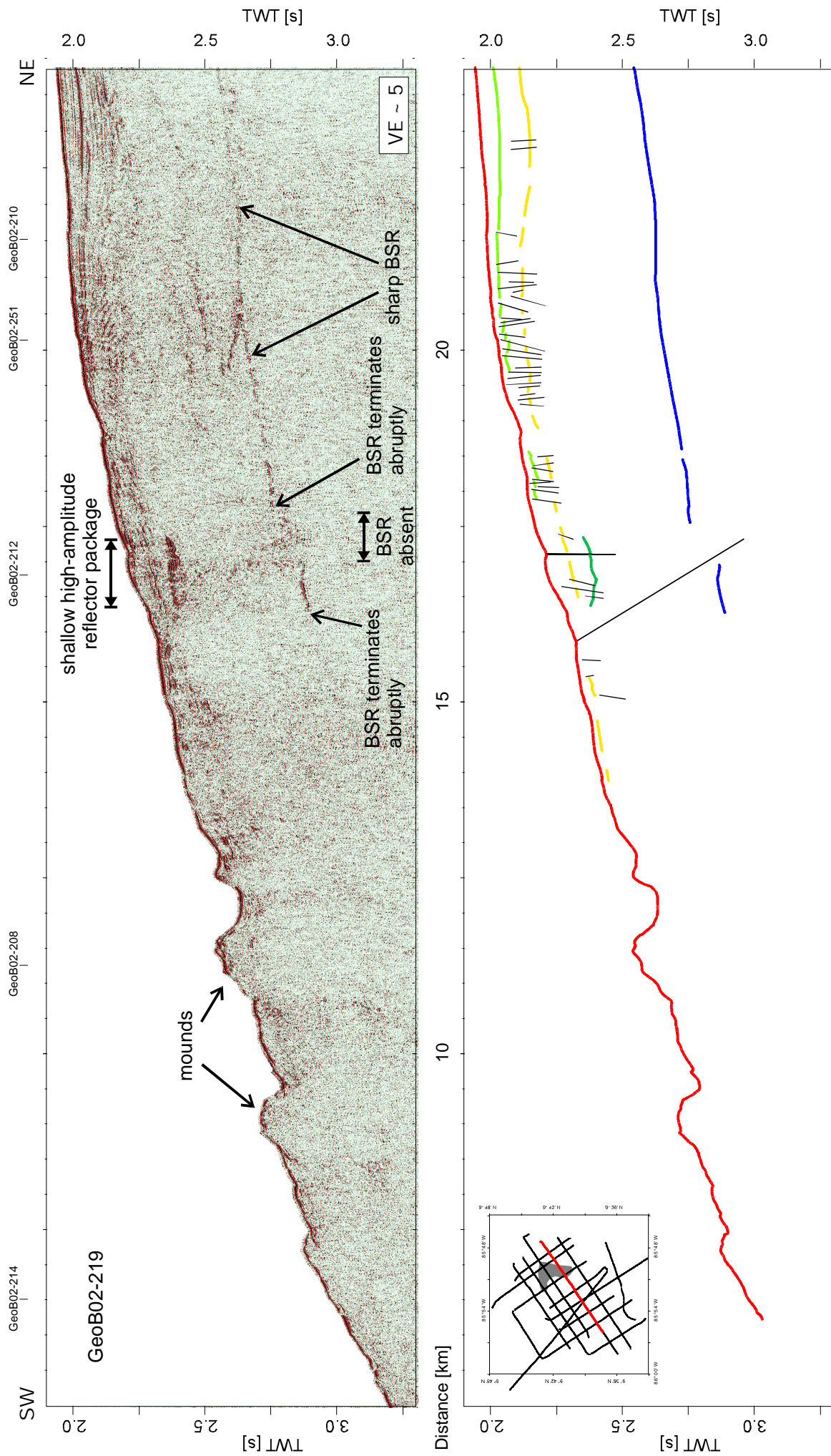
Figure 5.4 Seismic dip line GeoB02-219. The zone of coherent reflectors in the northeast portion thins downslope and finally disappears towards the trench, giving way to a seismically transparent region. The transition approximately coincides by the abrupt termination of BSR at offset 16 km. BSR disruption (at offset 17 km) and the associated vertical offset (90 ms) seems related to a high-amplitude shallow reflector package, whose lateral extent is shown in the inset.
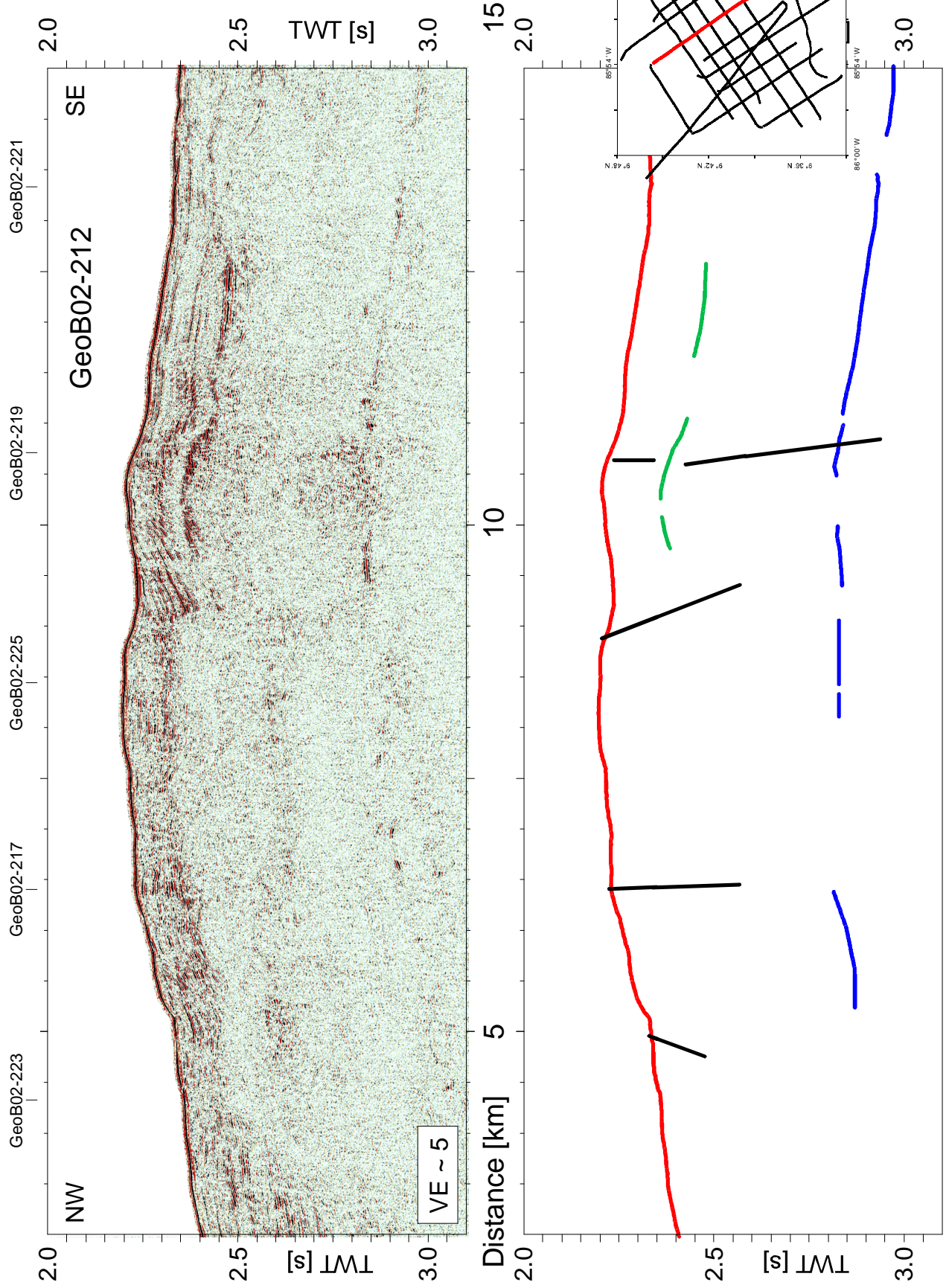
Figure 5.5 Seismic profile GeoB02-212, crossing the BSR disruption/offset seen in Figure 5.4. BSR appears diffuse or absent (offset 9.8 - 11 km), but not offset vertically. Seafloor above the feaure is slightly doming. Reflector segments of high amplitude are see at about 150 ms bsf.
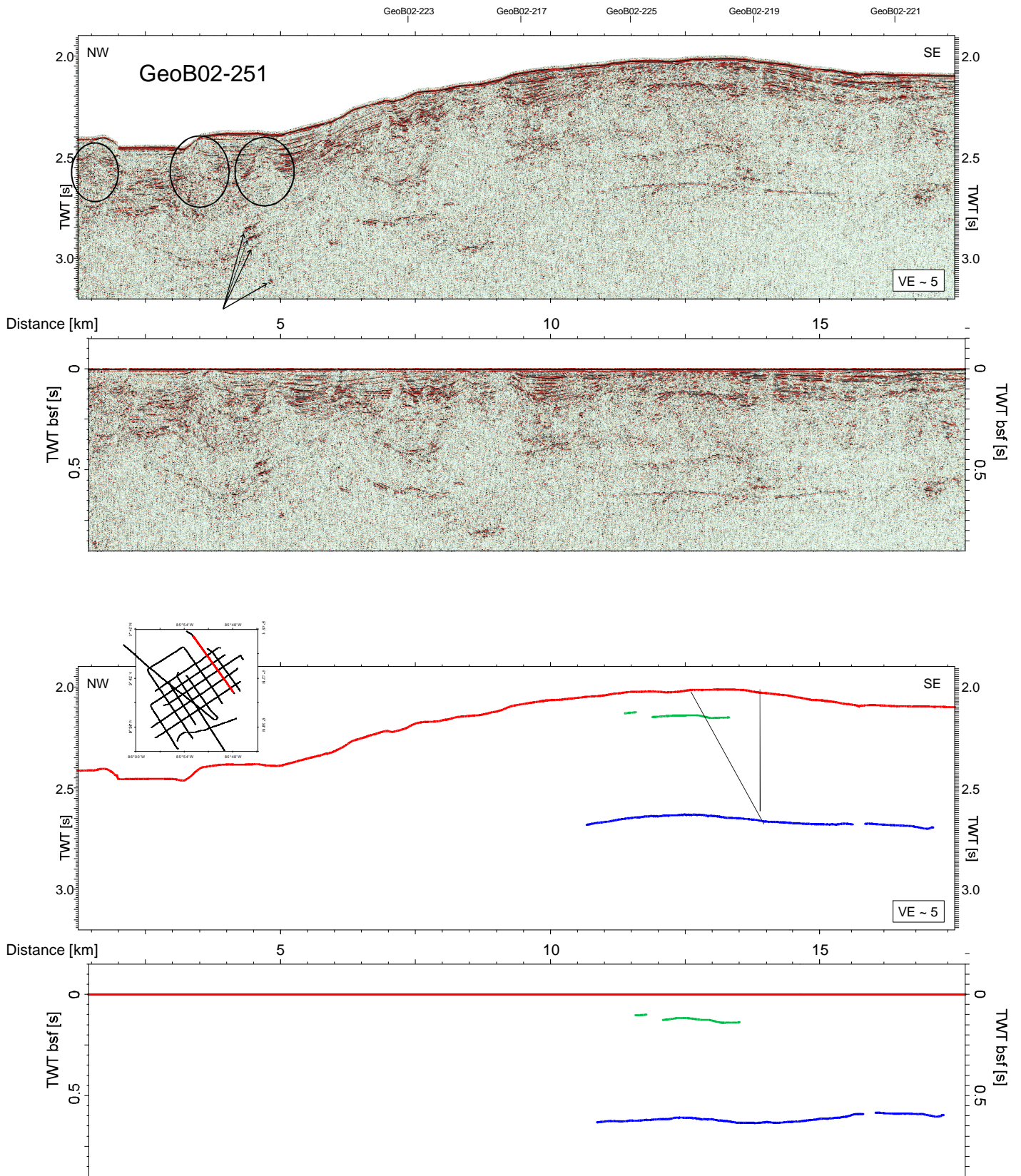
Figure 5.6 Seismic profile GeoB02-251, displaying a number of features. Offset 1.5 - 5 km: downward widening triangular structures of low reflection amplitude (ellipses), some associated with elevated seafloor topography. Near offset 4.5 km, a series of short, high-amplitude, reverse-polarity reflector segments are imaged (marked with arrows).

BSR topography outside the Hongo area

A significant change in BSR depth is observed on a transit profile into the study area. 16 km from the central Mound Jaguar, average BSR depths appear to be similar to those typical of the Hongo area (550 ms TWT bsf). Another 16 km further southeast, towards the other end of the profile, BSR is found at a sub-bottom depth of 300 ms TWT. In between the two locations, the reflector appears only as short, low-amplitude segments, and is at the limit of detectability (Fig. 5.8).

5.3 Discussion

The Hongo mounds

Of the several mounds found in the area, only the ones located landwards show different seismic properties from their surroundings. They are characterized by an apparent lack of internal layering, and reflectors terminate abruptly beneath their flanks. The same is true for several smaller seafloor structures, which are not classified as mounds but do not exceed a diameter of 1 km (cf. Sahling et al., in prep.). Their seismic transparency indicates a homogeneous, destroyed or masked internal structure. Together with a lack of microseismicity in the vicinity (Weinrebe and Flueh, 2002), this points to a probable diapiric origin of the structures.

Mud domes further trenchward are assumed to be of the same nature based on video and backscatter surveys, which have shown several of them to exhibit active or recent venting (Bohrmann et al., 2002, Weinrebe and Flueh, 2002). Although the lack of coherent reflectors in this domain removes most of the seismic contrast, scattered energy beneath the flanks points to changes in the physical properties. Therefore, all mud domes in the Hongo area are thought to consist of extensively sheared and deformed mud, while carbonates found on the summits of various hills are probably precipitated from expulsed fluids.

Deformation

Trench-parallel seafloor lineaments are proposed to be the surface manifestation of regional deep faults. This is suggested by their spatial correlation in the landward domain to vertically offset reflectors as well as BSR disruptions and enhanced amplitudes of shallow strata. Both normal and thrust faults occur in the Hongo area, however, because of lack of deeper reflectors, fault orientation cannot be determined. Some faults are associated with short high-amplitude reflector segments (bright spots), which are arranged near vertically. This provides seismic evidence that fractures act as pathways for advecting gases and fluids in the Hongo area.

Vertically offset shallow reflectors reveal small-scale fracturing in the landward portion of the area. These fractures are not associated with any surface expression and represent offsets on the meter scale. Although they occur in large numbers, their correlation across even neighbouring profiles is not possible. Their possible role is to locally compensate stresses caused by the regional tectonic movements.

Seaward of the mounds, slumping is identified in both bathymetric and seismic data. An embayment of variable topography is found here. Its floor is made up of terraces, and it terminates landward in a semicircular headwall. Its interior shows no seismic structure, but abundant incoherent, scattered energy with numerous side arrivals. The feature is associated with radially oriented seafloor steps upslope of its headwall, overprinting the regional pattern of trench-parallel lineaments. Because of its position opposite the subducting FZT ridge, which has been shown to continue beneath the slope (Barckhausen et al., 2001), the deformation pattern is thought to be formed as a consequence of local uplift, oversteepening, and slumping, much like other examples at locations of seamount subduction (Ranero and von Huene, 2000, Huenerbach et al., 2005, Dominguez et al., 2000, Bruening, 2006). Updoming further landward of the Hongo mounds is possibly also caused by this ridge.

Canyons

Seaward of the shelf break, the presence of downslope oriented canyons is observed in the bathymetry. They terminate just landward of the survey area, closest to the northwestern end of profile GeoB02-251 (Fig. 5.6). Bathymetric correlability supports the interpretation of triangular low-amplitude anomalies as buried canyon walls.

124

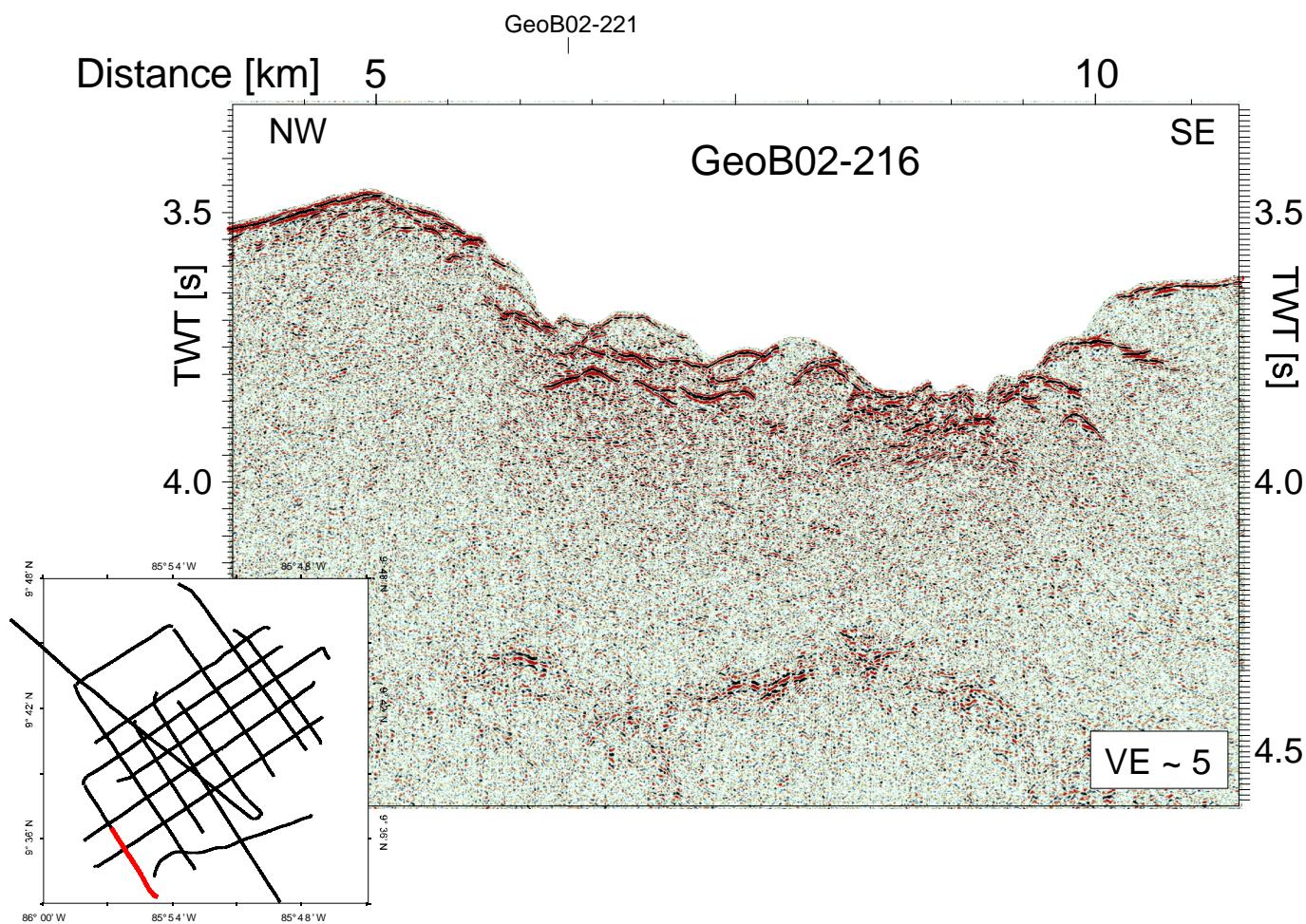Figure 5.7 Seismic profile GeoB02-216 crossing a slump. Note side arrivals near the seafloor.
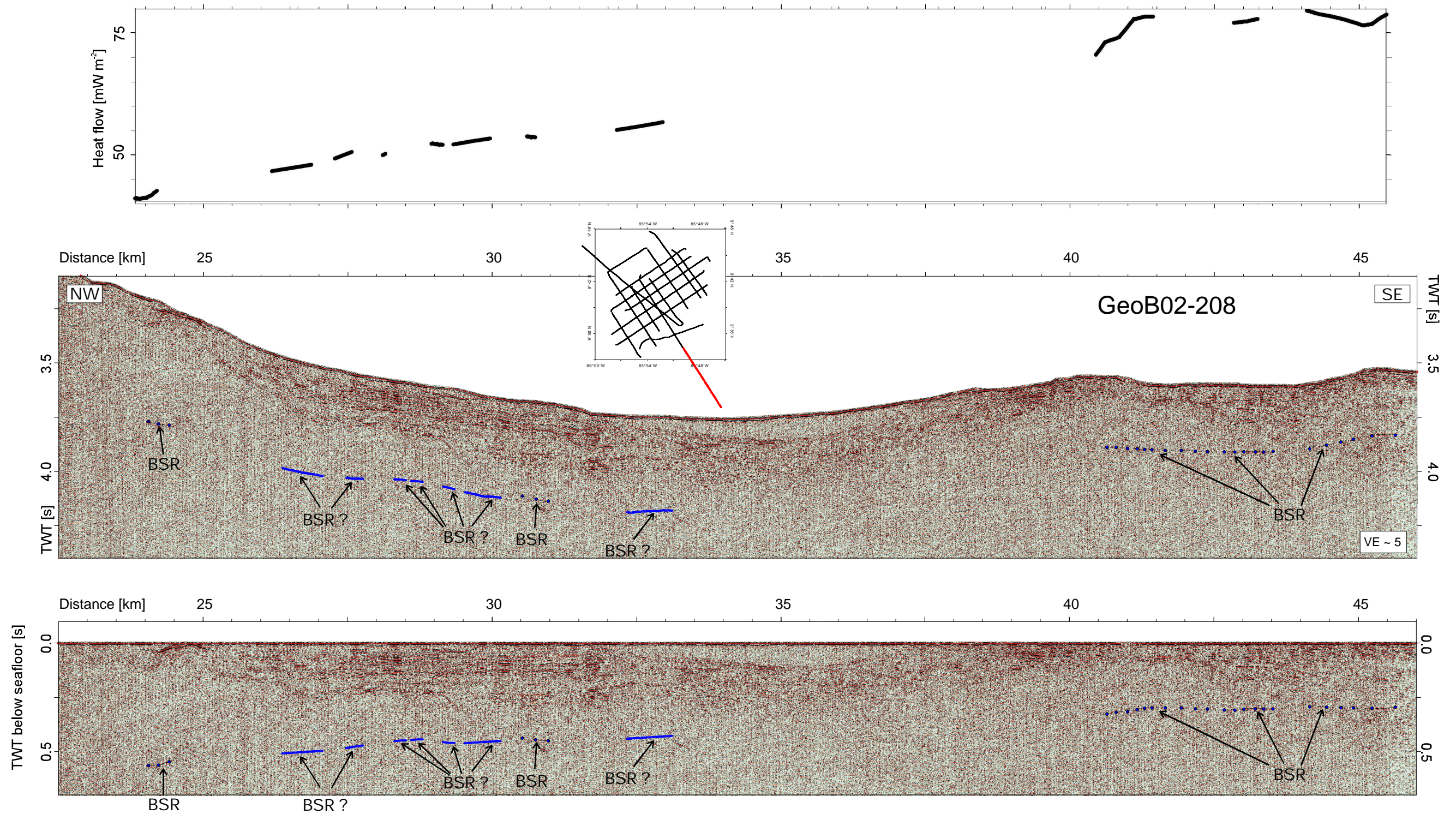
Figure 5.8 Tracing the BSR towards the CNS crust. Profile GeoB02-208 displays the BSR 600 ms TWT below seafloor near the Hongo mounds, but only 300 ms TWT bsf 16 km further southeast (dots). Inbetween, the reflector is at the limit of detectability (lines). Top: BSR-derived heat flow along the profile.

Enhanced reflection amplitudes at the sides are possibly of gradational origin and indicate fast, rather than gradual, filling of the canyon by turbidites. The upward bending of parallel reflectors (at offset 5 km) implies post-sedimentary relative movement. It may also be caused by a part of the sediments being pelagic, which tend to drape over topography rather than evening it out. The lack of corresponding features in neighbouring strike lines may be explained by the continuous deepening of the canyons beneath a thickened sediment cover.

Heat flow modelling

The BSR around the Hongo mounds has been interpreted to mark the base of hydrate stability zone. We used the reflector to calculate heat flow values in the shallow subsurface (Figure 5.9), through the method of Dickens and Quinby-Hunt (1994) described in Chapter 4. Modelling parameters were chosen to be the same as for the Mound Culebra area: thermal conductivity $k = 0.95$ W m^{-1} K^{-1}, acoustic velocity $v = 1750$ m s^{-1}, the density of seawater $\rho = 1035$ kg m^{-3} (assuming hydrostatic pressure in the sediments) and the constant of gravity $g = 9.782$ m s^{-2} (corrected for latitude). This is thought to be appropriate due to the geological similarity between the two survey areas. Heat flow values vary between 25 and 37 mW / m^2, with the lowest values found between the mounds, and highest ones at the edge of slump headwall. These latter are possibly a result of recent sediment removal on the surface, within a time frame too short for the BSR to have adjusted.

Considering only the region where a sharp BSR occurs, a general trend of heat flow decrease with distance from the trench can be inferred (Fig. 5.10). An increase further landward is perhaps related to localized seafloor structures near the profile ends. Due to the scarceness of profiles, local anomalies are not dealt with in the vicinity of Hongo mounds.

BSR-derived heat flow is in good agreement with values measured *in situ* along two nearby transects (Soeding et al., 2003).

5.4 Interpretation

Sediments in the Hongo area

The continental margin upslope of the Hongo mounds reveals morphological characteristics similar to those seen elsewhere in the Costa Rican fore-arc. Trenchward of the shelf break, an extensive canyon system is found, in which downslope sediment transport in the form of turbidites occurs. The canyons confine episodic mass transport and are in turn carved deeper by the sediment flows, their walls occasionally built higher by overspill material. However, unlike at many other locations, the canyon system does not cross the entire margin here, depositing turbidites near or into the trench. Instead, it outlets onto a flat basin on the middle slope.

This has two relevant consequences. One is, that the canyons get gradually infilled as the basin extends upslope. The other result is a comparably smaller amount of sediments arriving to the lower slope. This may be part of the explanation why, although the margin here exhibits a steepness of approximately 3.5°, there is no indication of either channelized sediment transport or gravity-driven mass creep across the survey area; the thickness of layered strata, which implies local sediment accumulation, also thins rapidly downslope. Alternatively, seismic layering of the trenchward region may have been destroyed by deformation.

Tectonic model

The tectonic setting of the Hongo area appears to be largely controlled by the subduction of FZT. Imprinted on the regional pattern of margin subsidence, frontal erosion, and steepening of the lower slope, local uplift is seen in the vicinity of the mounds and several kilometers further upslope. Steeply dipping trench-parallel normal faults, a probable result of erosive subsidence, show enhanced vertical offsets, and some are inverted to form thrust faults. Both phenomena are possibly related to the variable topography of downgoing plate. In consequence, faults are considered to affect both the sediment cover and the margin wedge. A subducting ridge segment causes compression at its front, and slumping in its wake. Landward of the survey area, sediments are captured in a local deposition center on the middle slope, which is possibly created by rough wedge topography. The upper slope is characterized by canyons. Although our survey does not provide any details about the middle and upper slope tectonic regimes, they are assumed to be similar to that described in the
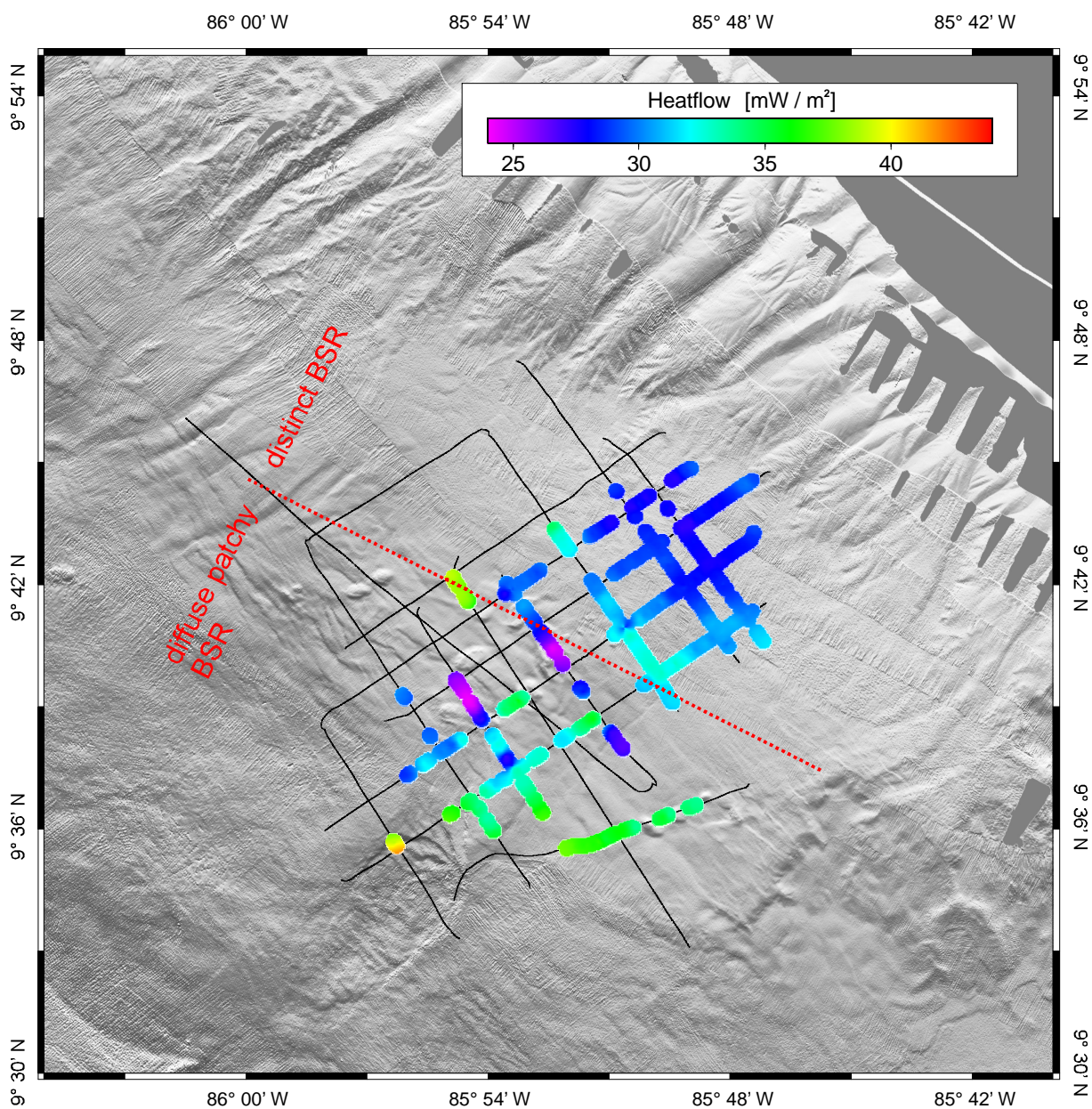
Figure 5.9 Map of BSR-derived heat flow. Although the presence of a sharp distinct BSR is limited to the landward portion of the study area (northeast of the dotted red line), short segments of it can be identified in the southwest as well. For discussion, see text.
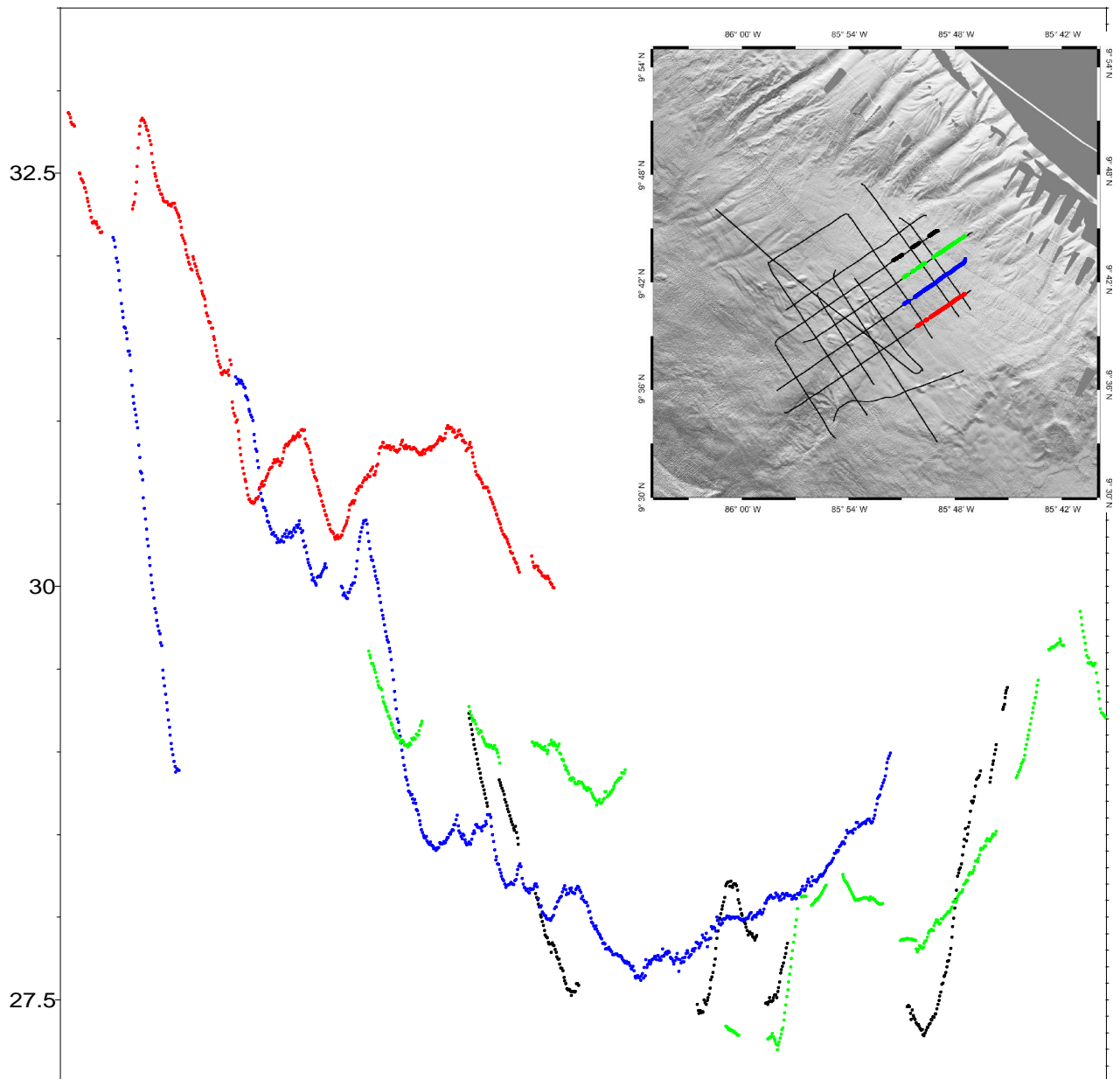
Figure 5.10 Dip lines of BSR-derived heat flow on the landward part of the survey area.
A clear decrease away from the trench is possibly followed by an increase further upslope.

vicinity of Mound Culebra (cf. Chapter 3). A schematic sketch of the tectonic settings of the Hongo area is shown in Figure 5.11.
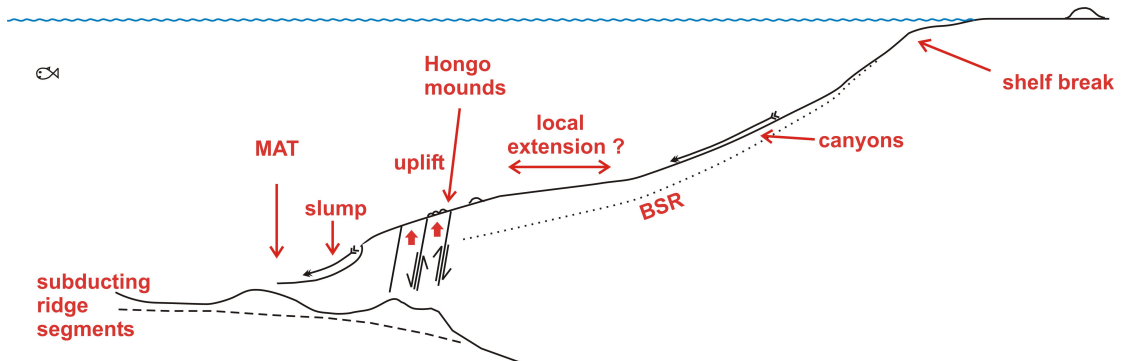
Figure 5.11 Schematic tectonic model of the Hongo area. The subducting segments of FZT create local uplift beneath the lower slope, increasing fault offsets and often reversing their throw direction. These effects cause the venting rate of the mounds to change, possibly to decrease. On the other hand, they provide pathways which affect the margin wedge as well as the sediment cover. In the wake of the ridge, slumping occurs. The presence of a distinct BSR and seismic layering are limited to the landward segment of the survey area. Further upslope, a local depocenter of possibly extensional tectonics is shown in the bathymetry, which traps a significant amount of sediment transported trenchward by the upper slope canyons. Also compare to Figure 3.16.

Dewatering in the Hongo area

Because of the spatial distribution of seismic properties in the survey area, indications of dewatering-related structures have only been identified in the landward, layered region. We rely, on one hand, on structural information associated with evidence of venting from other surveying methods. This indicates for several of the mounds to be, or have recently been, actively emitting fluids. The exact nature and probable source depth of these fluids is yet to be investigated.

Another way to trace pathways is to locate characteristic amplitude anomalies. The shallow, high-amplitude reflector package mapped in the northeastern portion of the area, related to a probable fault structure and the vertical offset of the BSR (Fig. 5.4), can be explained in terms of advecting fluids. According to this scenario, fluids would

migrate along the fault up to the reflector, at which point the vertical permeability decreases. Fluids would then be deviated sideways along stratigraphical units, and possibly reach the surface in a more diffusive manner.

The third way to detect upward flow is by locating and interpreting heat flow anomalies. However, these are strongly non-conclusive in the area. The only possible indication they carry is that dewatering on the landward edge of the region is stronger than closer to the trench. Should this be the case, it suggests a decreasing activity of the Hongo mounds, possibly caused by the tectonic disturbance of the subducting FZT. The emphasis in dewatering is placed on the numerous faults. The case when fluid and heat advection are decoupled must also be considered.

Heat flow above the subducting plate segment boundary

Heat flow measured on the oceanic plate opposite the Hongo area reveals an anomalously cold EPR lithosphere. BSR-derived values above the continental lower slope are in agreement with this anomaly. However, the mounds themselves are thought to be located exactly opposite the plate segment boundary, south of which the downgoing plate exhibits heat flow values in accordance with conductive estimates. The thermal boundary is found beneath the southeastward transit profile GeoB02-208 (Fig. 5.8). It represents a gradual heat flow increase from 40 mW m^{-2} to 80 mW m^{-2} in a lateral distance of approximately 16 km.

5.5 Comparison to observations at Mound Culebra

Multi-frequency seismo-acoustic imaging has revealed the Culebra and Hongo areas, analyzed in some detail throughout Chapters 3 to 5, to be characterized by a great number of similar properties. These, as well as the differences found, are listed and discussed on the following pages.

Seismic properties

In the seismic data sets, the following similarities and differences are observed. A well-layered shallow subsurface overlies a transparent interval in both survey areas. This indicates that, be its cause sedimentary or gas hydrate-related, it is a regional

phenomenon. A negative-polarity BSR is seen around 600 ms TWT bsf in both vicinities. A patchier BSR occurrence near the Hongo mounds is a probable indication of greater availability of pathways for gas to escape.

The upper, well-layered seismic facies is seen to undergo significant thinning towards the trench. This is a possible indication of enhanced subsidence of the middle slope and a gradual decrease of the amount of sediment deposited further seaward.

All mounds are imaged to be seismically transparent. Beneath their flanks, seismic amplitudes drop abruptly, and reflectors, including the BSR, are disrupted. This, together with indications of venting from different geological - geochemical investigations, supports their diapiric origin.

Surface morphology

A fundamental difference between the two study areas is their location relative to major tectonic features. Mound Culebra, located 35 km from the MAT, is on the middle slope above a subducting plate of clearly EPR origin. 90 km to the southeast, the Hongo mounds are only 15 km away from the trench, and close to the zone where properties of the incoming plate change profoundly. From a morphological point of view, Mound Culebra is a single dome with relatively high elevation, while the Hongos are a cluster of structures of variable shapes, sizes, and heights, all of them smaller than Culebra.

However, the survey areas host many morphological similarities. Both exhibit active, although not vigorous, fluid venting. Mounds host chemosynthetic communities of similar composition, and are covered in part by carbonate precipitates, in part by sediments. Several of them are elliptical in shape, elongated in a downslope direction. All larger mounds appear to have several summits, with a depression between them that is generally covered with sediment. In accordance with this, we propose that two small, elongated hills north of Mound Jaguar (1 and 2 in Fig. 5.1) actually belong to the same structure, with a size and shape comparable to the larger mounds, but no elevation above the surrounding seafloor.

The bathymetry of the margin at the two trench segments is largely comparable. The upper slope is covered by a canyon system, which terminates near water depths of 1500 - 1700 m. It gives way to an elliptical basin, which probably acts as sediment trap for material arriving within the canyons. Downslope of the basin, the number of trench-parallel seafloor steps increases. The lower slope steepens towards the trench.

Apart from mound size and location, the main differences are seen in lower slope morphology. Faults offsets are larger and throw directions more complex in the Hongo area. The lower slope itself is not as steep here, and formed by a slump.

Deformation, tectonics

The above-described morphological differences are the direct consequence of tectonic differences. In the Culebra area, trench-parallel seafloor lineaments appear to be related to listric growth faults, associated with gravity-driven downslope sediment creep. Vertical offsets remain well below the height of the mound, throw direction is trenchward down. In contrast, the Hongo area is characterized by large-offset steep faults, several of which throw landward down. Part of the area also displays faults oriented radially away from the slump headwall. While we interpret the upper and middle slopes of the two survey areas to be of similar tectonic setting, - faulting and tilting characteristic of the canyon system, local extension and relative subsidence forming the basin, - the subduction of ridge segments beneath the Hongo mounds causes enhanced deformation, uplift, and sediment destabilization in the region near the trench. The presence of small-scale fractures in dip lines in both areas supports their being a response to margin-wide processes, such as regional subsidence and the steepening of slope.

Dewatering

The indications of dewatering are remarkably different near the Hongo mounds as in the vicinity of Mound Culebra. In the northwestern target area, fluid flow patterns are primarily deduced from BSR topography and heat flow values calculated thereof. They appear to be related to the mud dome and one fault. Trench-parallel lineaments

seem not to play a major role in providing pathways for fluids and gases migrating upward from depth.

On the other hand, the Hongo mounds display no seismic evidence of ongoing venting: their internal structure, interpreted to be of diapiric origin, as well as the carbonates and chemosynthetic fauna found on their surface, do not provide direct proof of present activity. Instead, amplitude anomalies, BSR disruptions, and reversed-polarity reflector segments in association with large-offset trench-parallel faults indicate an increasing importance of these latter features in the dewatering of the fore-arc. This is a possible consequence of the subduction of ridge segments beneath the area: a decrease of venting through mounds is achieved through enhanced movement along faults.

The fate of mounds

Based on the observations described so far, an outline of the possible fate of these mud domes is attempted.

Where exactly mounds are created is uncertain, at any rate they are sometimes observed on the upper slope and are present in greater numbers on the middle slope along the entire margin. According to the least restrictive of our hypotheses (cf. Chapter 3), they are a consequence of negative wedge topography, where the sediment thickness is locally increased. Since the wedge is brittle enough here to host earthquakes (Arroyo, pers. comm.), it can also undergo faulting, thus providing pathways for lower plate fluids. These create an overpressure at the base of sediment cover and mobilize solid material, which starts its buoyant ascent.

On the middle slope, the diapir is set in the context of enhanced sediment deposition. In order to maintain a positive surface morphology, it needs to be rising until it leaves the domain of local extension. Gas leaving solution from the pore fluid as well as hydrates dissociating because of excess heat may promote this process.

In accordance with the frontal erosion and regional subsidence of the margin, mounds "travel" downslope and eventually leave the middle slope basin. The sediment cover is gradually more deformed here, which also affects the conduits of the mud domes and will eventually influence their venting activity. Fluid expulsion on the lower slope is more likely to occur along faults that cut through both the sediments and the margin wedge.

Some of the predictions of the above theory are the following.

The Hongo mounds are thought to represent a more mature life stage of mud domes than does Mound Culebra. They have, or are about to, stop venting, while Culebra may still be active for a while.

Lower slope mounds always occur in association with steep, deep-reaching faults. This is likely if a wedge fault is needed to form mounds. Provided it remains active, faults will develop above it through the sediment cover to enable mechanical adjustment. However, the phenomenon may be related to subducting topography and not a general lower slope property.

Thermal observations

The thermal setting of Hongo area reveals a primary influence from EPR-produced material. Its low values, while anomalous relative to a conductive model of lower slope above a 24-Ma-old subducting plate, are in accordance with heat mining documented on the oceanic side of the trench. BSR-derived heat flow values are variable, but average around values calculated in the Culebra area. This contradicts expectations slightly: under similar circumstances, being closer to the trench should yield higher heat flow values. The discrepancy indicates a difference in the local thermal regime, as is also seen in the background heat flow data acquired *in situ*. The effect of trench proximity at the Hongo domes is perhaps counteracted by a lesser degree of reheating of the subducted plate beneath them, or a great variability of the thermal state of the EPR lithosphere.

The thermal regime of both study areas is clearly in contrast to values calculated 15 - 20 km further southeast. Although not supported by a dense grid of data, BSR depth towards the end of the profile clearly reveals a completely different region with heat flow values about 3 times higher, up to 80 mW / m^2. The width of thermal transition zone does not exceed 16 km along the trench.

5.6 Conclusions

In this paper we have presented structural and thermal investigations of the Hongo mounds. Data used for the study includes bathymetric as well as high-resolution streamer seismic profiles.

Derived from observations of seafloor morphology, the spatial extent of seismic layers, reflector amplitude variations, and changes in the BSR depth, the nature of specific features were analyzed. In particular, the Hongo mounds are proposed to be of diapiric origin with a decreasing role in fore-arc dewatering. Buried canyons have been identified in the landward part of study area, along with manifestations of slumping, normal and thrust faulting in the entire Hongo vicinity. Heat flow values have been calculated from BSR depth near the mounds and further southeast, beyond the subducting plate segment boundary.

Based on the above, as well as on results presented in Chapter 3, the tectonic context of the Hongo mounds was outlined. This is proposed to be controlled by two factors, the regional influence of erosive margin and a local effect from the subducting Fracture Zone Trace underneath the study area. While the former is thought to cause a steepening and normal faulting of the lower slope, the latter may invert some of the faults, enhances fault throw, and induces slumping behind the passing ridge segments. Its effect on dewatering is also significant: it possibly causes steep faults to become the pathway of preference instead of mud domes.

Finally, a direct comparison of the Culebra and Hongo areas was presented. Major similarities include the proposed diapiric nature of mounds, the vertical distribution of seismic facies in the subsurface, the middle and upper slope morphologies of relevant margin segments, the presence of trench-parallel seafloor steps, and the heat flow values calculated from BSR depth. Significant differences are observed in the deformation pattern and local tectonics of the lower slopes as well as in the importance of mud domes and faults in fore-arc dewatering. A possible fate of mud mounds offshore northern Costa Rica was also outlined, from their onset on the upper slope, through the peak of venting activity as they reach greater water depth, to their probable shutting down by enhanced deformation near the trench.

6

Conclusions

Throughout the previous chapters, investigations are presented concerning the role of mud mounds in the dewatering of Middle American continental fore-arc. Two mound areas were imaged by multi-frequency seismo-acoustic techniques in order to determine the nature, internal structure, and possible fluid contribution of mud domes, their relation to local and regional tectonic elements, and the role of gas hydrates present in the subsurface.

Structural investigations in the vicinity of Mound Culebra indicate the mud dome to be a diapir. This is supported by seismo-acoustic observations - internal transparency, disruption and upward bending of reflectors beneath its flanks - as well as results from visual observations and sedimentological analysis of shallow cores. It is found to be situated in a local deposition center, fed by a canyon system further upslope and crossed by trench-parallel seafloor steps seaward of the mound. These lineaments, associated with trenchward-dipping low-angle faults in the subsurface, appear to represent the most common type of deformation downslope from Mound Culebra, and are proposed to reveal gravity-driven sediment creep on the lower slope. A proposed tectonic model divides the margin into domains of faulting and tilting landwards, local extension and enhanced subsidence near the mound, and oversteepening and low-angle faulting towards the trench. Hypotheses have been confronted in order to evaluate the regional significance of this model. In subsequent investigations, we utilized the least restrictive one, which connects the formation of mud diapirs to local lows in margin wedge topography and a related deep fluid source.

The widespread occurrence of a distinct, negative-polarity bottom simulating reflector in the area provides means to study the thermal regime of subsurface and thus identify probable locations of intense fluid upflow. Interpreted to mark the lower boundary of gas hydrate stability, a sensitive indicator of temperature and pressure variations, the reflector's depth can be used to estimate heat flow in the shallow sediments. The observed general landward decrease is discussed in the context of an anomalously cold subducting plate segment and its explanation by subsurface hydrothermal circulation. Locally elevated heat flow values highlight the significance of Mound Culebra, the Culebra Fault, and a largely uninvestigated circular bathymetric feature in the upward flow of warm fluids.

In order to put the previous results in a wider perspective, similar investigations above another group of mounds have been carried out. The Hongo mud domes are proposed to be of diapiric origin, inferred from their seismic contrast to their surroundings in the landward segment of the area and a complete lack of mud flows in their vicinity. Deformation nearby appears in the form of slumping as well as normal and thrust faulting. Several faults step landward down, pointing to a local tectonic influence by subducting segments of the Fracture Zone Trace. These are interpreted to potentially invert faults and increase their throw. The significant consequence for dewatering is that faults rather than mud mounds appear to be the preferred location of fluid advection in the Hongo area. This is also supported by estimated heat flow values.

A comparison between the study areas reveals similarities primarily in morphological, structural, and thermal observations. Principal differences are found in the tectonic settings of lower slope and in the patterns of dewatering. As a final synthesis, a possible fate of mud mounds offshore northern Costa Rica was outlined, from their onset on the upper slope, through the peak of venting activity as they reach greater water depth, to their probable shutting down by enhanced deformation near the trench.

However, many questions remain yet to be answered. One concerns the presence of carbonates covering mud domes. Numerical modelling (Luff et al., 2004) has shown that carbonate crusts in the sediments can only form over a relatively narrow range of upward fluid flow velocities ($20 - 60$ cm a^{-1}). These are over an order of magnitude beyond what Mound Culebra is thought to produce, the discrepancy to the Hongo mounds is possibly even greater. Could these domes have exhibited a period of such vigorous venting in the past?

Mounds have been found in the southeast, offshore central Costa Rica. Prominent examples like Mounds 11 and 12 are identified as mud volcanoes, with significant amount of fluid output (e.g. Mau et al., 2006, Hensen et al., 2004). Their low topography indicates a much lower viscosity than that found in Mound Culebra. What are the structural controls that influence the ratio of fluids to solid material in mud domes?

Numerous mounds have been recently discovered offshore Nicaragua. They are generally larger in size, and appear arranged in line with ridges or along faults (Buerk, pers. comm., Talukder, pers. comm.). What is the role of the canyon system in the location of mud domes? These and similar issues provide sufficient scientific targets.

References

Bangs N.L.B., Sawyer D.S., Golovchenko X. (1993): Free gas at the base of the gas hydrate zone in the vicinity of the Chile triple juction. Geol. 21, 10, 905-908

Barckhausen U., Ranero C.R., von Huene R., Cande S.C., Roeser H.A. (2001): Revised tectonic boundaries in the Cocos Plate off Costa Rica: Implications for the segmentation of the convergent margin and for plate tectonic models. JGR 106, B9, 19207-19220

Bialas J., Flueh E., Bohrmann G. (1999): RV SONNE Cruise Report SO144-1&2. PAGANINI: Panama Basin and Galapagos "Plume" - New Investigations of Intraplate Magmatism. GEOMAR Report 94.

Bohrmann G., Heeschen K., Jung C., Weinrebe W., Baranov B., Cailleux B., Heath R., Huehnerbach V., Hort M., Kath T., Masson D. and Trummer I. (2002): Widespread fluid expulsion along the seafloor of Costa Rica convergent margin. Terra Nova 14, 69-79

Bruening M. (2006): Sedimentdeformation an subduzierten Seamounts, seismoakustische Untersuchungen am Parrita Scar vor Costa Rica. Unpublished diploma thesis, Bremen

Caress D.W., Chayes D.N.: MB-System. www.ldeo.columbia.edu/res/pi/MB-System

Chan L.-H., Kastner M. (2000): Lithium isotopic compositions of pore fluids and sediments in the Costa Rica subduction zone: implications for fluid processesand sediment contribution to the arc volcanoes. EPSL 183, 275-290

Christeson G.L., McIntosh K.D., Shipley T.H., Flueh E.R., Goedde H. (1999): Structure of the Costa Rica convergent margin, offshore Nicoya Peninsula. JGR 104, B11, 25443-25468

Coulbourn W.T., Hesse R., Azema J., Shiki T. (1982): A summary of the sedimentology of DSDP Leg 67 sites: the Middle America Trench and slope off Guatemala - an active margin transect. in: Aubouin J., von Huene R. et al: Init. Repts. DSDP 67; U.S. Printing Office, Washington, D.C.

Damuth J.E. (1975): Echo character of the western equatorial Atlantic floor and its relationship to the dispersal and distribution of terrigenous sediments. Marine Geology, 18, 17-45.

Damuth J.E., Hayes D.E. (1977): Echo character of the east Brazilian continental margin and its relationship to sedimentary processes. Marine Geology, 24, 73-95.

Damuth J.E. (1980): Use of High-Frequency (3.5-12 kHz) Echograms in the Study of Near-Bottom Sedimentation Processes in the Deep-Sea: A review. M.G. 38, 51-75

DeMets C., Gordon R.G., Argus D.F., Stein S. (1994): Effect of recent revisions to the geomagnetic reversal time scale on estimates of current plate motions. GRL 21, 20, 2191-2194

DeMets C. (2001): A new estimate for present-day Cocos-Caribbean plate motion: Implications for slip along the Central American volcanic arc. GRL 28, 21, 4043-4046

Dickens G.R. (2001): The potential volume of oceanic methane hydrates with variable external conditions. Org. Geochem. 32, 1179-1193

Dickens G.R., Quinby-Hunt M.S. (1994): Methane hydrate stability in seawater. GRL 21, No 19m 2115-2118

Dominguez S., Malavieille J., Lallemand S.E. (2000): Deformation of accretionary wedges in response to seamount subduction: Insights from sandbox experiments. Tectonics 19, 182-196

Ecker C. (2001): Seismic characterization of methane hydrate structures. Dissertation, Stanford Univ.

Fisher A.T., Stein C.A., Harris R.N., Wang K., Silver E.A., Pfender M., Hutnak M., Cherkaoui A., Bodzin R., Villinger H. (2003): Abrupt thermal transition reveals hydrothermal boundary and role of seamounts within the Cocos Plate. GRL 30, 11

Fisher D.M., Gardner T.W., Marshall J.F., Sak P.B., Protti M. (1998): Effect of subducting sea-floor roughness on fore-arc kinematics, Pacific coast, Costa Rica. Geology 26, No 5, 467-470

Flueh E.R., Soeding E., Suess E. (eds.) (2004): RV SONNE Cruise Report SO173/1, SO173/3 and SO173/4: SUBDUCTION-II: The Central American Continental Margin. GEOMAR Report 115, 492 pp.

Ganguly N., Spence G.D., Chapman N.R., Hyndman R.D. (2000): Heat flow variations from bottom simulating reflectors on the cascadia margin. Marine Geology 164, 53-68

Grevemeyer I., Villinger H. (2001): Gas hydrate stability and the assessment of heat flow through continental margins. GJI 145, 647-660

Grevemeyer I., Kopf A.J., Fekete N., Kaul N., Villinger H., Heesemann M., Wallmann K., Spiess V., Gennerich H.H., Mueller M. and Weinrebe W. (2004): Fluid flow trough active mud dome Mound Culebra offshore Nicoya Penisula, Costa Rica: evidence from heat flow surveying. Marine Geology 207: 145-157

Han X., Suess E., Sahling H. and Wallmann K. (2004): Fluid venting activity on the Costa Rica margin: New results from authigenic carbonates. Int. Jou. Earth Sci. (Geol Rundschau) 93, 596-611

Hensen C., Wallmann K., Schmidt M., Ranero C.R., Suess E. (2004): Fluid expulsion related to mud extrusion off Costa Rica - A window to the subducting slab. Geology 32, 201-204

Hensen C., Wallmann K. (2005): Methane formation at Costa Rica continental margin - constraints for gas hydrate inventories and cross-décollement fluid flow. EPSL 236, 41-60

Huehnerbach V., Masson D.G., Bohrmann G., Bull J.M., Weinrebe W. (2005): Deformation and submarine landsliding caused by seamount subduction beneath the Costa Rica Continental margin – new insights from high-resolution sidescan sonar data. In: Hodgson, D.M., Flint, S.S. (eds): Submarine slope systems, processes and products. Geological Society Special Publication 244, 195-205.

Hyndman R.D., Davis E.E. (1992): A Mechanism for the Formation of Methane hydrate and Seafloor Bottom-Simulating Reflectors by Vertical Fluid Expulsion. JGR 97, No B5, 7025-7041

Kahn L.M., Silver E.A., Orange D., Kochevar R., McAdoo B. (1996): Surficial evidence of fluid expulsion from the Costa Rica accretionary prism. GRL 23, 8, 887-890

Keil H. (1995): Migration von PARASOUND-Daten. Unpublished diploma thesis

Kimura G., Silver E.A., Blum P. et al. (1997): Proceedings of the Ocean Drilling Program, Initial Reports, Vol. 170, College Station, TX

Kopf A., Deyhle A. and Zuleger E. (2000): Evidence for deep fluid circulation and gas hydrate dissociation using boron and boron isotopes of pore fluids in forearc sediments from Costa Rica (ODP Leg 170). Marine Geology 167, 1-28.

Kopf A. (2002): Significance of mud volcanism. Rev. Geoph. 40, 2, 1005

Kvenvolden, K.A. (1988) Methane hydrate—A major reservoir of carbon in the shallow geosphere? Chemical Geology, v. 71, p. 41–51.

Lance S., Henry P., Le Pichon X., Lallemant S., Chamley H., Rostek F., Faugeres J.C., Gonthier E., Olu K. (1998): Submersible study of mud volcanoes seaward of the Barbados accretionary wedge: sedimentology, structure and rheology. Marine Geology 145, 255-292

Langseth M.G., Silver E.A. (1996): The Nicoya convergent margin - a region of exceptionally low heat flow. GRL 23, 8, 891-894

Mau S., Sahling H., Rehder G. , Suess E., Linke P., Soeding E. (2006): Estimates of methane output from mud extrusions at the erosive convergent margin off Costa Rica. Marine Geology 225, 129-144

McAdoo B.G., Orange D.L., Silver E.A., McIntosh K., Abbott L., Galewsky J., Kahn L., Protti M. (1996): Seafloor structural observations, Costa Rica accretionary prism. GRL 23, 8, 883-886

McIntosh K., Silver E., Shipley T. (1993): Evidence and mechanism for forearc extension at the accretionary Costa Rica convergent margin. Tectonics 12, 6, 1380-1392

McIntosh K., Silver E.A. (1996): Using 3D Seismic reflection data to find fluid seeps from the Costa Rica accretionary prism. GRL 23, 8, 895-898

Melles M., Kuhn G. (1993):Sub-bottom profiling and sedimentological studies in the southern Weddell Sea, Antarctica; evidence for large-scale erosional/ depositional processes. Deep-Sea Res. I (Oceanographic Res. Papers), 40, 4, 739-760.

Meschede M., Zweigel P., Kiefer E. (1999): Subsidence and extension at a convergent plate margin: evidence for subduction erosion off Costa Rica. Terra Nova 11, 112-117

Mienert J., Vanneste M., Buenz S., Andreassen K., Haflidason H., Sejrup H. P. (2005): Ocean warming and gas hydrate stability on the mid-Norwegen margin at the Storegga Slide. Marine and Petroleum Geology, 22, 233-244

Moerz T., Kopf A., Brueckmann W., Fekete N., Huenerbach V., Masson D., Hepp D.A., Suess E. and Weinrebe W. (2005a): Styles and productivity of mud diapirism along the Middle American Margin / Part 1: Margin Evolution, Segmentation, Dewatering and Mud Diapirism. Nato science series, Kluwer Academic Publishers, Dordrecht/Boston/London

Moerz T., Fekete N., Kopf A., Brueckmann W., Kreiter S., Huehnerbach V., Masson D., Hepp D. A., Schmidt M., Kutterolf S., Sahling H., Abegg F., Spiess V., Suess E. and Ranero C. R. (2005b): Styles and productivity of mud diapirism along the Middle American Margin / Part 2: Mound Culebra and Mounds 11 and 12. Nato science series, Kluwer Academic Publishers, Dordrecht/Boston/London

Morris J., Valentine R., Harrison T. (2002): [10]Be imaging of sediment accretion and subduction along the northeast Japan and Costa Rica convergent margins. Geology 30, 59-62

Pecher I. (1996): Seismic Studies of Bottom Simulating Reflectors at the Convergent Margins Offshore Peru and Costa Rica: nature and formation, results from full waveform inversion heat flux from the depth of bottom simulating reflectors. Geomar Report 47, Kiel

Pecher I.A., Ranero C.R., von Huene R., Minshull T.A., Singh S. (1998): The nature and distribution of bottom simulating reflectors at the Costa Rican convergent margin. GJI 133, 219-229

Pecher I.A., Kukowski N., Ranero C.R., von Huene R. (2001): Gas hydrates along the Peru and Middle America Trench Systems. in: Natural Gas Hydrates: Occurrence, Distribution, and Detection (Geophys. Monogrpah 124)

Protti M., Guendel F., McNally K. (1994): The geometry of the Wadati-Benioff zone under Southern Central America and its tectonic significance: results from a high-resolution local seismographic network. Physics of the Earth and Planetary Interiors 84, 271-287

Ranero C.R., von Huene R. (2000): Subduction erosion along the Middle America convergent margin. Nature 404, 748-752

Ranero C.R., Phipps-Morgan J., McIntosh K. and Reichert C. (2003): Bending-related faulting and mantle serpentinization at the Middle America trench. Nature 425, 367-373

Saffer D.M., Silver E.A., Fisher A.T., Tobin H., Moran K. (2000): Inferred pore pressures at the Costa Rica subduction zone: implications for dewatering processes. EPSL 177, 193-207

Sahling H., Masson D.G., Ranero C.R., Huehnerbach V., Weinrebe W., Klaucke I., Buerck D., Brueckmann W., Suess E. (in prep.): Methane seepage at the continental margin off Costa Rica and Nicaragua revealed by high-resolution swath bathymetry, sidescan sonar, and seafloor observations.

Sallares V., Danobeitia J.J., Flueh E.R. (2000): Seismic tomography with local earthquakes in Costa Rica. Tectonophys 329, 61-78

Shipley T.H., Stoffa P.L., Dean D.F. (1990): Underthrust Sediments, Fluid Migration Paths, and Mud Volcanoes Associated With the Accretionary Wedge off Costa Rica: Middle America Trench. JGR 95, B6, 8743-8752

Shipley T.H., McIntosh K.D., Silver E.A., and Stoffa P.L. (1992): Three-dimensional seismic imaging of the Costa Rica accretionary prism: structural diversity in a small volume of the lower slope. JGR 97, 4439–4459

Silver E.A. (2000): Leg 170: synthesis of fluid-structural relationships of the Pacific margin of Costa Rica. In: Silver E.A., Kimura G., Shipley T.H. (eds.): Proceedings of the Ocean Drilling Program, Scientific Results, Vol. 170

Silver E., Kastner M., Fisher A., Morris J., McIntosh K., Saffer D. (2000): Fluid flow paths in the Middle America Trench and Costa Rica margin. Geology 28, 8, 679-682

Soeding E., Wallmann K., Suess E. and Flueh E.R. (eds.) (2003): RV METEOR Cruise Report M54/2+3: Fluids and Subduction Costa Rica 2002. GEOMAR Report 111

Spiess V. (1993): Digitale Sedimentechographie - neue Wege zu einer hochaufloesenden Akustostratigraphie. Berichte, Fachbereich Geowissenschaften, Universitaet Bremen, Germany, Nr. 35, 199 S.

van Rensbergen P., Morley C. K., Ang D. W., Hoan T. Q., Lam N. T. (1999): Structural evolution of shale diapirs from reactive rise to mud volcanism: 3D seismic data from the Baram delta, offshore Brunei Darussalam. Journal of the Geological Society, London, 156, pp. 633-650

Vannucchi P., Scholl D.W., Meschede M., McDougall-Reid K. (2001): Tectonic erosion and consequent collapse of the Pacific margin of Costa Rica: combined implications from ODP Leg 170, seismic offshore data, and regional geology of the Nicoya Peninsula. Tectonics 20, 5, 649-668

Vannucchi P., Ranero C.R., Galeotti S., Straub S. M., Scholl D.W. and McDougall-Ried K. (2003): Fast rates of subduction erosion along the Costa Rica Pacific margin: Implications for non-steady rates of crustal recycling at subduction zones. JGR 108, B11, 2511

von Huene R., Ranero C.R., Weinrebe W., Hinz K. (2000): Quarternary convergent margin tectonics of Costa Rica, segmentation of the Cocos Plate, and Central American volcanism. Tectonics 19, 2, 314-334

von Huene R., Ranero C.R., Vannucchi P. (2004): Generic model of subduction erosion. Geology 32 No 10 pp 913-916

Walther C.H.E., Flueh E.R., Ranero C.R., von Huene R., Strauch W. (2000): Crustal structure across the Pacific margin of Nicaragua: evidence for ophiolitic basement and a shallow mantle sliver. GJI 141, 759-777

Walther C.H.E. (2003): The crustal structure of the Cocos Ridge off Costa Rica. JGR 108, B3, 21 pp.

Weinrebe W., Flueh E.R. (eds.) (2002): RV SONNE Cruise Report SO163: SUBDUCTION-I: Multi-System Analysis of Fluid Recycling and Geodynamics at the Continental Margin off Costa Rica. GEOMAR Report 106

Wessel, P., and W. H. F. Smith (1998): New, improved version of Generic Mapping Tools released. EOS Trans. Amer. Geophys. U., 79 (47), pp. 579

Appendix

Excerpt from binning statistics with occupation (GeoB02-216):

GeoAPP-Part II: statistics

binning along midpoints of channel   12
used channels: 48
number of shots: 406
number of traces: 19488
number of bins: 1136
radius of bins: 30.00000
distance of bins: 10.0000000000000
length of profile (m):   11358.0000000000

optimization on!

     554 midpoints not binned
(cdp=0 for these traces!)
     97 percent of midpoints binned.

   1. bin occupied with: 9
     2. bin occupied with: 3
     3. bin occupied with: 5
     4. bin occupied with: 5
     5. bin occupied with: 6
     6. bin occupied with: 6
     7. bin occupied with: 5
     8. bin occupied with: 6
     9. bin occupied with: 7
     10. bin occupied with: 6
etc.
     1127. bin occupied with: 15
     1128. bin occupied with: 10
     1129. bin occupied with: 13
     1130. bin occupied with: 10
     1131. bin occupied with: 12
     1132. bin occupied with: 11
     1133. bin occupied with: 7
     1134. bin occupied with: 9
     1135. bin occupied with: 9
     1136. bin occupied with: 19

maximum occupation: 23
number of empty bins :   0
average occupation (without empty bins):   16.00000
end of binning!

Excerpt from failed bins, with shot number, channel number, cdp coordinate:

```
1706  33 -85.913335   9.555747
1706  34 -85.913305   9.555702
1706  35 -85.913272   9.555653
1706  36 -85.913242   9.555608
1706  37 -85.913209   9.555559
1706  38 -85.913178   9.555514
1706  39 -85.913146   9.555465
1706  40 -85.913115   9.555420
1706  41 -85.913082   9.555371
1706  42 -85.913052   9.555326
1706  43 -85.913019   9.555277
1706  44 -85.912989   9.555232
1706  45 -85.912956   9.555184
1706  46 -85.912925   9.555138
1706  47 -85.912892   9.555090
1706  48 -85.912862   9.555044
1707  33 -85.913569   9.555901
1707  34 -85.913538   9.555856
1707  35 -85.913505   9.555807
1707  36 -85.913475   9.555762
1707  37 -85.913442   9.555713
1707  38 -85.913412   9.555668
1707  39 -85.913379   9.555619
1707  40 -85.913348   9.555574
1707  41 -85.913315   9.555525
1707  42 -85.913285   9.555480
1707  43 -85.913252   9.555431
1707  44 -85.913222   9.555386
1707  45 -85.913189   9.555337
1707  46 -85.913158   9.555292
1707  47 -85.913125   9.555243
1707  48 -85.913095   9.555198
1708  42 -85.913372   9.555778
1708  43 -85.913339   9.555729
1708  44 -85.913309   9.555684
1708  45 -85.913276   9.555635
1708  46 -85.913246   9.555590
1708  47 -85.913213   9.555541
1708  48 -85.913182   9.555496
```

Raw (right) and corrected (left, without outliers and smoothed) heading values from ta
Digi bird, GeoB02-216, average heading 313°
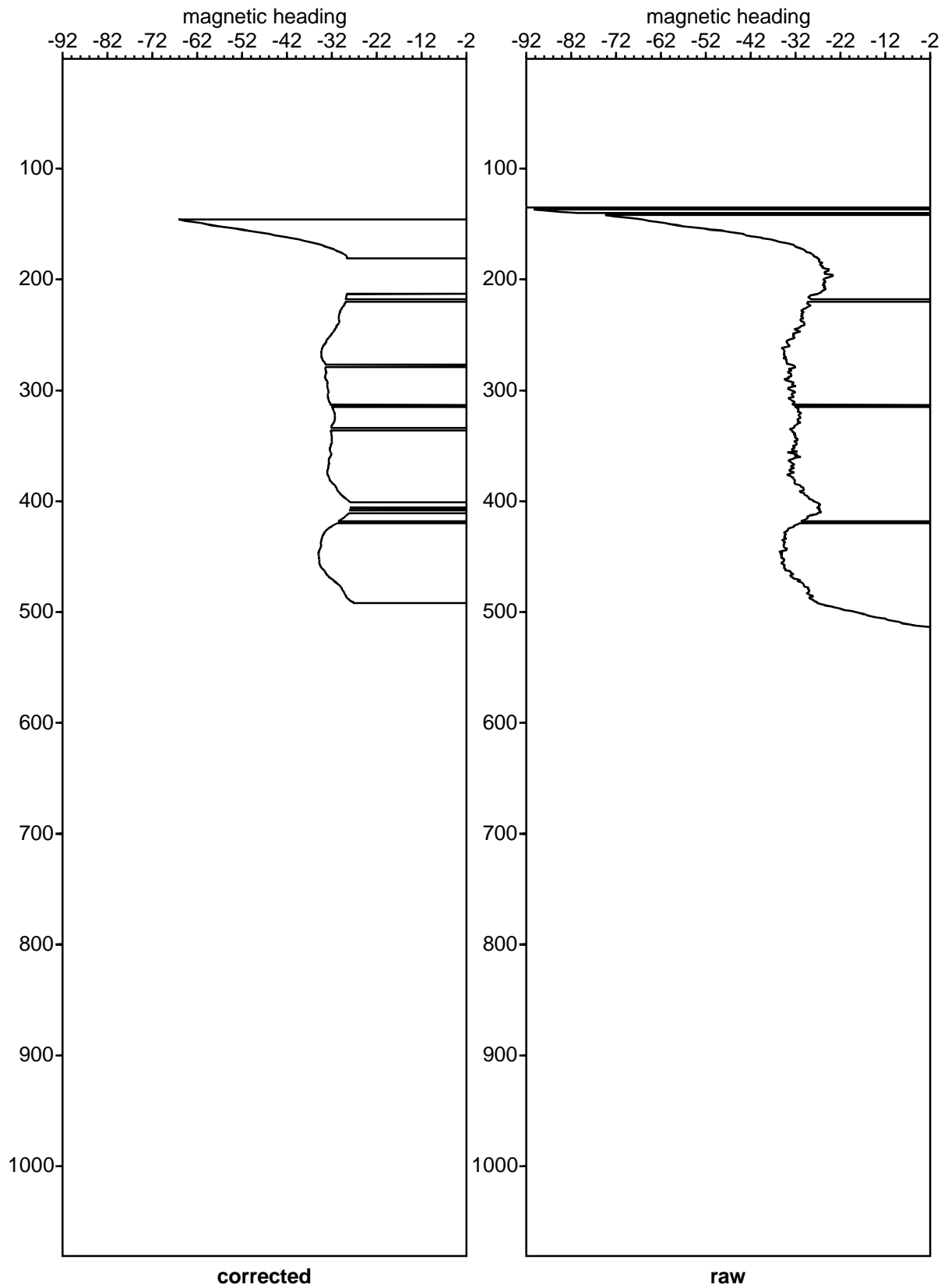
Acknowledgements

I would like to thank my supervisor, Tim Reston, for his scientific guidance throughout the years. Without his unique personality, work would have been less rewarding, and less fun.

To Volkhard Spiess I owe a great deal. As the source of "my data", he led me through the ungrateful first part of processing. He was ready for discussions or to provide his opinion to the very last day, and could also motivate me in periods of frustration. Without him, I would not have gotten far. Thank you.

Thanks are due to Ingo Grevemeyer for help and discussions concerning heat flow.

I am grateful to Lars Zuehlsdorff, Hanno Keil, and Sebastian Krastel, for many hours of bug hunting in GeoApp and their patience for simpleton questions. Thanks to Dirk Klaeschen for his help with Seismos, and the removal of lots of noise from the data. My gratitude goes to the fellow members of the SFB 574 for fruitful discussions and a cheerful atmosphere, and to the Geodynamics group for their helpfulness. Special thanks to Karen, Michael, Juergen, both Martins, Andreas, Peter, Gerald, Dietmar, and the others, for the great company in both in and out of science. Thanks to Gregor for the book, and to Ernst for the cruises. To Steve for his script on gas hydrate thickness, and for his pearls of wisdom on how science works. To Steffen for sedimentation rates. To Arnim for his Seismos experience and spontaneous user support.

Since marine data can not be collected alone, thanks are due to the crews of various Meteor and Sonne cruises. Equally important, although perhaps not so spectacular, has been the patient guidance from Ulrike, Silke, Martina, and several other ladies in the administration, through a forest of rules and forms.

And last but not least, I would like to thank Gerd, for providing a peaceful background for the writing, and bearing with me through the stress and hectics.

Curriculum Vitae

Personal details

Name:	FEKETE, Noémi Mária
Nationality:	Hungarian
Place/date of birth:	Gyor (Hungary), 13th July 1976
Marital status:	single

Education, qualifications

1990 - 1995:	English-Hungarian Dual Language Secondary School, Balatonalmádi, Hun.
1995:	Certificate of General Education
1995 - 2000:	Geophysics major, Eötvös Loránd University, Budapest, Hun.
2000:	M. Sc. in Geophysics
	supplementary diploma in Translating (English, specialized in Earth Sciences)
2000 - 2002:	3 semesters of PhD studentship at the Dept. of Geophysics, Eötvös Loránd Univ., Budapest, Hun.
2003- 2006:	6 semesters of PhD studentship at the Christian Albrecht University, Kiel, Germany

Positions

2000 – 2002:	GEOMEGA Ltd., Budapest, Hun.
2002 – 2005:	SFB 574, Christian Albrecht University, and Leibniz Institut of Marine Sciences (IFM-GEOMAR), Kiel, Germany
since 01. 01. 2006:	University of Bremen, Bremen, Germany

Erklärung

Hiermit erkläre ich, dass die von mir für das Promotionsverfahren vorgelegte Abhandlung "Dewatering Through Mud Mounds on the Continental Fore-arc of Costa Rica" – abgesehen von der Beratung durch die Betreuer – nach Inhalt und Form meine eigene Arbeit ist und bisher noch nicht an anderer Stelle im Rahmen eines Prüfungsverfahrens vorgelegt wurde.